REPORT 1218

EFFECT OF GROUND INTERFERENCE ON THE AERODYNAMIC AND FLOW CHARACTERISTICS OF A 42° SWEPTBACK WING AT REYNOLDS NUMBERS UP TO 6.8×10⁶ [†]

By G. Chester Furlong and Thomas V. Bollech

SUMMARY

The effects of ground interference on the aerodynamic characteristics of a 42° sweptback wing have been investigated at distances 0.68 and 0.92 of the mean aerodynamic chord from the simulated ground to the 0.25-chord point of the mean aerodynamic chord. Survey data behind the wing, both with and without the simulated ground, are presented in the form of contour charts of downwash, sidewash, and dynamic-pressure ratio at longitudinal stations of 2.0 and 2.8 mean aerodynamic chords behind the wing.

The nature and magnitudes of the effects of ground interference on the aerodynamic characteristics of the sweptback wing are, in general, comparable to those obtained on unswept wings. The longitudinal stability at the stall for the sweptback wing with and without flaps deflected was not materially affected by the presence of the ground for the ground heights available in the tests.

The qualitative results of the airstream survey for the ground-out condition are, in general, consistent with the results which would be expected from a consideration of the span loading of sweptback wings. It was found also that without the ground present the tip vortices for the plain wing were shed at a position that would be expected for a straight tapered wing.

The variations of average downwash and average dynamic-pressure ratio with angle of attack indicate that, for either model configuration, the most preferable tail location would be below the chord plane extended and at the most rearward survey position. In the presence of the ground, negative variations of average downwash with angle of attack were obtained, and although such variations would increase the degree of stability, they may be undesirable from the standpoint of trim.

The lifting-line procedure used for calculating the downwash behind unswept wings has been extended to include the effects of sweep. Calculations of downwash by the lifting-line method (as applied) underestimated the experimental downwash at the plane of symmetry but resulted in reasonable estimates of the experimental downwash outboard of the plane of symmetry.

INTRODUCTION

Certain aspects of the effects of the ground interference on the aerodynamic characteristics of unswept wings have been thoroughly investigated both theoretically and experimentally (refs. 1 to 6). The experimental results of these investigations have shown that, in the high-lift range, theoretical calculations by existing methods do not provide either a reliable estimate of the magnitude of the ground effects or an explanation of the phenomena involved at the stall.

Extensive theoretical and experimental studies have been made of the flow behind straight wings with the result that reasonable estimates of the flow inclination and wake characteristics can be made for a straight wing either with or without the ground present (refs. 5, 7, and 8). Theoretical and experimental studies of the flow behind sweptback wings are, at present, limited in scope and, hence, no adequate means for proper empennage design exists. The experimental data that are available for sweptback wings were obtained without the ground present and at relatively low values of Reynolds number (for example, ref. 9). Some large-scale data have been published in reference 10.

Inasmuch as extensions of theoretical calculations into the high-lift range are not reliable and the available experimental data in the high-lift range are confined to wings having little or no sweepback, it appears that a knowledge of the effects of the ground on a highly sweptback wing can only be acquired by means of experiment. Accordingly, an investigation has been conducted in the Langley 19-foot pressure tunnel to determine the effects of ground interference on a highly sweptback wing and to indicate whether the ground effects on a sweptback wing are of the same general nature and magnitude as those on an unswept wing. These tests were to provide not only additional flow-inclination and wake data behind a sweptback wing not in the presence of the ground but also flow data obtained with the wing in the presence of the ground.

The model used for the present investigation had 42° sweepback of the leading edge, an aspect ratio of 4.01, a taper ratio of 0.625, and NACA 64₁–112 airfoil sections normal to the 0.273-chord line. Tests were made with and without a simulated ground for two model configurations; namely, the plain wing and the wing with inboard trailing-edge split flaps and outboard leading-edge flaps deflected.

The present report contains force and moment data obtained throughout the angle-of-attack range at several values of Reynolds number and contour charts of downwash, sidewash, and dynamic-pressure ratio at two longitudinal

stations behind the wing (2.0 and 2.8 mean aerodynamic chords). The locations of the tip vortices have been shown on the contour charts of dynamic-pressure ratio for the plain wing without the ground present. Integrations have been made to obtain variations of average downwash and dynamic pressure with angle of attack. Values of downwash have been calculated by extending the method presented in references 7 and 8 to account for the sweep of the 0.25-chord line.

The ground was simulated in the tunnel by means of a ground board. Although this method of ground representation is not ideal, the results of the present tests are believed to be indicative of the ground-interference effects on a sweptback wing.

SYMBOLS

C_L lift coefficient, $\dfrac{\text{Lift}}{qS}$

C_D drag coefficient, $\dfrac{\text{Drag}}{qS}$

C_m pitching-moment coefficient about $0.25c$, $\dfrac{\text{Pitching moment}}{qS\bar{c}}$

α angle of attack of wing root chord, deg

q free-stream dynamic pressure, $\dfrac{\rho V^2}{2}$, lb/sq ft

R Reynolds number, $\dfrac{\rho V\bar{c}}{\mu}$

S wing area, sq ft

b wing span, ft

c local chord, ft

$\bar{c}$ mean aerodynamic chord, $\dfrac{2}{S}\displaystyle\int_0^{b/2} c^2\,dy$, ft

ρ mass density of air, slugs/cu ft

V stream velocity, ft/sec

q_t local stream dynamic pressure, lb/sq ft

ϵ local downwash angle, deg

Λ sweep angle of 0.25-chord line, deg

σ sidewash angle, inflow positive, deg

μ coefficient of viscosity of air, slugs/ft-sec

q_t/q ratio of local-stream dynamic pressure to free-stream dynamic pressure

z vertical distance from chord plane extended, ft

x longitudinal distance from 0.25-chord point of root chord

s vortex semispan (always positive), ft

y lateral distance from plane of symmetry, ft

g downwash factor

w total induced downward velocity, ft/sec

c_l section lift coefficient

τ vortex strength

ϵ' calculated downwash angle, deg

h downward displacement, measured normal to the relative wind, of the center line of the wake and the trailing vortex sheet from its origin at the trailing edge, ft

Integrated air-stream surveys:

$(q_t/q)_{av}$ average q_t/q, obtained by

$$\left[\left(\frac{q_t}{q}\right)_{av}=\frac{2}{S_t}\int_0^{b_t/2}\left(\frac{q_t}{q}\right)c_t\,dy_t\right]$$

ϵ_{av} average ϵ, obtained by

$$\left[\epsilon_{av}=\frac{2}{\left(\dfrac{q_t}{q}\right)_{av}S_t}\int_0^{b_t/2}\epsilon\left(\frac{q_t}{q}\right)c_t\,dy_t\right]$$

where

c_t chord of fictitious tail

b_t span of fictitious tail

S_t area of fictitious tail

y_t spanwise distance

$\dfrac{d\epsilon_{av}}{d\alpha}$ rate of change of ϵ_{av} with angle of attack

GROUND, MODEL, AND APPARATUS

### GROUND REPRESENTATION AND GROUND DISTANCE

Several methods such as the reflection method, the partial plate and reflection method, and the plate method are available for ground simulation in a wind tunnel (refs. 4 to 6). The most feasible arrangement for ground tests in the Langley 19-foot pressure tunnel is the plate method (commonly referred to as the ground-board method).

The vertical distance from the $0.25\bar{c}$ to the ground board (regardless of boundary-layer thickness on the ground board) is referred to as the ground distance. Inasmuch as no standard point of reference exists, the $0.25\bar{c}$ has been used because it was the most convenient point of reference from considerations of test procedure. The model was supported in the tunnel at the $0.25\bar{c}$, and to maintain a constant ground distance for any other point of reference would have necessitated moving the ground board as the angle of attack of the wing was changed.

Based on the preceding definition of ground distance, the ground distances used in the present tests were $0.68\bar{c}$ and $0.92\bar{c}$.

MODEL

The model mounted on the normal wing-support system of the Langley 19-foot pressure tunnel is shown in figure 1. The wing had 42° sweepback of the leading edge, a taper ratio of 0.625, an aspect ratio of 4.01, and NACA 64_1–112 airfoil sections normal to the 0.273-chord line. The principal dimensions of the model and flaps are given in figure 2. It was found that a slight discontinuity existed along the 0.20-chord line of the wing. The results obtained in the present tests, therefore, do not necessarily represent exactly those which would be obtained on a wing with true NACA 64_1–112 airfoil sections. The model was maintained in a smooth condition during the tests. For tests with flaps deflected, the $0.20c$ trailing-edge split flaps were deflected 60° from the lower surface and extended from the root to $0.50\dfrac{b}{2}$. The leading-edge flaps extended spanwise from $0.400\dfrac{b}{2}$ to $0.975\dfrac{b}{2}$.
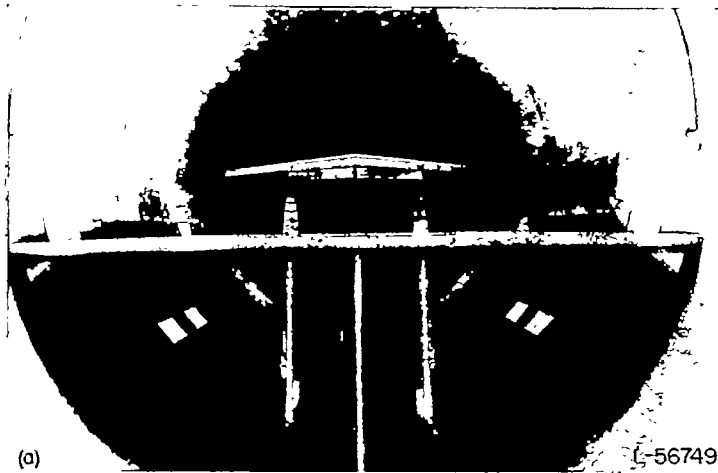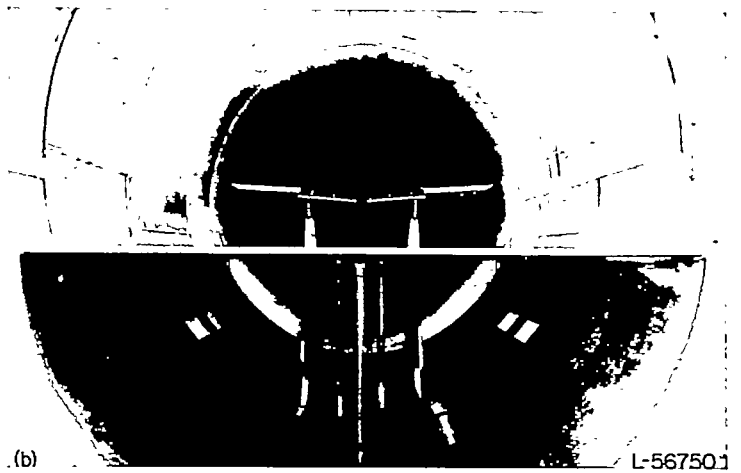
(a) Front view.

FIGURE 1.—A 42° sweptback wing mounted in the Langley 19-foot pressure tunnel. Flaps deflected; ground board in. Ground distance, 0.92c̄.
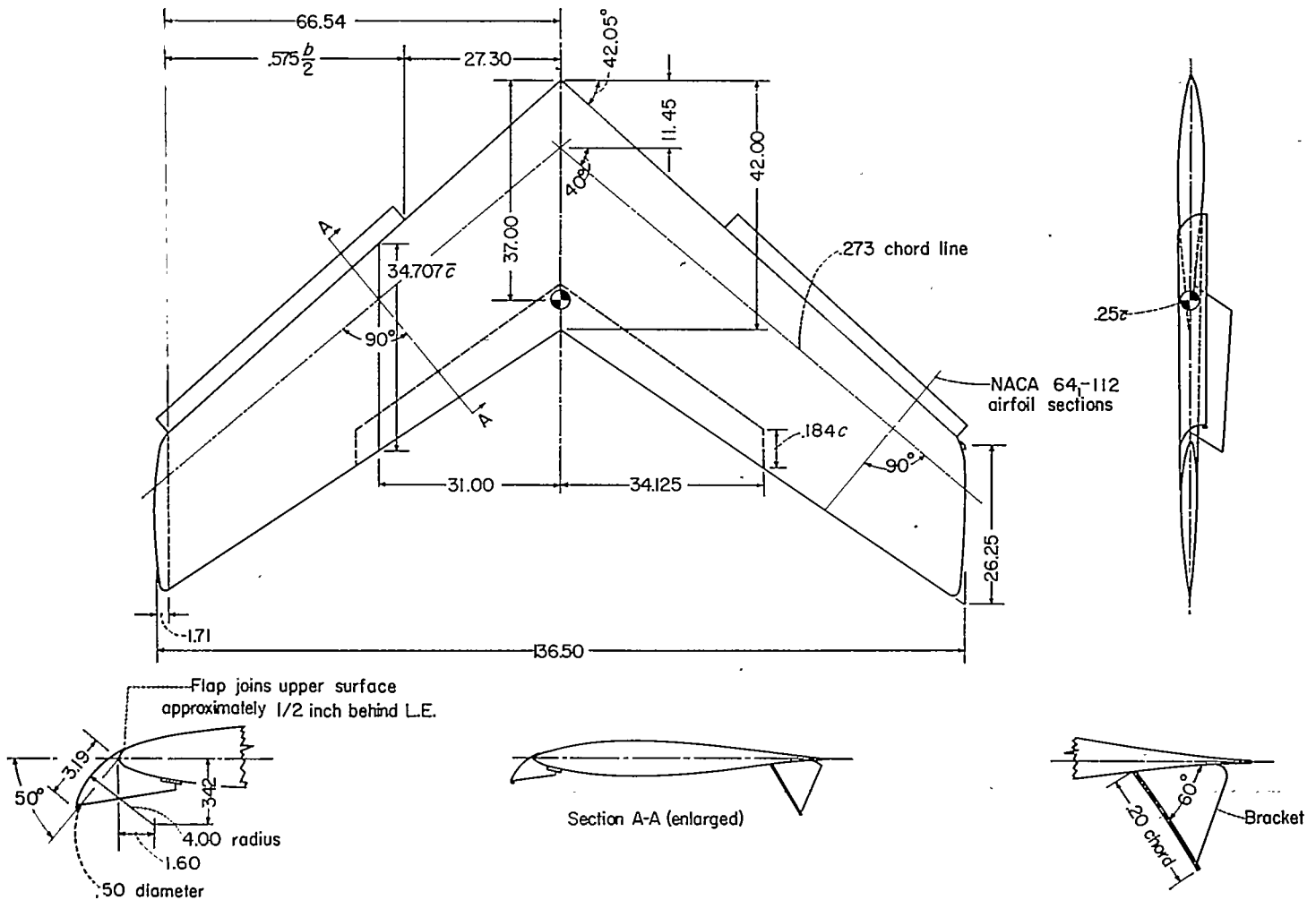
(b) Rear view.

FIGURE 1.—Concluded.

FIGURE 2.—Layout of 42° sweptback wing. (All dimensions are in inches.)

APPARATUS

The aerodynamic forces were measured by a simultaneously recording, six-component balance system.

Survey apparatus.—The Langley 19-foot-pressure-tunnel survey apparatus and multiple-tube survey rake (fig. 3) were used to obtain downwash and dynamic pressure behind the wing. The multiple-tube survey rake consists of six pitot-static tubes with pitch and yaw orifices in the hemispherical tips. The survey apparatus maintained the rake in a vertical position as it was moved laterally along the span. This survey rake had been previously calibrated through known pitch and yaw angles. All pressure leads were conducted to a multiple-tube manometer and during the tests the data were photographically recorded.

A probe containing three tufts spaced 1.5 inches was used to locate the tip vortex. The probe was attached to the survey strut.

Ground board.—The ground board consisted of a steel framework covered with plywood on both the upper and lower surfaces, which resulted in an overall thickness of 4 inches. (See fig. 4.) A slot extending the full width of the ground board and located 1 foot in front of the $0.25\bar{c}$ of the wing was provided as a means of boundary-layer control. The ground board was supported in the tunnel test section by means of wall brackets and center posts. (See figs. 1 and 4.) The support system allowed a ground-board travel from 16.0 to 31.9 inches below the center line of the tunnel (center of rotation of the model).

L-47123
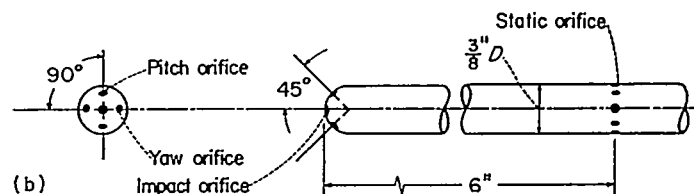
(a) Photograph of survey rake.
(b) Sketch of survey-rake tube.

FIGURE 3.—Langley 19-foot pressure tunnel airstream survey rake.
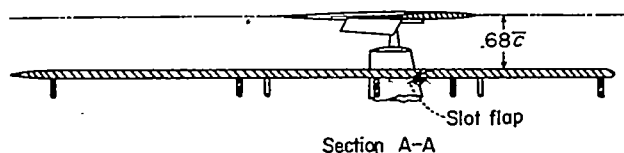

View B-B

Section A-A
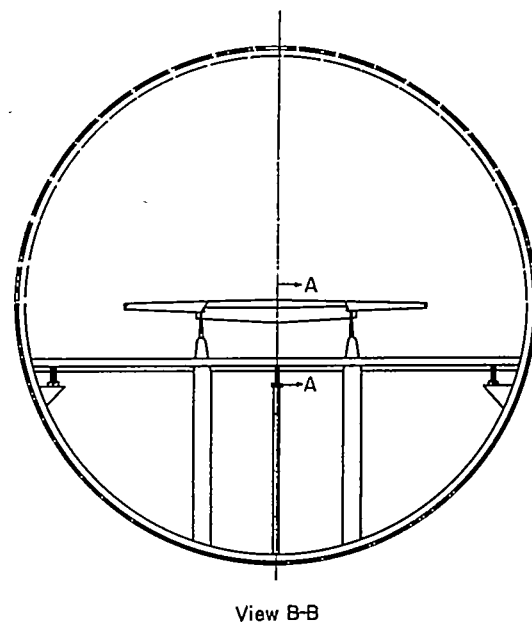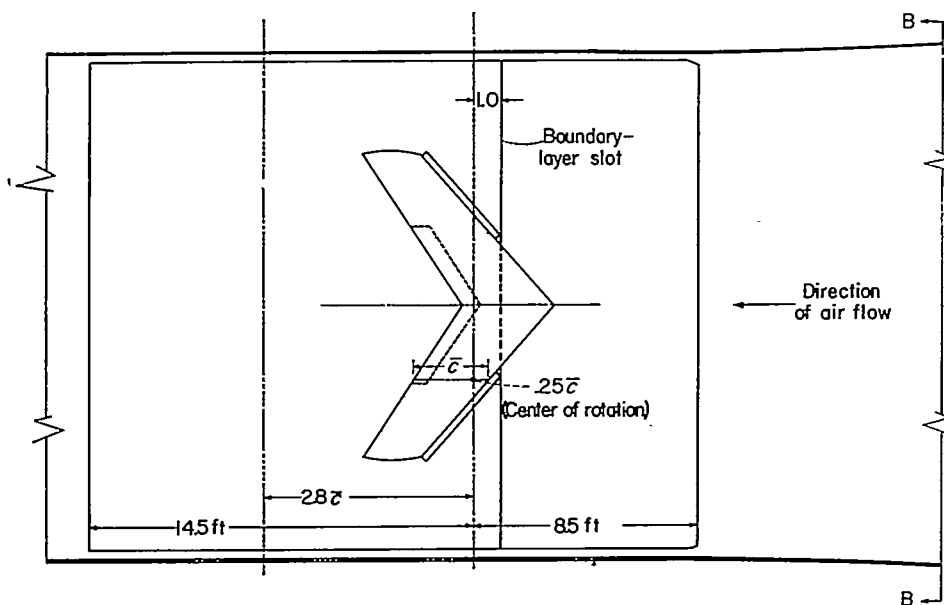
FIGURE 4.—Sketch of 42° sweptback wing and ground board used in the Langley 19-foot pressure tunnel. Ground distance, $0.68\bar{c}$.

TESTS AND CORRECTIONS

TESTS

The air in the tunnel was compressed to approximately 33 pounds per square inch absolute for all tests. The tests were made at Reynolds numbers up to 6.8×10^6 (based on $\bar{c}$), which corresponded to a dynamic pressure of approximately 80 pounds per square foot and a Mach number of 0.14.

Exploratory tests.—An exploratory investigation was conducted to determine the flow characteristics on the ground board and in the tunnel test section both with and without the model in the tunnel.

The change in velocity distribution in the tunnel due to the ground board was determined with the ground board in the tunnel and the model out. Measurements of the flow beneath the board indicated that the increase in flow due to the presence of the model was hardly measurable; hence the usual model blockage correction has been applied to the dynamic-pressure measurements. The ground board reduced the tunnel-clear stream angle approximately 0.15°.

Visual tuft studies of the flow on the ground board with the boundary-layer slot closed and open were made through the angle-of-attack range of the model. When the slot was closed but not completely sealed, an unsteady flow condition existed along the nose of the slot. The flow condition at the nose of the slot was improved when the slot was open. An unsteady flow condition existed in an area near the center of the board between $2.0\bar{c}$ and $2.8\bar{c}$ with either the slot open or closed. This unsteady flow condition can be attributed to the diffusion of the flap wake. There was no indication of actual flow separation on the board throughout the angle-of-attack range of the model. By use of the boundary-layer-control slot the maximum thickness of the boundary layer was reduced from approximately 1.0 inch to 0.4 inch beneath the wing and from 1.6 inches to 1.0 inch at a distance $2.8\bar{c}$ rearward of the $0.25\bar{c}$. The flow through the slot was not materially affected by the presence of the model. The discontinuity in boundary-layer thickness due to the flow through the slot corresponds to an effective discontinuity in ground distance, which, however, is believed to have a negligible effect on the test results. Presence of a boundary layer on the ground board may be less troublesome under a sweptback wing than under an unswept wing, mainly because the maximum lift is considerably lower for the sweptback wing.

Force and moment tests.—Force and moment data were obtained for the two model configurations through an angle-of-attack range from −4° through the stall. The tests were made with the ground board out and with the ground board located at ground distances of $0.68\bar{c}$ and $0.92\bar{c}$ for several values of Reynolds number. The Reynolds numbers of the tests based on $\bar{c}$ were 3.0, 4.3, 5.2, and 6.8×10^6.

Airstream surveys.—Downwash, sidewash, and dynamic-pressure surveys were made for each model and ground-board configuration at two longitudinal stations. The positions for the survey apparatus were selected so that they approximated, through the angle-of-attack range of the tests, stations $2.0\bar{c}$ and $2.8\bar{c}$ behind the $0.25\bar{c}$ of the wing measured along the chord plane extended. The maximum variation of the stations $2.0\bar{c}$ and $2.8\bar{c}$ from the locations of the survey apparatus was only 0.5 inch through the angle-of-attack

range of the test. Due to the fact that the trailing edge of the wing was swept back, the distance between the survey rake and the trailing edge of the wing decreased as the rake was moved from the plane of symmetry. Data were obtained at three angles of attack for the wing with flaps neutral and at four angles of attack for the flapped wing. The angles of attack for the tests in the presence of the ground were selected so that the values of lift coefficient obtained were of approximately the same magnitude as those obtained with the ground board out.

In conjunction with the airstream surveys, the tip-vortex core was located by observing the rotational movement of a wool tuft on a probe.

CORRECTIONS

The lift, drag, and pitching-moment data have been corrected for support tare and strut interference as determined from tare tests. The angles of attack, drag data, and moment data have been corrected for jet-boundary effects. In addition, the angles of attack have been corrected for airstream misalinement.

The airstream-survey data have been corrected for jet boundary effects which consist of an angle change to the downwash $\Delta\epsilon$ and a downward displacement of the flow field. The magnitude of the angular corrections $\Delta\epsilon$ at the two survey stations are given in the following table:

Longitudinal survey position	$2.0\bar{c}$	$2.8\bar{c}$
$\Delta\epsilon$	$\dfrac{1.36C_L}{\sqrt{q_i/q}}$	$\dfrac{1.53C_L}{\sqrt{q_i/q}}$

With the ground board in the tunnel test section, it was not possible to obtain corrections for support-tare and strut interference. The ground-board-out corrections for support-tare and strut interference, however, have been applied to the ground-board-in data in the belief that they would be of the same nature, although not necessarily of the same magnitude, as would be obtained with the ground board in.

Calculations made for other ground investigations (such as ref. 4) have shown that at small ground heights, jet-boundary corrections are negligible; hence, they have been neglected in the present tests.

EFFECTS OF GROUND INTERFERENCE

A discussion of the concepts of ground interference appears pertinent before the results of the present tests of a sweptback wing are presented. Although the concepts have been derived largely to explain the effects of ground interference on an unswept wing, they should, in general, apply to a sweptback wing as well.

The ground effect on a wing may be considered as the interference due to the reflected image of the wing in the ground. Computations of the effects of the image wing on the real wing can be made by replacing it with a bound vortex and a system of trailing vortices. Inasmuch as these computations are based on thin-wing theory, the effect of the thickness of the image wing must also be determined. The separate effects of the bound vortex, trailing vortices,

and wing thickness can then be added. In reference 1 the interference from the trailing vortices of the image wing was considered in detail; whereas in reference 6 the interferences from the bound vortex and wing thickness of the image wing were also considered. Although the calculations of the separate interference effects for unswept wings have been shown experimentally to be inadequate in the high angle-of-attack range, the separate effects may be used to describe qualitatively the combined effects of angle of attack and ground distance.

The image trailing vortices induce an upwash at the wing which is stronger at the center than near the tips. Figure 5 (a) shows the trailing vortices of the wing and the image

(a) Trailing vortices.

(b) Bound vortex (low angle (c) Bound vortex (high angle
　　of attack).　　　　　　　　　 of attack).

(d) Wing thickness doublet (e) Wing thickness doublet
　　(low angle of attack).　　　 (high angle of attack).
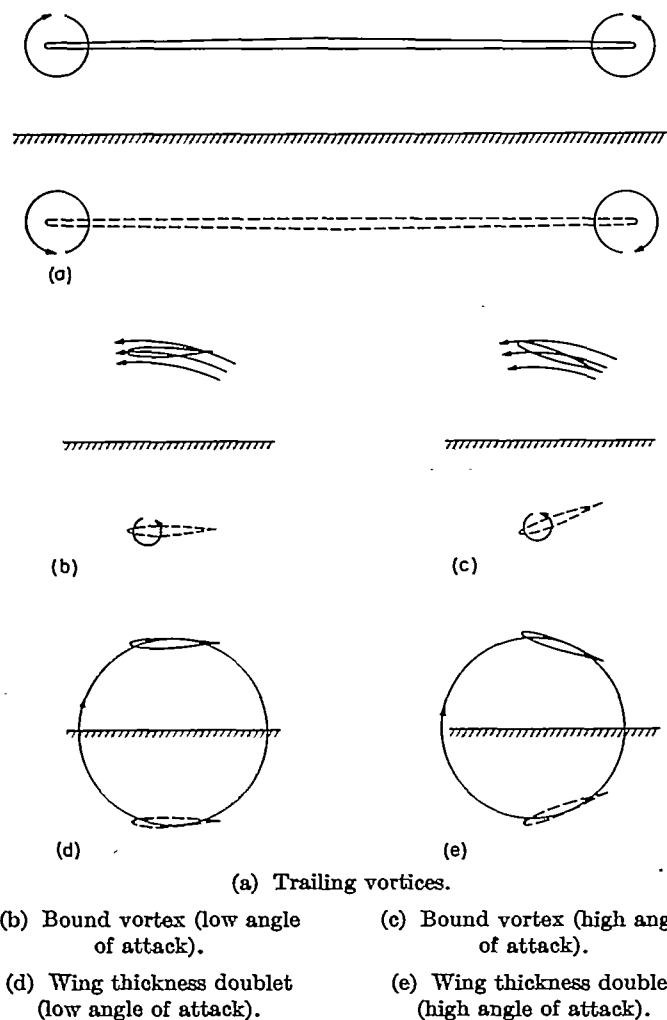
FIGURE 5.—Sketch showing the interference effects of the reflected image of a wing in the presence of the ground.

vortices. The main effects resulting from this vortex pattern are an increase in lift-curve slope, a reduction in induced drag, and a concentration of lift toward the center of the wing. The effects are increased by decreasing the ground distance and are relatively independent of the angle of attack.

The induced flow over the wing due to the image bound vortex is shown by a side view of the wing and its image (fig. 5 (b)). The flow, which is from rear to front, reduces the stream velocity in the vicinity of the wing and thereby tends to reduce the lift. If, however, the wing is fairly close to the ground, is at a low or moderate angle of attack, and is

uncambered, the induced flow also has a vertical component near the rear (fig. 5 (b)), which corresponds to an effective increase in camber and a corresponding increase in lift. As either the angle of attack or the camber is increased, however, the induced flow crosses the wing from above (as in fig. 5 (c)) with a corresponding effective decrease in camber and reduction in lift. For a highly cambered airfoil, such as a flapped wing, this effect is very pronounced. The decrease in camber and reduction in lift as the angle of attack is increased is also a function of ground distance. As the ground distance becomes very small, the effects mentioned are delayed to higher and higher angles of attack.

The thickness of the image wing may be roughly represented by a source near the airfoil nose and an equivalent sink near its trailing edge. The corresponding streamlines are circles through the source and sink, as indicated in figures 5 (d) and 5 (e). The velocity is in such a direction as to increase the stream velocity in the vicinity of the wing. The induced flow (figs. 5 (d) and 5 (e)) is seen to be essentially independent of angle of attack and is downward near the trailing edge and upward at the nose. This induced flow corresponds to a negative induced camber and a reduction in lift. The induced-flow effect of the doublet is increased as the ground distance is reduced, but in any case this effect is small compared with the induced-flow effect of the bound vortex (figs. 5 (b) and 5 (c)).

In general, the induced flows indicated in figures 5 (a), 5 (b), 5 (d), and 5 (e) serve to increase the slope of the lift curve. As the angle of attack and lift coefficient become very large or when the flaps are deflected, the induced flow indicated in figure 5 (c) becomes increasingly strong and serves to reduce the lift-curve slope. The overall influence of these effects on the maximum lift is too complex to be explained without a more quantitative analysis.

Experimental results provide some indication of the important factors determining the maximum lift as the ground is approached. Data for straight, unflapped wings (refs. 1 and 6) show that the maximum lift is decreased and then increased as the ground is approached. The reduced stream velocity and the negative induced angle and camber indicated in figure 5 (c) appear to combine with the small induced flow of figure 5 (e) to effect a decrease in maximum lift at moderate ground distances. As previously mentioned, the negative induced angle and camber effect (fig. 5 (c)) are reduced appreciably for uncambered wings as the ground distance becomes small; hence the maximum lift begins to increase. The experimental data for straight, flapped wings (ref. 4) show a decrease in maximum lift at all ground distances down to $0.50\bar{c}$. In this case the wing is originally very highly cambered and the negative induced angle and camber indicated in figure 5 (c) are not materially decreased by a decrease in ground distance.

For sweptback wings most of the effects just described would probably remain the same. With regard to the spanwise distribution of loading, however, calculations made as a part of the present investigation have indicated that, when the effect of the swept bound vortices is included with the effect indicated in figure 5 (a) (calculated in ref. 1), the induced upwash distribution should tend to concentrate the
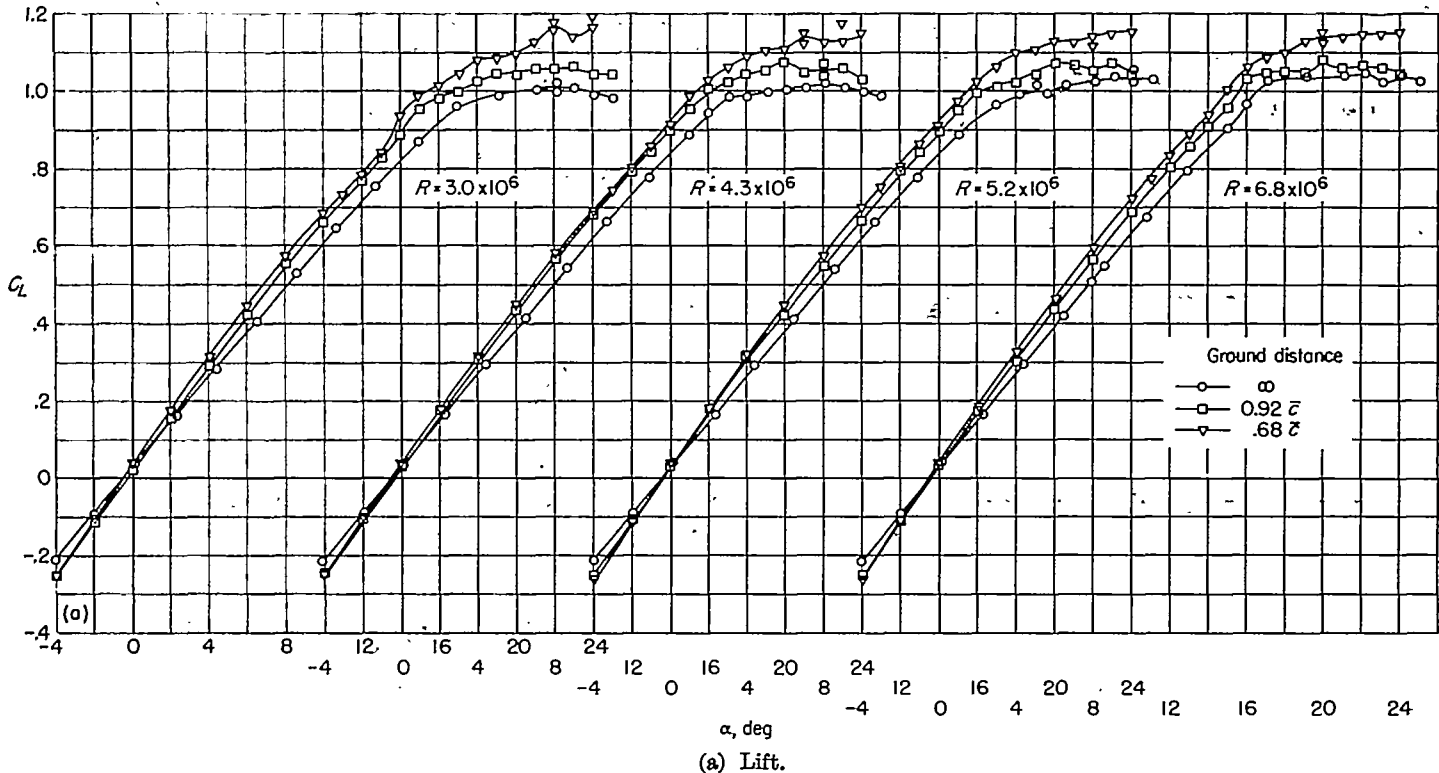
(a) Lift.

FIGURE 6.—Effect of ground on the aerodynamic characteristics of a 42° sweptback wing for various Reynolds numbers.   Flaps neutral.

loading near the tips instead of near the center. This effect, combined with the fact that the tip sections of a sweptback wing are much closer to the ground than the root sections, would be expected to result in a noticeable outboard shift in load. The tip stall usually associated with sweptback wings might be increased in severity by such an outboard shift in load.

RESULTS AND DISCUSSION

The lift, drag, and pitching-moment data are presented in figures 6 and 7. The stalling characteristics are presented in figures 8 and 9.

The greater part of the present discussion is for data obtained at a Reynolds number of 6.8×10^6.

LIFT-CURVE SLOPE

The slope of the lift curve near $C_L=0$, for the wing with flaps both neutral and deflected 60°, increased as the distance to the ground decreased (figs. 6 (a) and 7 (a)). The increase is, in general, comparable to the increase obtained for an unswept wing with flaps neutral (ref. 4). The data do not indicate a shift in angle of zero lift. Such a shift is indicated by the theory and test data for an unswept wing presented in reference 6. No such shift, however, was indicated by the unswept-wing data of reference 4. The reduction in lift-curve slope attributable to ground interference in the high angle-of-attack range was much more severe for the flaps-deflected configuration (fig. 7 (a)) than for the flaps-neutral configuration (fig. 6 (a)).

MAXIMUM LIFT

The data of figure 6 (a) for the wing with flaps neutral show an increasing maximum lift coefficient at the ground

(b) Drag.
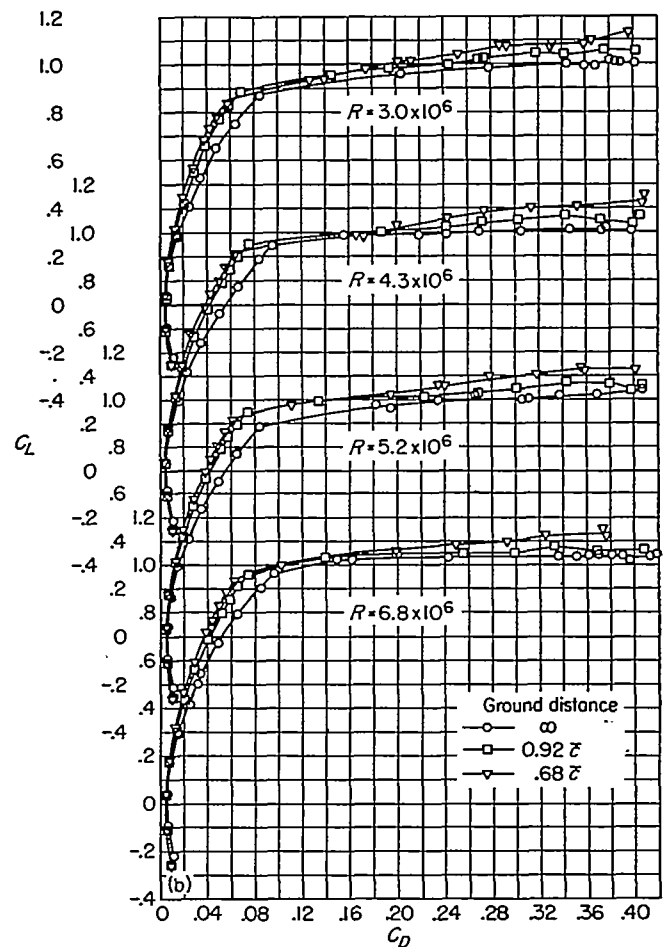
FIGURE 6.—Continued.
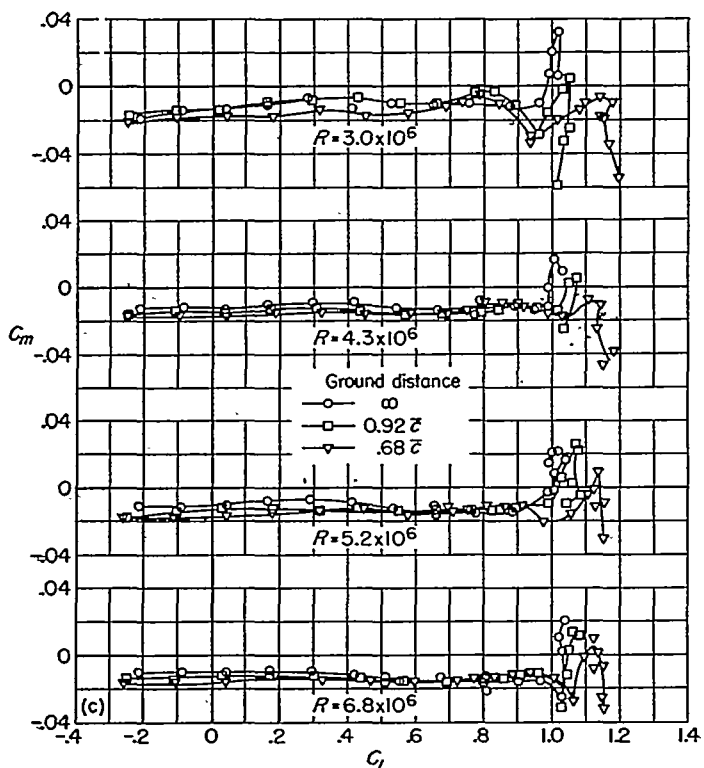
(c) Pitching moment.

FIGURE 6.—Concluded.

distances of the present tests (less than $1.0\bar{c}$). The data of the present tests do not extend to sufficiently high ground distances to show whether a sweptback wing will sustain a loss in maximum lift when first entering the presence of the ground. Both the magnitude of the increase in maximum lift and the magnitude of the ground distances at which the increase in lift is obtained appear to be greater than the magnitudes obtained for unswept wings (refs. 4 and 6). It should be remembered, however, that the points of reference used to determine the ground distances for a sweptback wing and an unswept wing are not directly comparable.

The data for the sweptback wing with flaps deflected (fig. 7 (a)) show an appreciable loss in maximum lift at the same gound distances at which increases in maximum lift were obtained for the flaps-neutral configuration (fig. 6 (a)). The decrease in maximum lift at small ground distances is in general agreement with the results obtained on unswept wings with flaps deflected (ref. 4).

DRAG

A reduction in drag (figs. 6 (b) and 7 (b)) was obtained when both model configurations were tested in the presence of the ground board. Throughout the comparable lift range the model with flaps deflected encountered slightly larger decreases in drag than were encountered with the flaps-retracted configuration. The reductions in drag are, in general, comparable with the reductions obtained for unswept wings (ref. 4).

α, deg
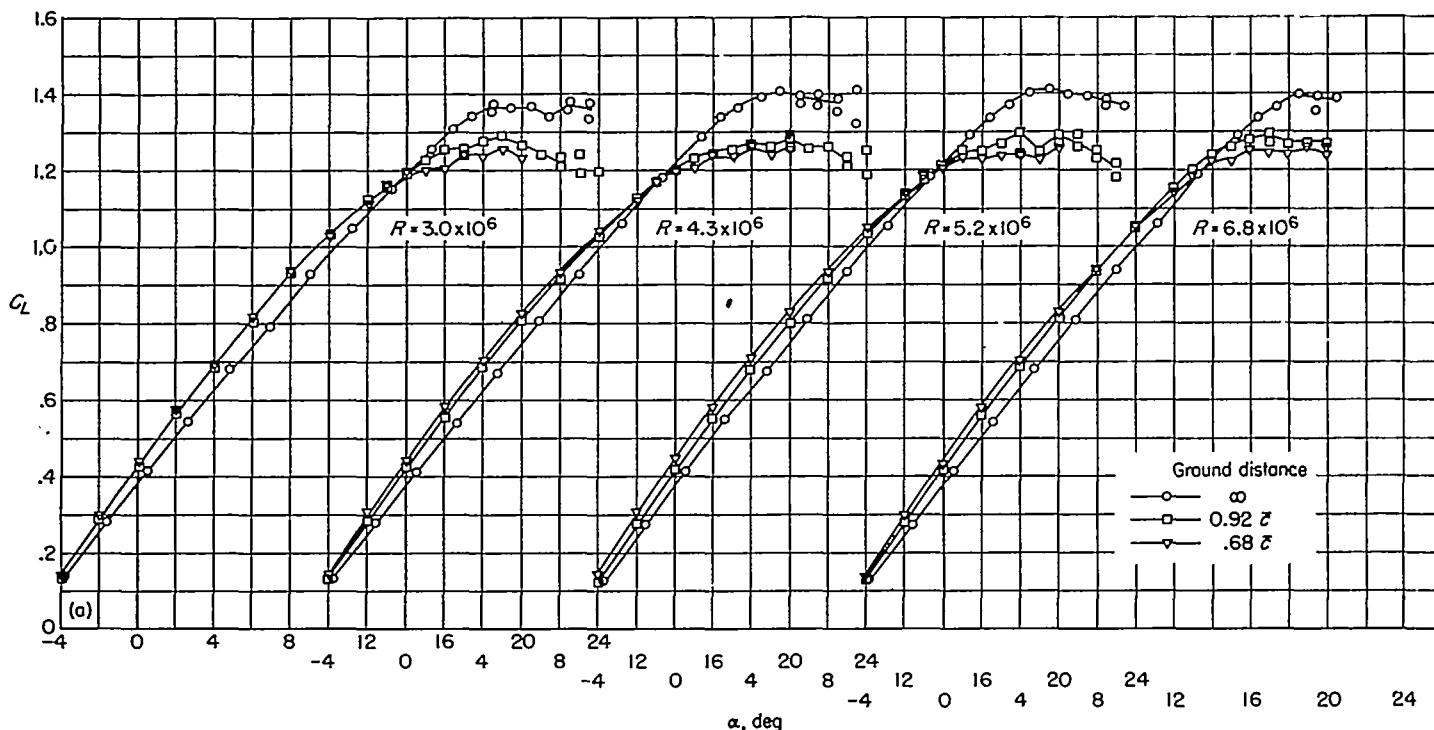
(a) Lift.

FIGURE 7.—Effect of ground on the aerodynamic characteristics of a 42° sweptback wing for various Reynolds numbers. Flaps deflected 60°.
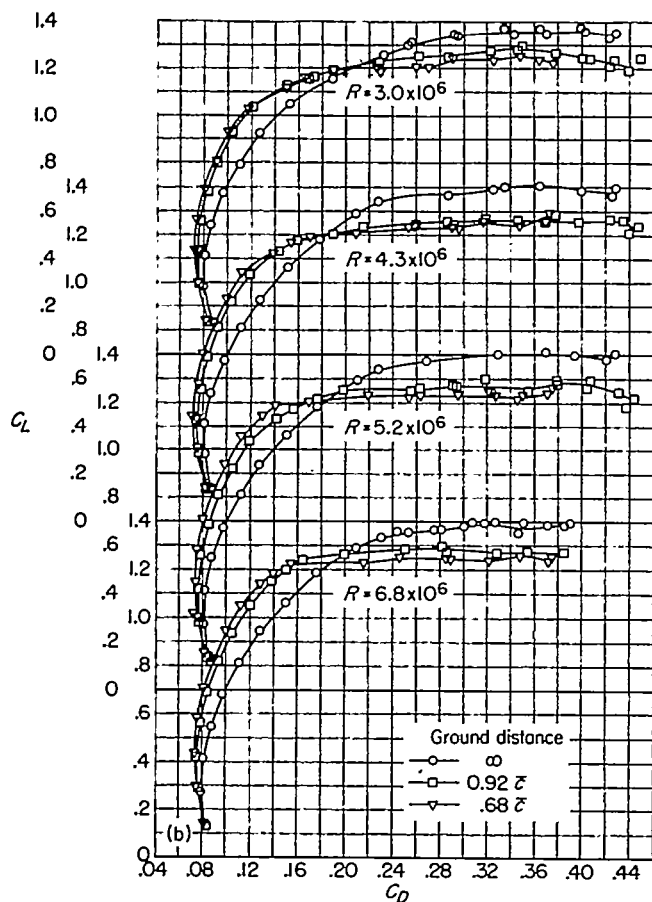
(b) Drag.

FIGURE 7.—Continued.

(c) Pitching moment.

FIGURE 7.—Concluded.

STALLING PATTERNS

The results of the visual stall observations (figs. 8 and 9) show that, for the configuration with flaps deflected, the presence of the ground precipitated a stall on the upper surface of the wing at a slightly lower angle of attack. Stall studies with the ground board out are not available for the wing with flaps neutral. The stall studies indicate that, in general, the origin and progression of the stall are little affected by the presence of the ground.

PITCHING MOMENT

The presence of the ground did not materially affect the longitudinal stability at the stall for either model configuration of the sweptback wing. The wing with flaps neutral remained unstable (fig. 6(c)) at the stall and the wing with flaps deflected remained stable (fig. 7(c)). At the lowest ground distance ($0.68\bar{c}$), a noticeable destabilizing change in pitching-moment slope in the lift-coefficient range just prior to stall was obtained for the flaps-deflected configuration. These effects are similar to those reported for an unswept wing (ref. 4).

It appears from the present data that, at the ground distances of the present tests, the outboard shift in load that might be expected with a sweptback wing is effectively counterbalanced by the increase in effective camber and by a reduction in adverse pressure gradients at the tip sections. The net result is that the origin and progression of the stall are little affected by the presence of the ground and hence the stability at the stall is not changed. The possibility of severe tip stalling and accompanying instability at the stall for the sweptback wing at ground distances greater than those of the present tests could not be ascertained and remains a problem to be investigated.

SCALE EFFECTS

For the configuration with flaps neutral, there appears to be some scale effect on the lift in the high-lift and stalling region. Because of this effect, the stabilizing change in pitching-moment slope obtained at a lift coefficient of 0.8 for a Reynolds number of 3.0×10^6 is delayed to a lift coefficient of approximately 1.0 at a Reynolds number of 6.8×10^6 (fig. 6(c)). The slight improvement in the stability at the stall, which is obtained for the smallest ground distance and a Reynolds number of 3.0×10^6, is not obtained at a Reynolds number of 6.8×10^6. The effects of Reynolds number on the lift, drag, and pitching moments for the wing with flaps deflected (fig. 7) appear to be small.
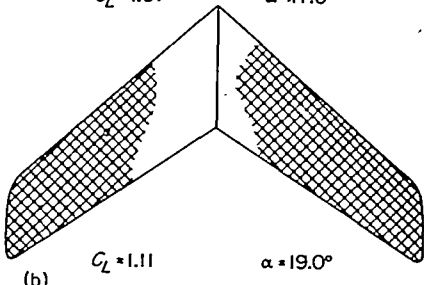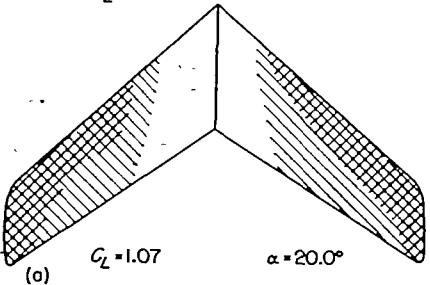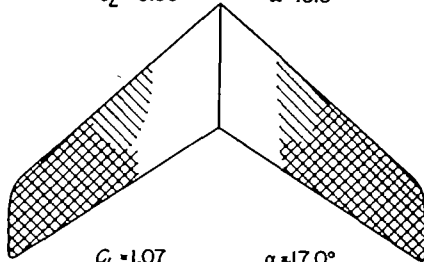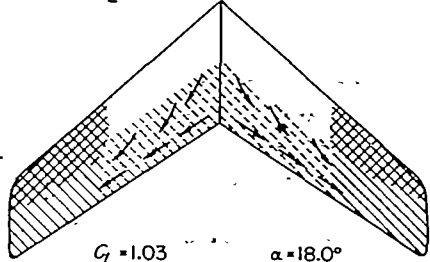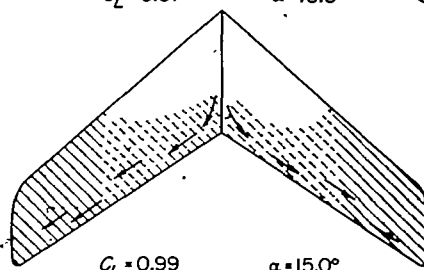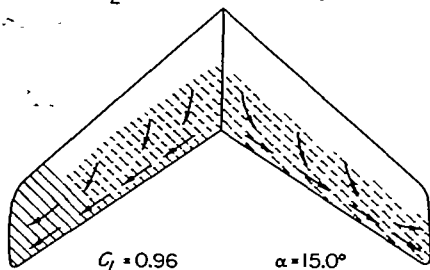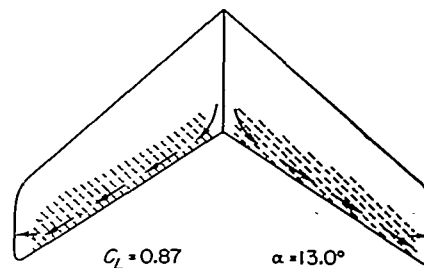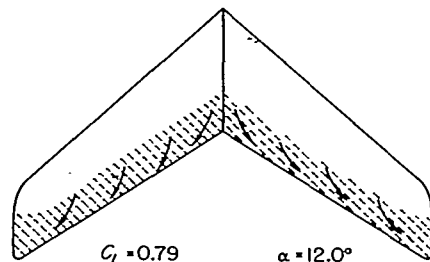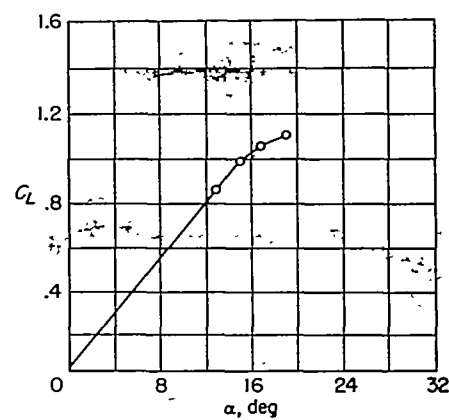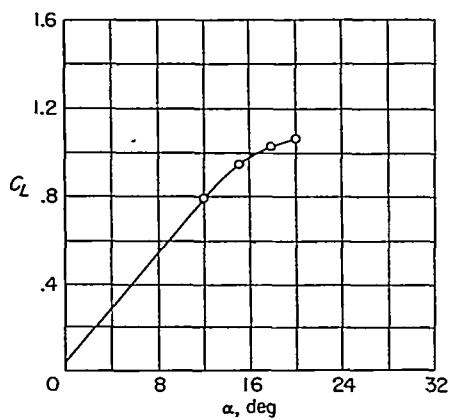
(a) Ground distance, $0.92\bar{c}$.   (b) Ground distance, $0.68\bar{c}$.

FIGURE 8.—Effect of ground on the stalling characteristics of a 42° sweptback wing. Renolds number=6.8×10⁶; flaps neutral.

(a) Ground distance, ∞.
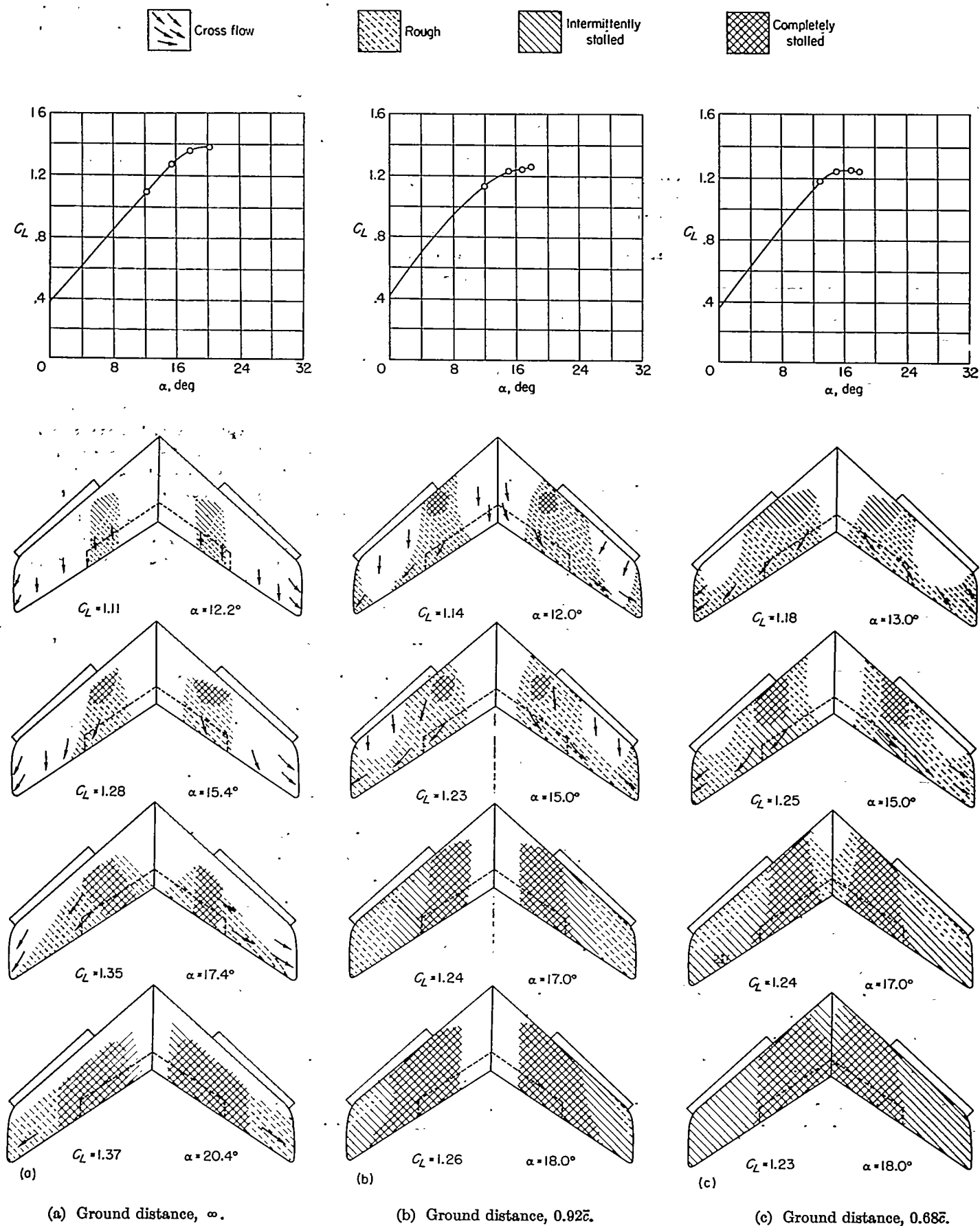
(b) Ground distance, 0.92c̄.

(c) Ground distance, 0.68c̄.

FIGURE 9.—Effect of ground on the stalling characteristics of a 42° sweptback wing. Reynolds number=6.8×10⁶; flaps deflected 60°

AIRSTREAM SURVEYS

The airstream-survey data have been cross-plotted to obtain contour charts of dynamic-pressure ratios, downwash, and sidewash in vertical planes $2.0\bar{c}$ and $2.8\bar{c}$ behind the $0.25\bar{c}$. The charts are presented in figures 10 to 21 and, for reference, the data presented are summarized in table I.

TABLE I

LIST OF DOWNWASH ANGLE, SIDEWASH ANGLE, AND DYNAMIC-PRESSURE-RATIO CONTOUR CHARTS PRESENTED

Figure	Flaps	Plane of survey	Ground distance	Angle of attack and lift coefficient
10	Neutral	$2.0\bar{c}$	∞	(a) $\alpha=7.9°$; $C_L=0.51$. (b) $\alpha=13.1°$; $C_L=0.81$. (c) $\alpha=16.0°$; $C_L=0.97$.
14	Neutral	$2.0\bar{c}$	$0.92\bar{c}$	(a) $\alpha=6.7°$; $C_L=0.48$. (b) $\alpha=11.9°$; $C_L=0.80$. (c) $\alpha=14.6°$; $C_L=0.95$.
18	Neutral	$2.0\bar{c}$	$0.68\bar{c}$	(a) $\alpha=6.7°$; $C_L=0.51$. (b) $\alpha=11.9°$; $C_L=0.83$. (c) $\alpha=14.6°$; $C_L=0.98$.
11	Neutral	$2.8\bar{c}$	∞	(a) $\alpha=7.9°$; $C_L=0.51$. (b) $\alpha=13.1°$; $C_L=0.81$. (c) $\alpha=16.0°$; $C_L=0.97$.
15	Neutral	$2.8\bar{c}$	$0.92\bar{c}$	(a) $\alpha=6.7°$; $C_L=0.48$. (b) $\alpha=11.9°$; $C_L=0.80$. (c) $\alpha=14.6°$; $C_L=0.95$.
19	Neutral	$2.8\bar{c}$	$0.68\bar{c}$	(a) $\alpha=6.7°$; $C_L=0.51$. (b) $\alpha=11.9°$; $C_L=0.83$. (c) $\alpha=14.6°$; $C_L=0.98$.
12	Deflected	$2.0\bar{c}$	∞	(a) $\alpha=3.6°$; $C_L=0.61$. (b) $\alpha=8.5°$; $C_L=0.91$. (c) $\alpha=13.5°$; $C_L=1.20$. (d) $\alpha=16.8°$; $C_L=1.35$.
16	Deflected	$2.0\bar{c}$	$0.92\bar{c}$	(a) $\alpha=2.4°$; $C_L=0.59$. (b) $\alpha=7.1°$; $C_L=0.89$. (c) $\alpha=9.7°$; $C_L=1.04$. (d) $\alpha=12.5°$; $C_L=1.18$.
20	Deflected	$2.0\bar{c}$	$0.68\bar{c}$	(a) $\alpha=2.4°$; $C_L=0.62$. (b) $\alpha=7.3°$; $C_L=0.91$. (c) $\alpha=10.0°$; $C_L=1.00$. (d) $\alpha=13.6°$; $C_L=1.20$.
13	Deflected	$2.8\bar{c}$	∞	(a) $\alpha=3.6°$; $C_L=0.61$. (b) $\alpha=8.5°$; $C_L=0.91$. (c) $\alpha=13.5°$; $C_L=1.20$. (d) $\alpha=16.8°$; $C_L=1.35$.
17	Deflected	$2.8\bar{c}$	$0.92\bar{c}$	(a) $\alpha=2.4°$; $C_L=0.59$. (b) $\alpha=7.1°$; $C_L=0.89$. (c) $\alpha=9.7°$; $C_L=1.04$. (d) $\alpha=12.5°$; $C_L=1.18$.
21	Deflected	$2.8\bar{c}$	$0.68\bar{c}$	(a) $\alpha=2.4°$; $C_L=0.62$. (b) $\alpha=7.3°$; $C_L=0.91$. (c) $\alpha=10.0°$; $C_L=1.00$. (d) $\alpha=13.6°$; $C_L=1.20$.

The effect of the model support struts on the flow at the survey planes was small even though tuft studies indicated that flow separation on the struts occurred at moderate angles of attack with the ground board present. The regions affected are easily discernible on the contours of dynamic-pressure ratio for the plain wing as areas of reduced dynamic-pressure ratio in the vicinity of $0.50\frac{b}{2}$. When the flaps were deflected the wing and strut wakes intermixed and hence the strut wake lost its identity.
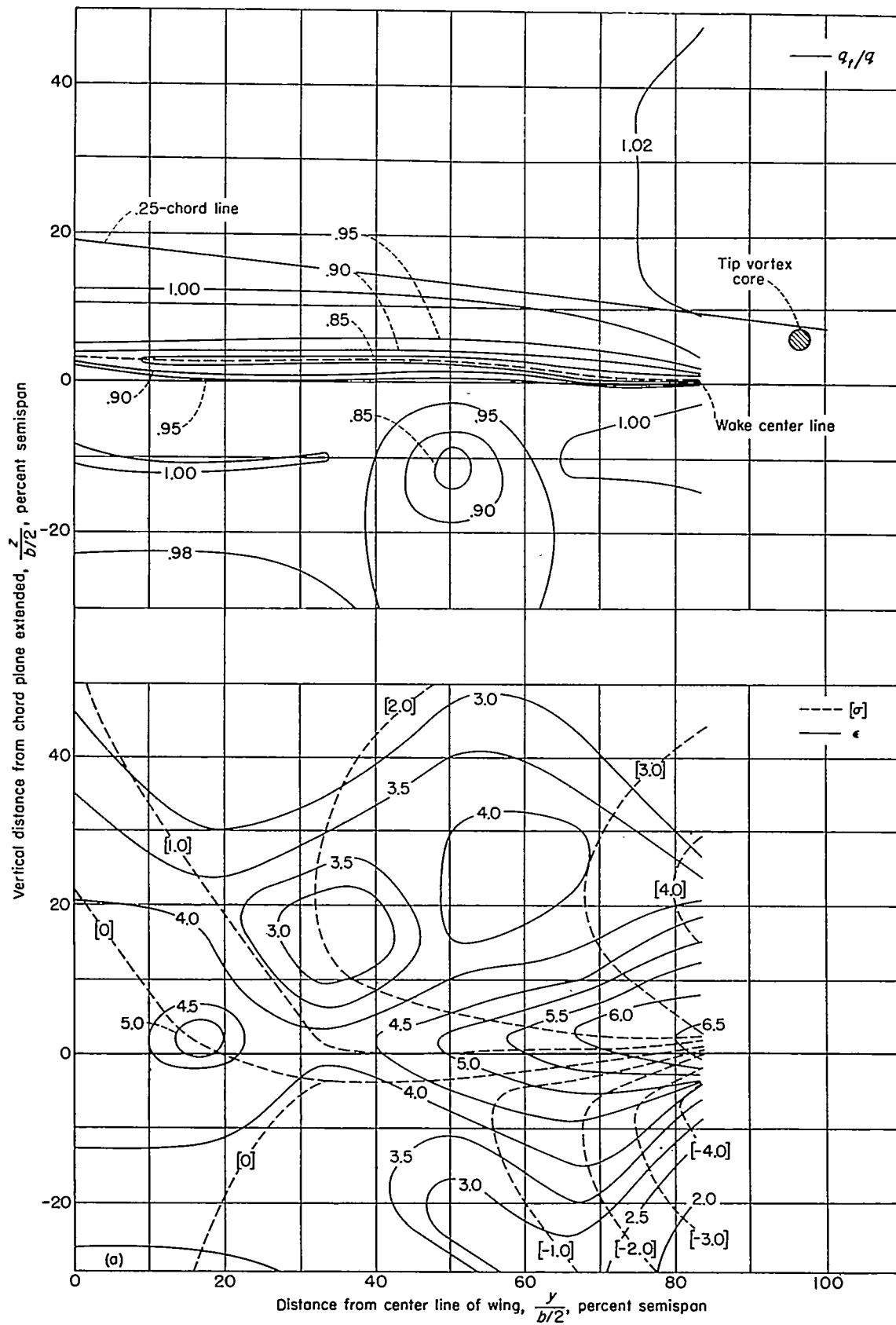
The contours of dynamic-pressure ratio, downwash, and sidewash have been shown with reference to the chord plane extended. The intersection of the chord plane extended with the plane of survey has been arbitrarily selected as the reference line and any horizontal tail will remain a constant distance from this line as the angle of attack of the wing is changed. In order to indicate the position of the flow field of the wing with respect to the wing, the 0.25-chord line of the wing has been projected onto the plane of survey in the contours of dynamic-pressure ratio.

The qualitative results of the airstream survey for the ground-out condition are, in general, consistent with the results which would be expected from a consideration of the spanwise lift distribution associated with sweptback wings. The spanwise lift distribution for the wing with flaps neutral, computed by the empirical method presented in reference 11, indicates that negative vorticity is shed over the inboard sections of the wing, and hence, it should be expected that the maximum downwash would occur outboard of the plane of symmetry. For an unswept wing of the same taper ratio, the lift would increase to the plane of symmetry and it would be here that the maximum downwash is reached. In the present tests, the reduced downwash at the plane of symmetry (figs. 10 and 11) is also due in part to the fact that the distance from the wing to the plane of survey is greatest at the plane of symmetry. The vortex sheet is displaced downward and the magnitude appears to be of the same order as for unswept wings. The wake center line traveled from just above the chord plane extended to a maximum height of $0.17\frac{b}{2}$ at the highest angle of attack ($\alpha=16.0°$) and most rearward survey position ($2.8\bar{c}$).

The airstream surveys behind the wing with flaps deflected $60°$ (figs. 12 and 13) show to some extent the strong effect of the flap tip vortex and secondary effect of the increase in strength of the bound vortex produced inboard by the flap on the flow field. The downwash is increased and the wake is lowered behind the flapped portion of the wing.

The tip vortices, as indicated by the present surveys for the plain wing, are shed and located in approximately the same position as would be expected for a straight tapered wing. In the range of the tests there is very little rolling-in of the vortex, a fact not unreasonable when it is realized that the distance rearward of the geometric tip is much less than the $2.8\bar{c}$ measured from $0.25\bar{c}$.

The presence of the ground for both model configurations caused the usual reduction in downwash and upward displacement of the wake (figs. 14 to 21). Inasmuch as the reflected tip vortex is opposite in direction to the real tip vortex, it would increase the negative values of sidewash (outflow) and decrease the positive values of sidewash (inflow).

(a) $\alpha = 7.9°$; $C_L = 0.51$.

FIGURE 10.—Contours of downwash and sidewash angles in degrees and of dynamic-pressure ratio behind a 42° sweptback wing. Longitudinal plane of survey at $2.0\bar{c}$; flaps neutral; ground distance, ∞.
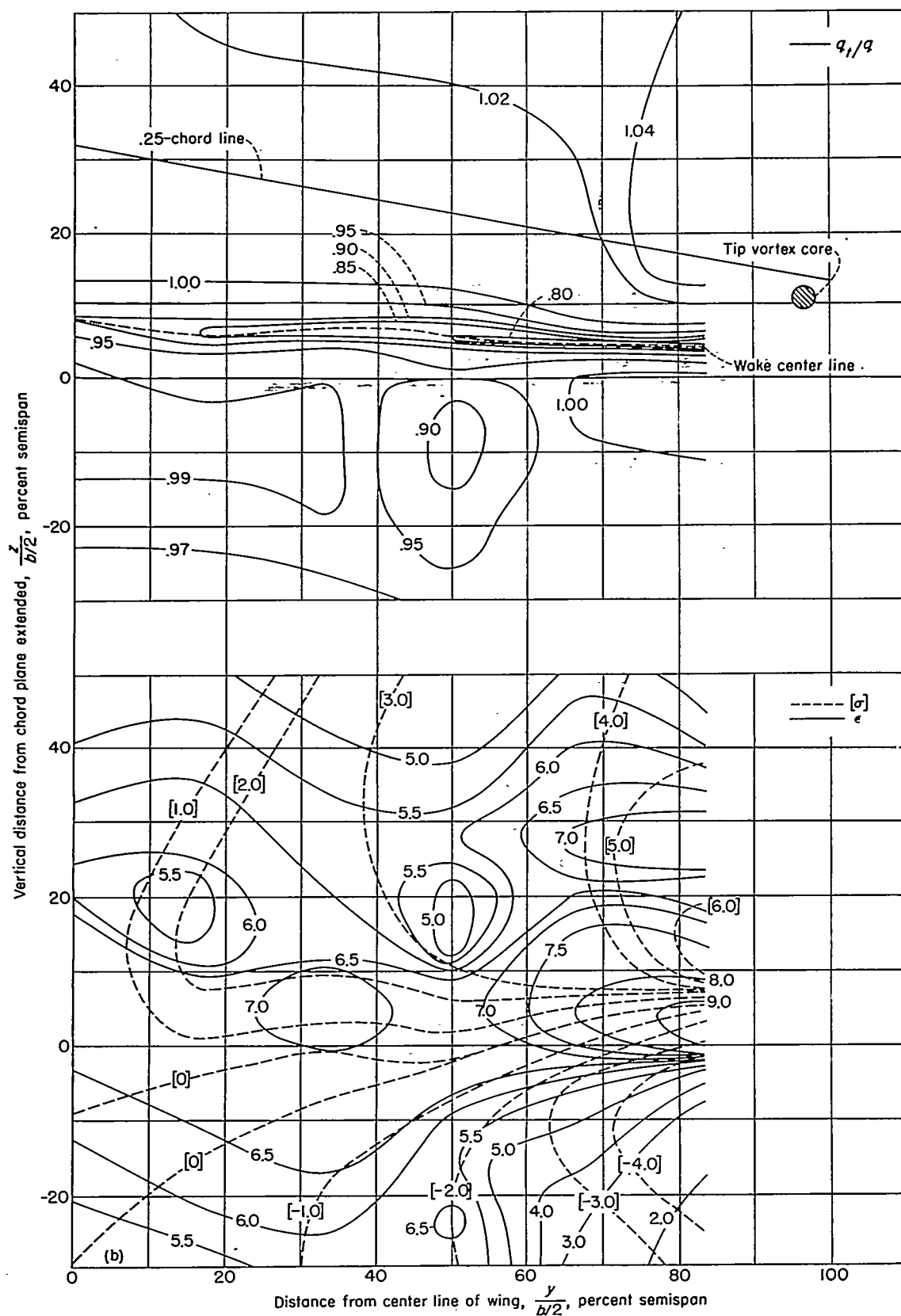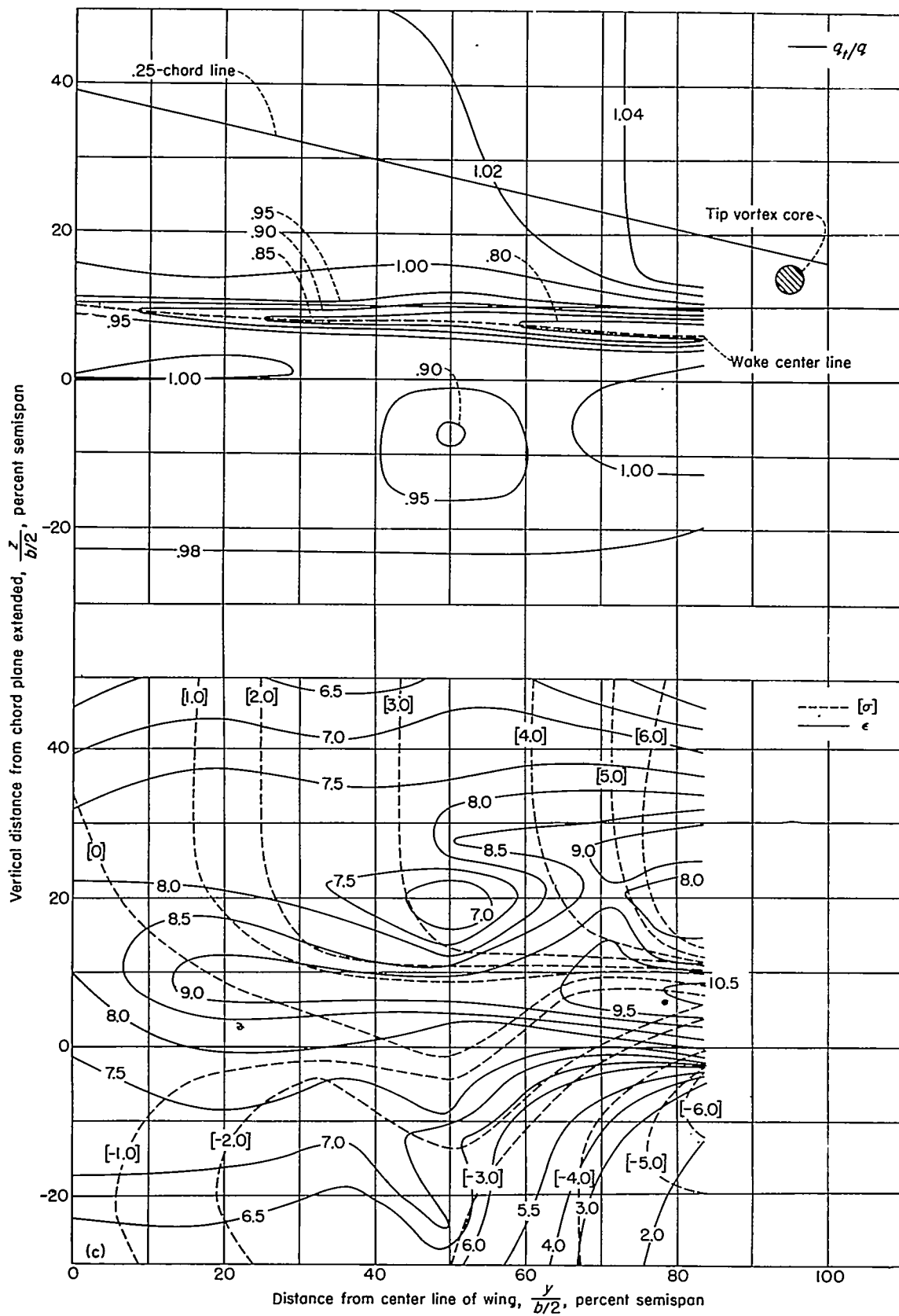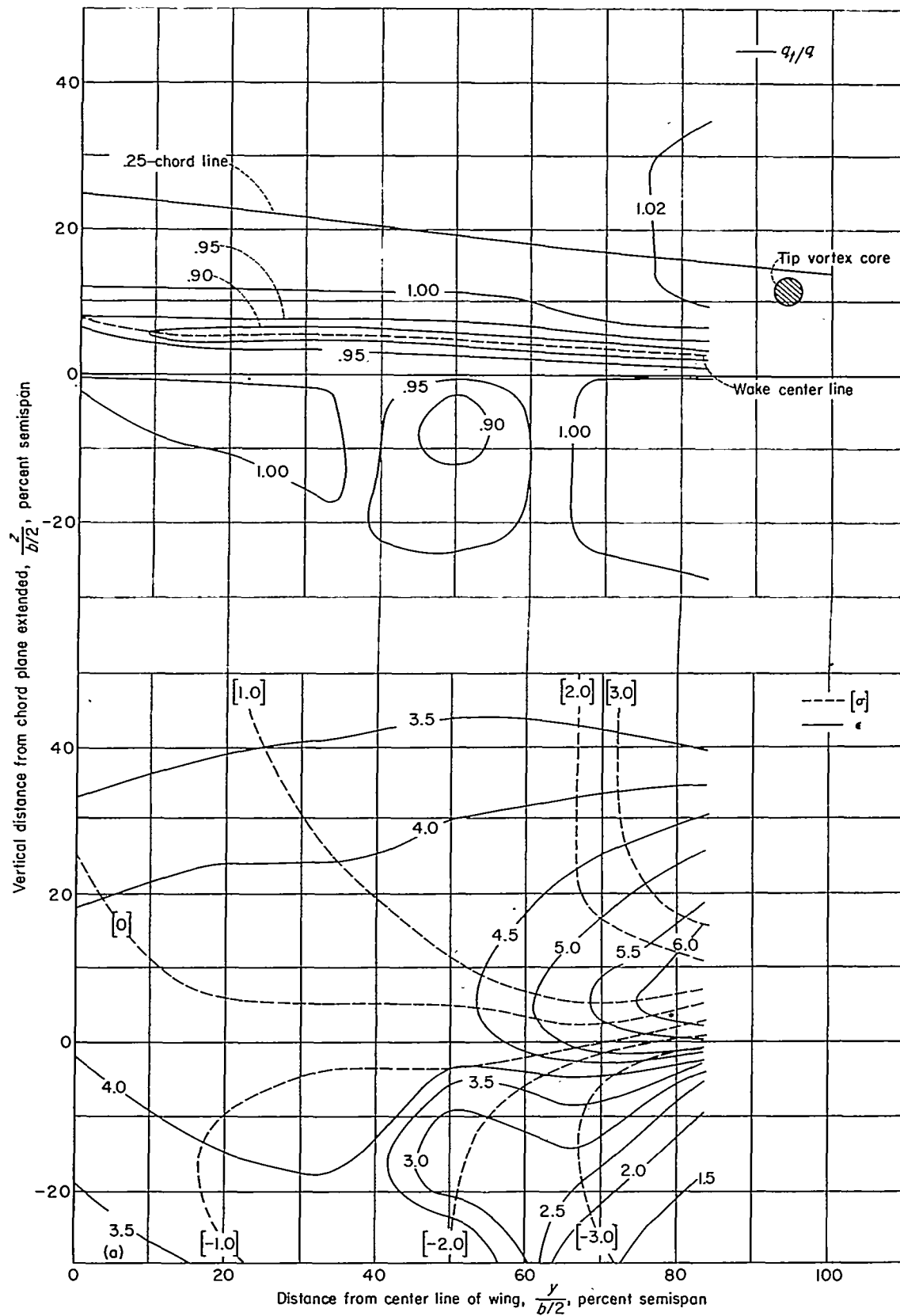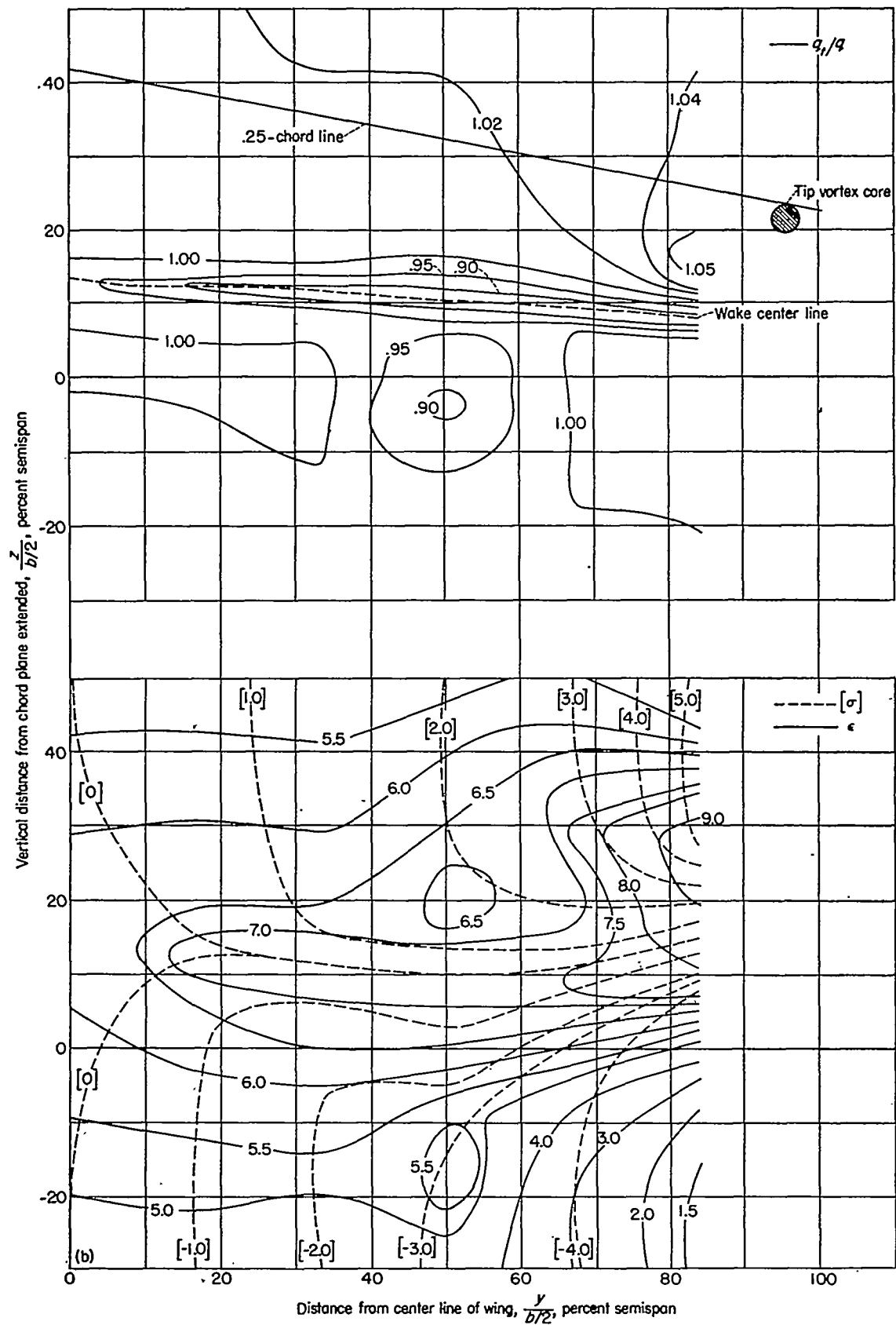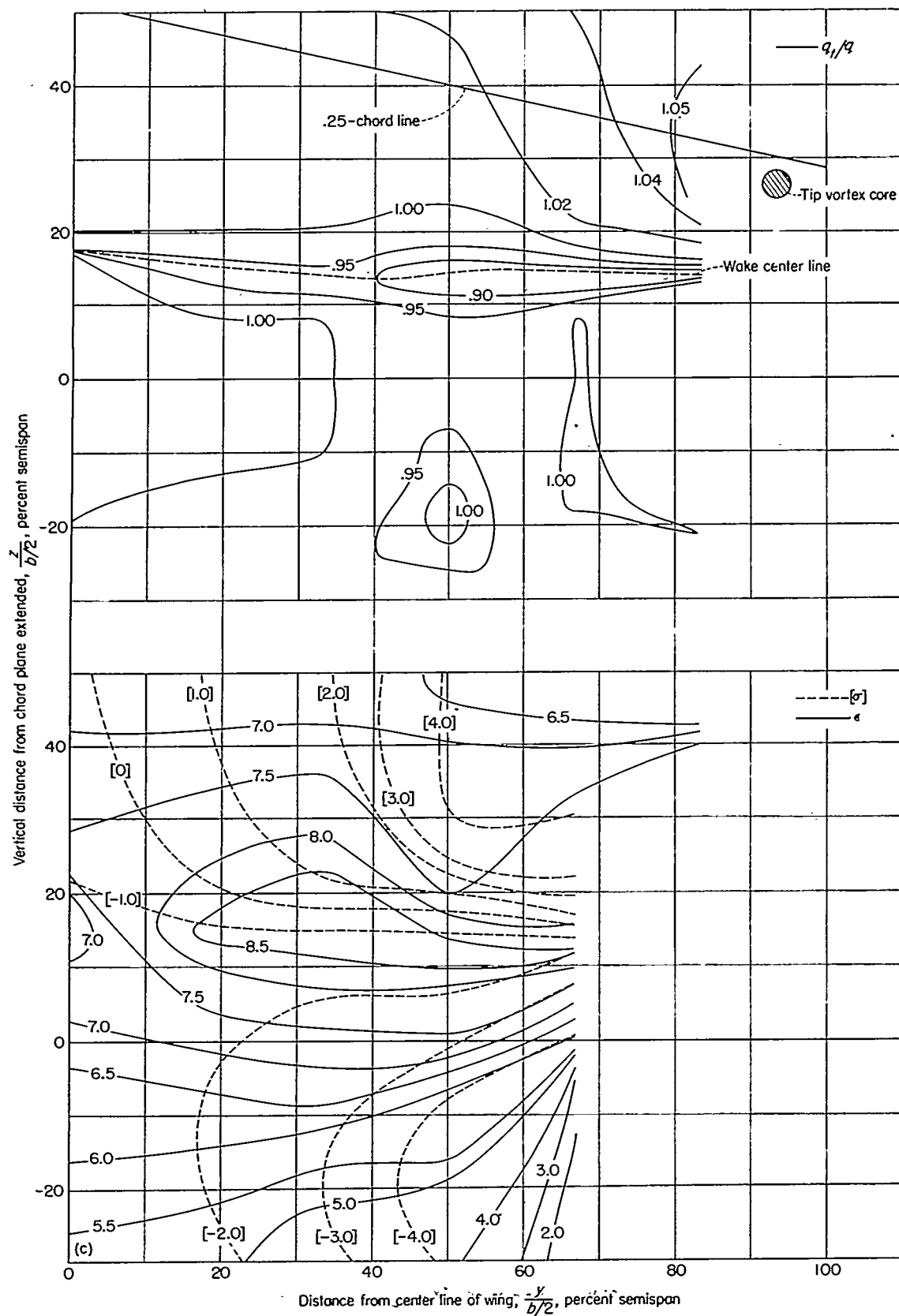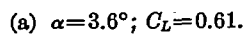
(b) $\alpha=13.1°$; $C_L=0.81$.
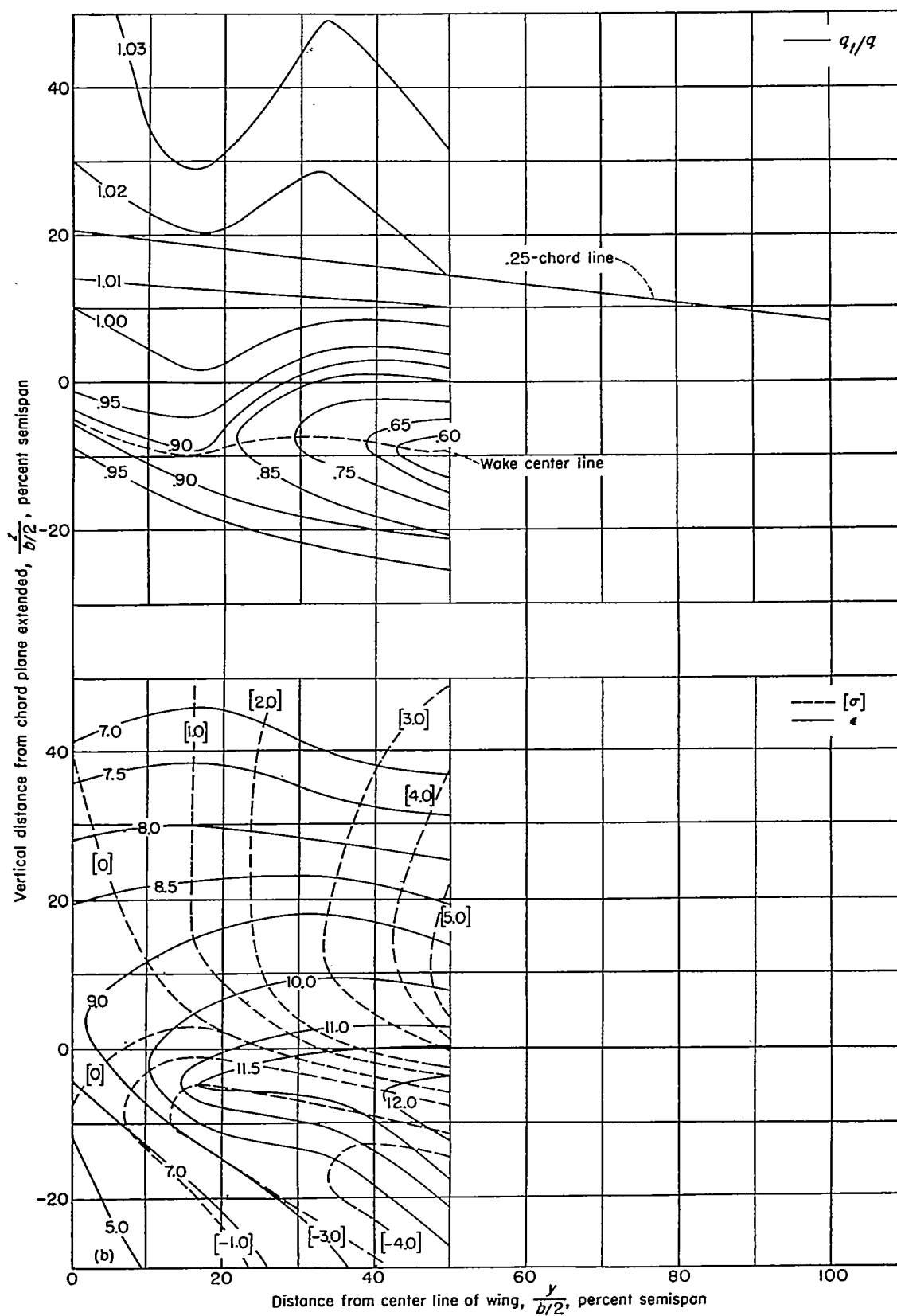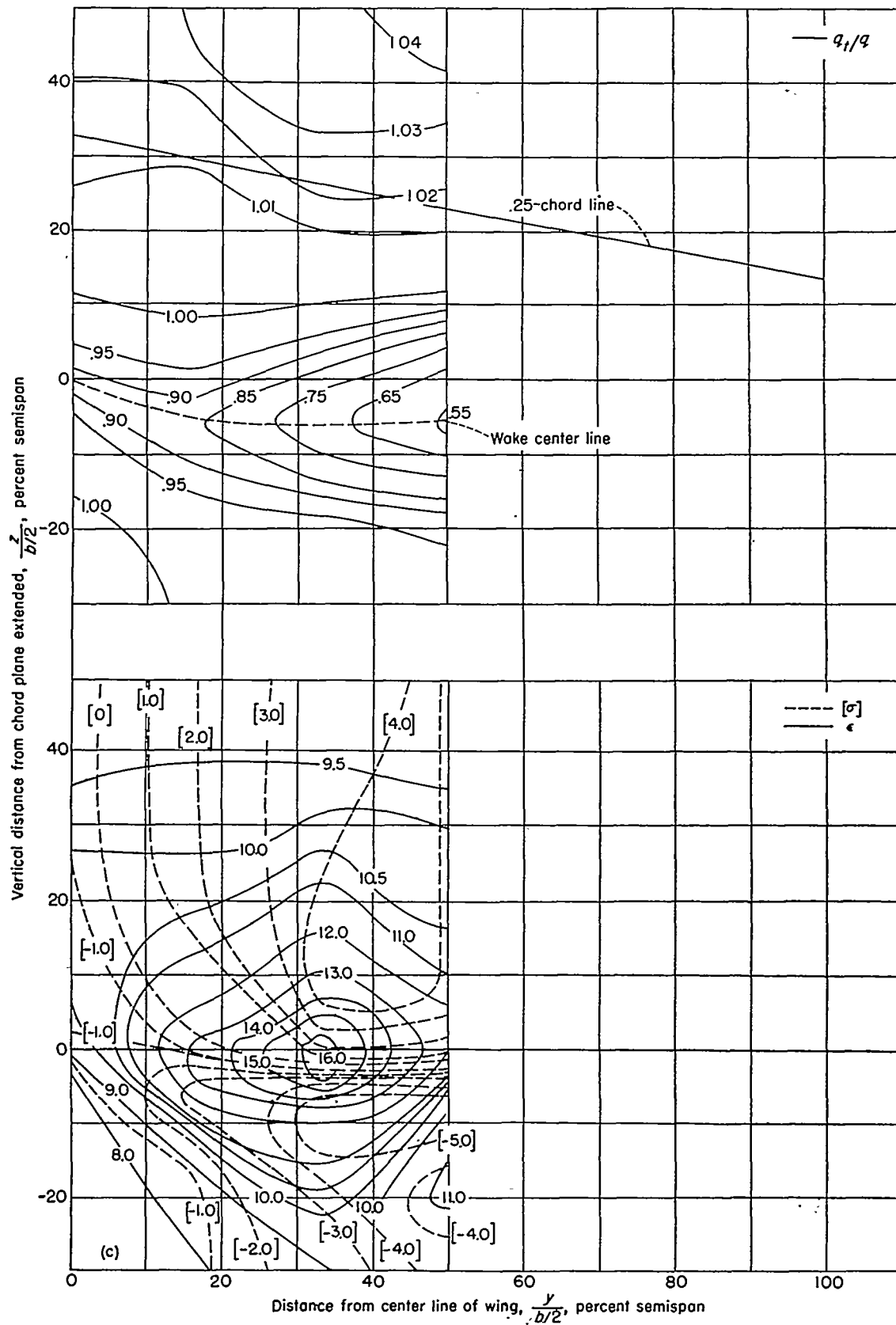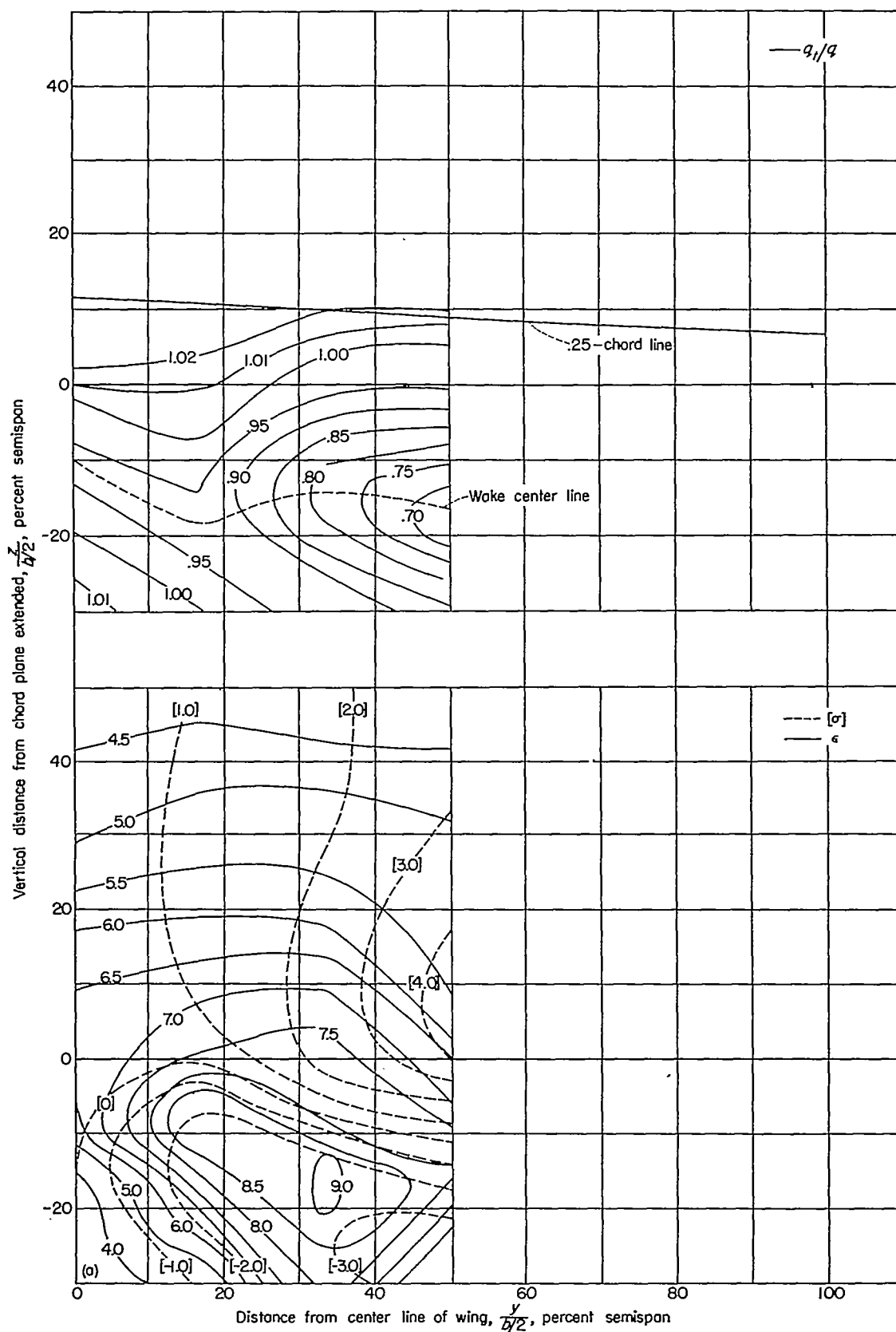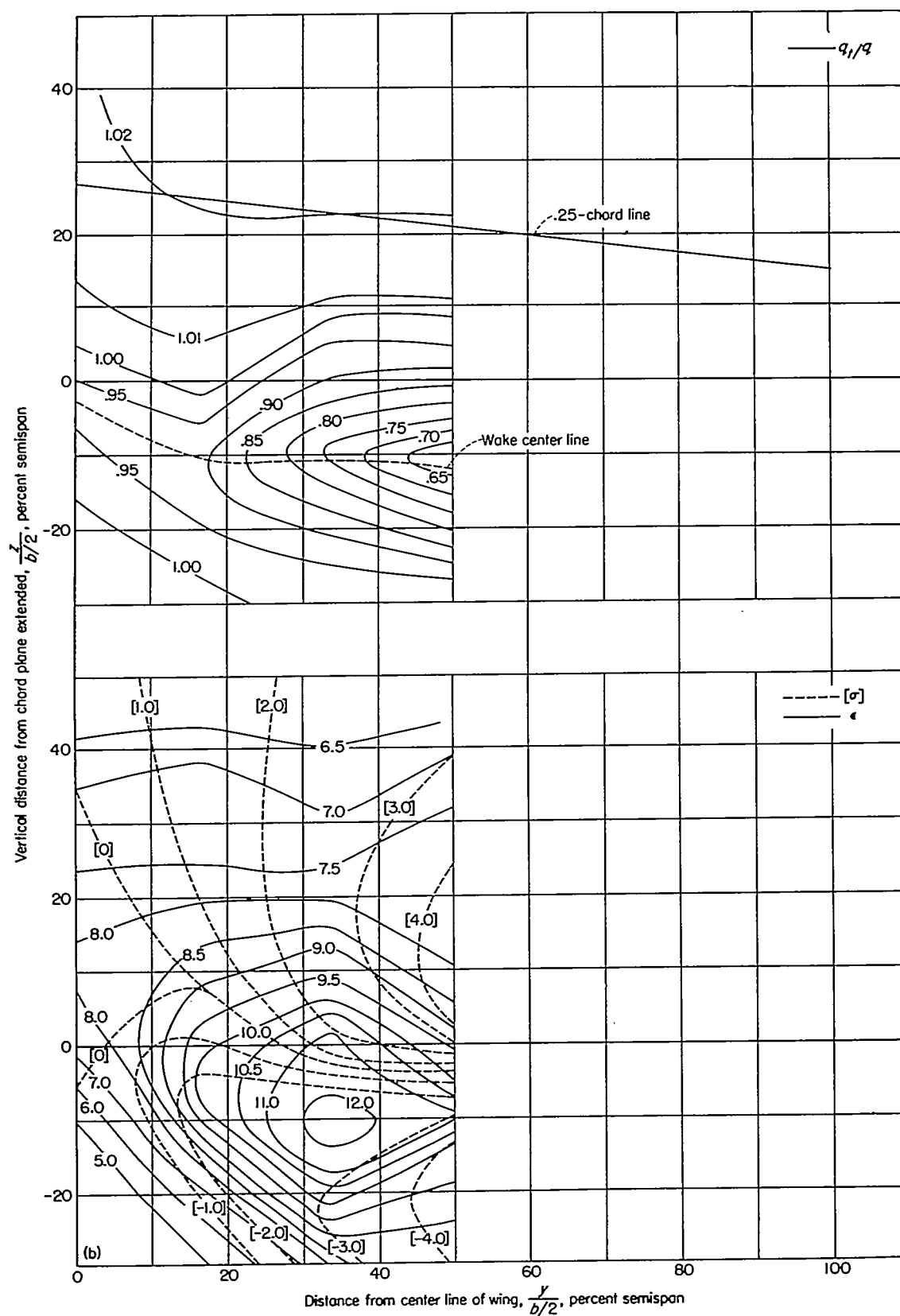
FIGURE 10.—Continued.

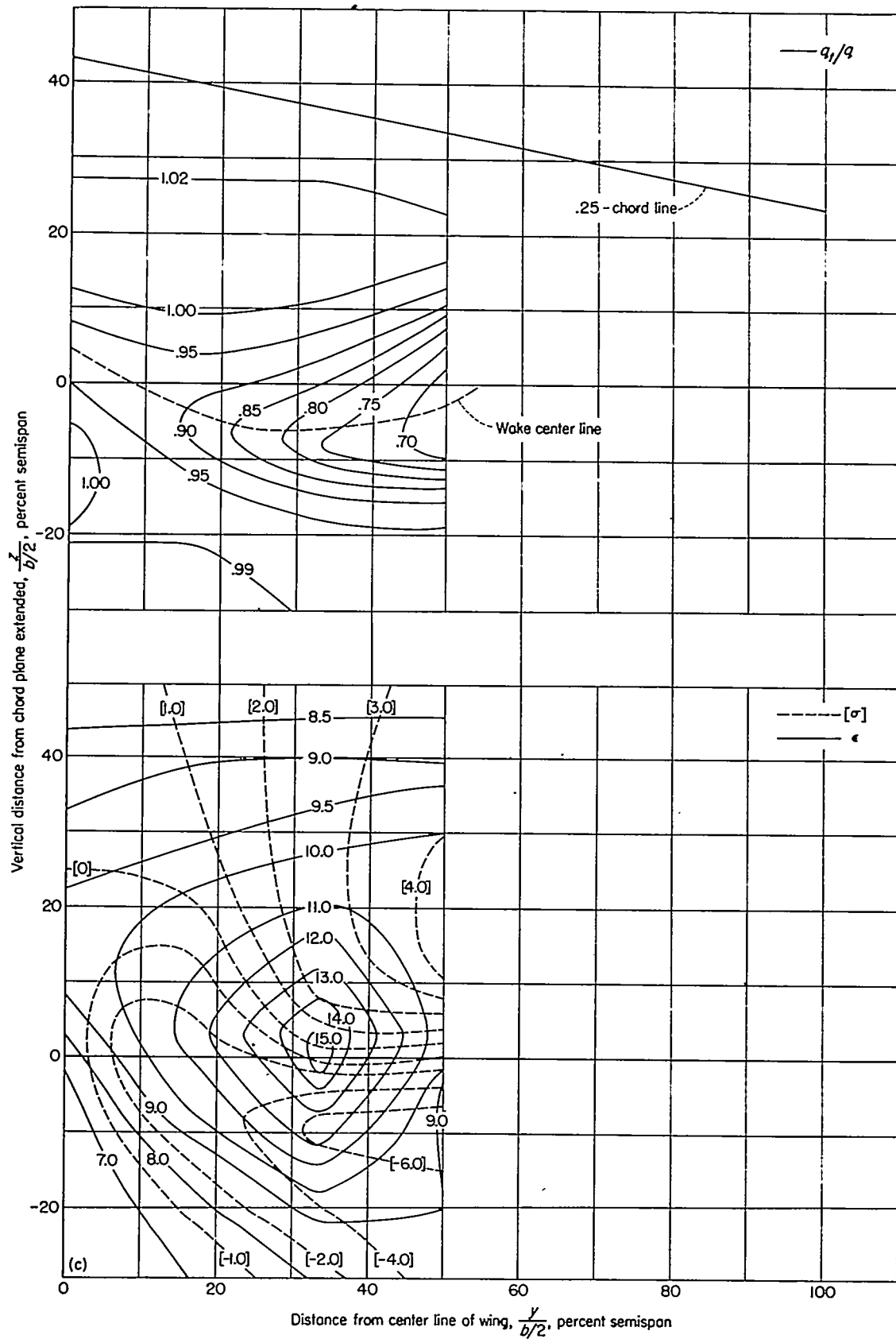(c) α=16.0°; C_L=0.97.

FIGURE 10.—Concluded.

(a) $\alpha=7.9°$; $C_L=0.51$.

FIGURE 11.—Contours of downwash and sidewash angles in degrees and of dynamic-pressure ratio behind a 42° sweptback wing. Longitudinal plane of survey at $2.8\bar{c}$; flaps neutral; ground distance, ∞.

(b) $\alpha = 13.1°$; $C_L = 0.81$.

FIGURE 11.—Continued.

(c) $\alpha = 16.0°$; $C_L = 0.97$.

FIGURE 11.—Concluded.

(a) $\alpha=3.6°$; $C_L=0.61$.

FIGURE 12.—Contours of downwash and sidewash angles in degrees and of dynamic-pressure ratio behind a 42° sweptback wing. Longitudinal plane of survey at 2.0$\bar{c}$; flaps deflected 60°; ground distance, ∞.
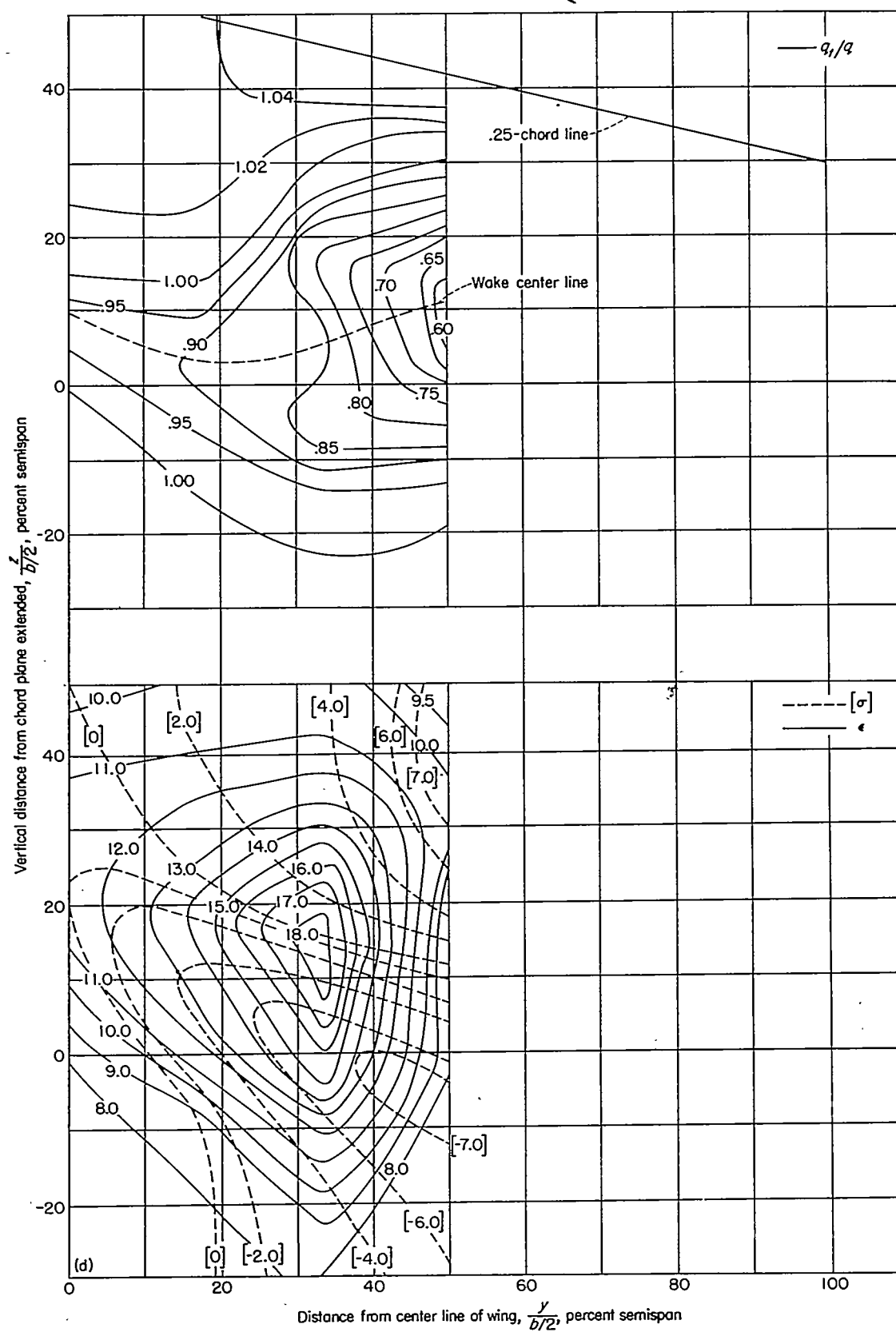
(b) $\alpha=8.5°$; $C_L=0.91$.

FIGURE 12.—Continued.

(c) $\alpha = 13.5°$; $C_L = 1.20$.

FIGURE 12.—Continued.
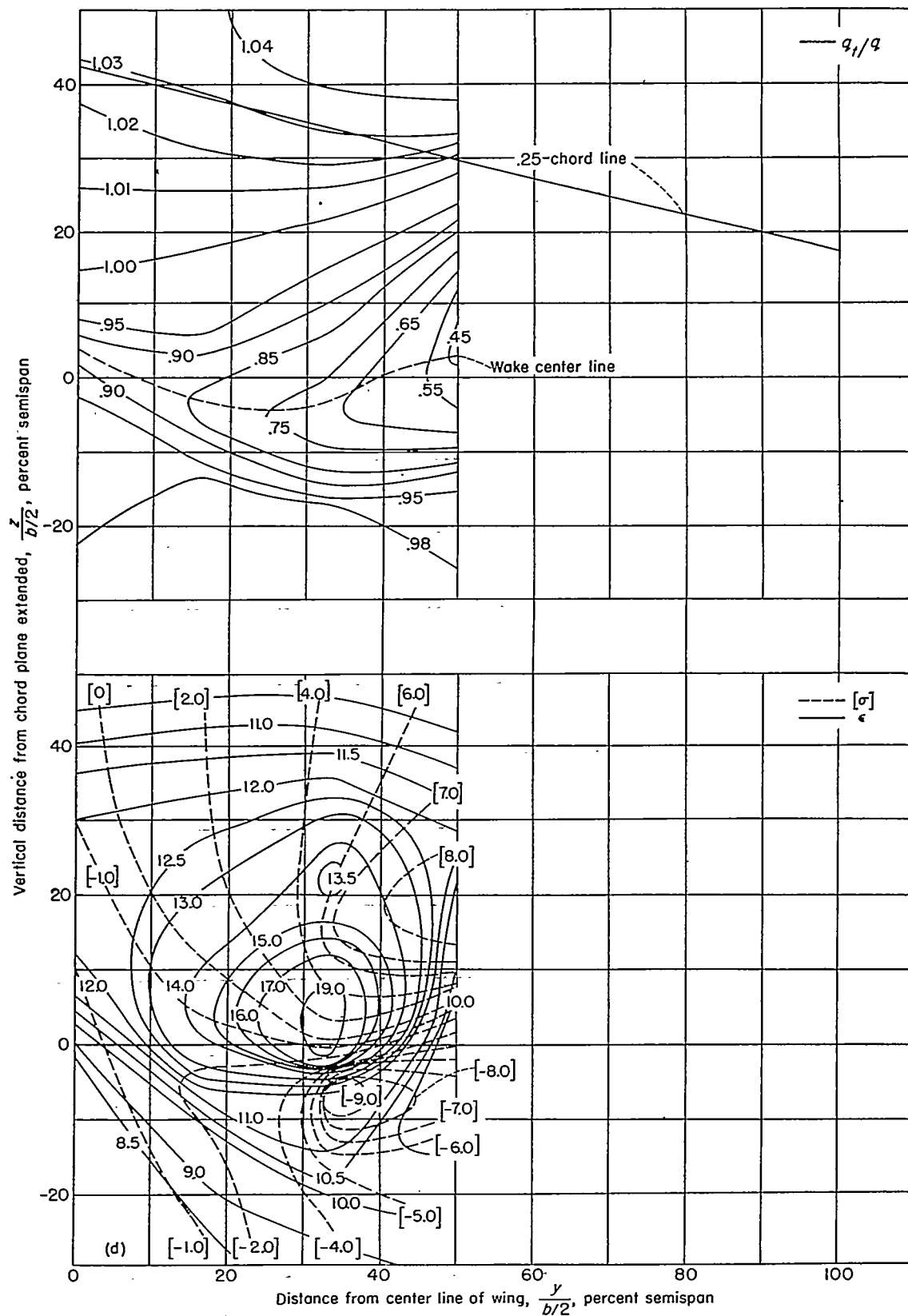
(d) $\alpha=16.8°$; $C_L=1.35$.

FIGURE 12.—Concluded.

(a) $\alpha=3.6°$; $C_L=0.61$.

FIGURE 13.—Contours of downwash and sidewash angles in degrees and of dynamic-pressure ratio behind a 42° sweptback wing. Longitudinal plane of survey at 2.8$\bar{c}$; flaps deflected 60°; ground distance, ∞.

(b) $\alpha=8.5°$; $C_L=0.91$.

FIGURE 13.—Continued.

(c) $\alpha=13.5^\circ$; $C_L=1.20$.

FIGURE 13.—Continued.

(d) $\alpha=16.8°$; $C_L=1.35$.

FIGURE 13.—Concluded.

(a) $\alpha = 6.7°$; $C_L = 0.48$.
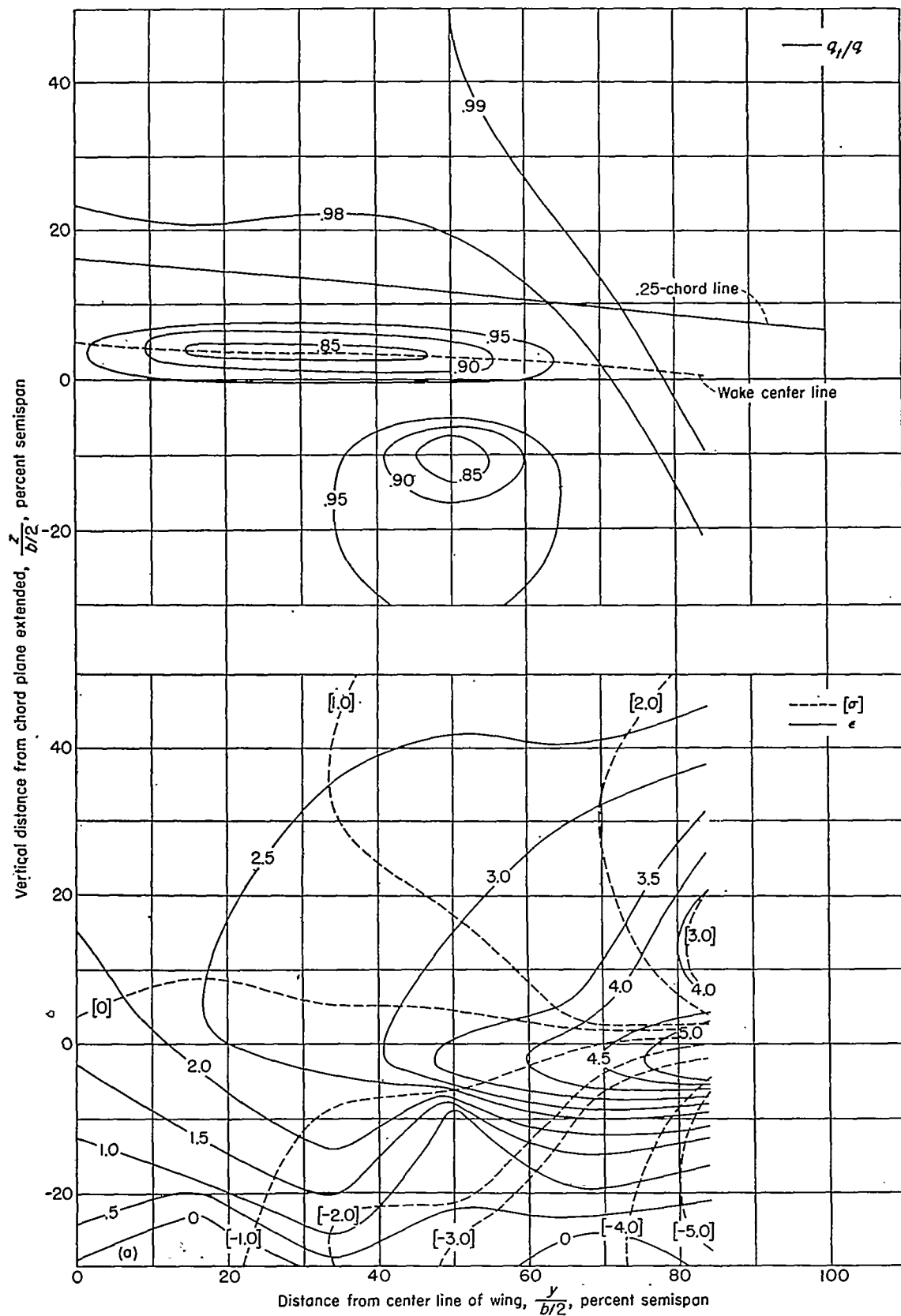
FIGURE 14.—Contours of downwash and sidewash angles in degrees and of dynamic-pressure ratio behind a 42° sweptback wing. Longitudinal plane of survey at $2.0\bar{c}$; flaps neutral; ground distance, $0.92\bar{c}$.
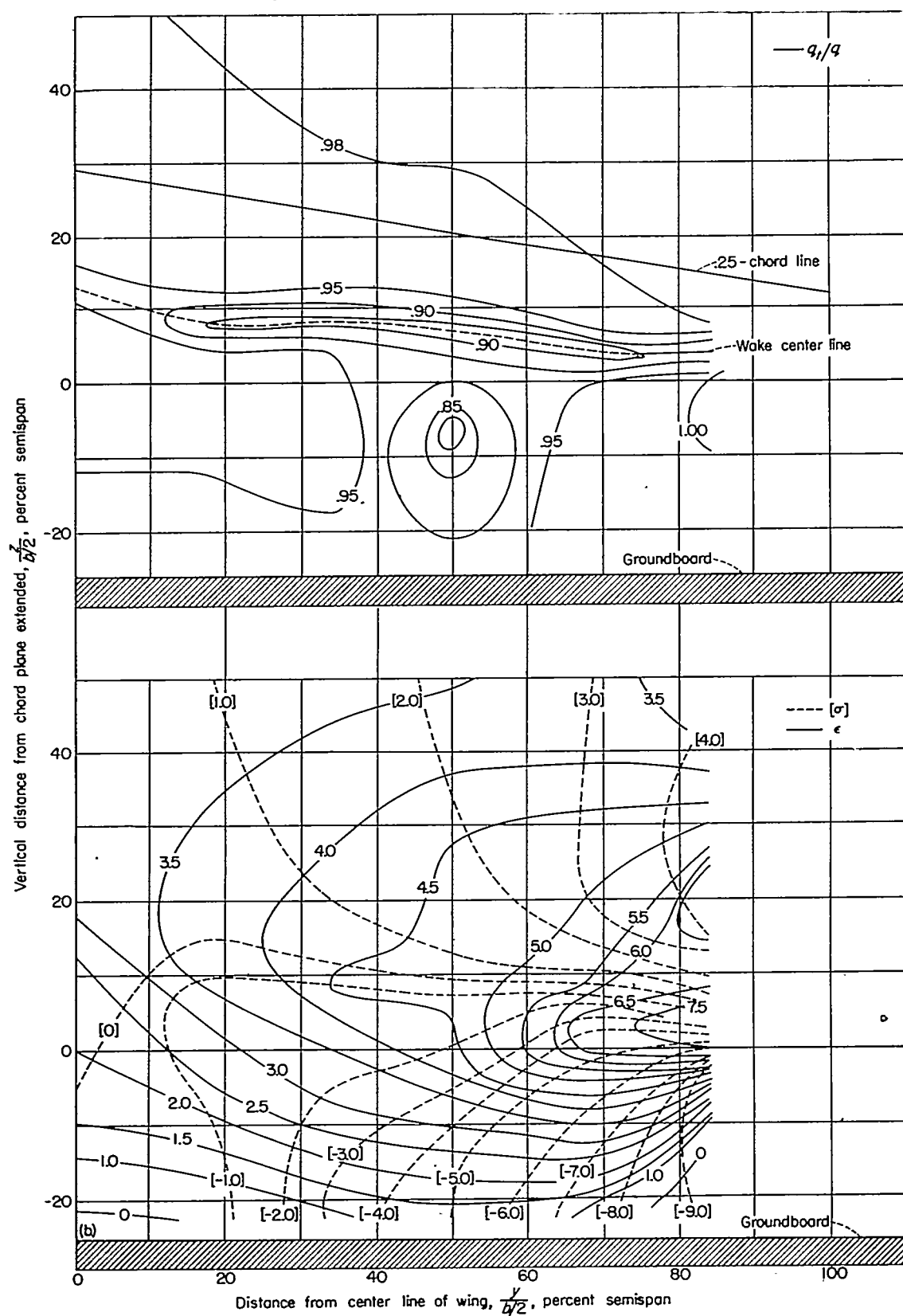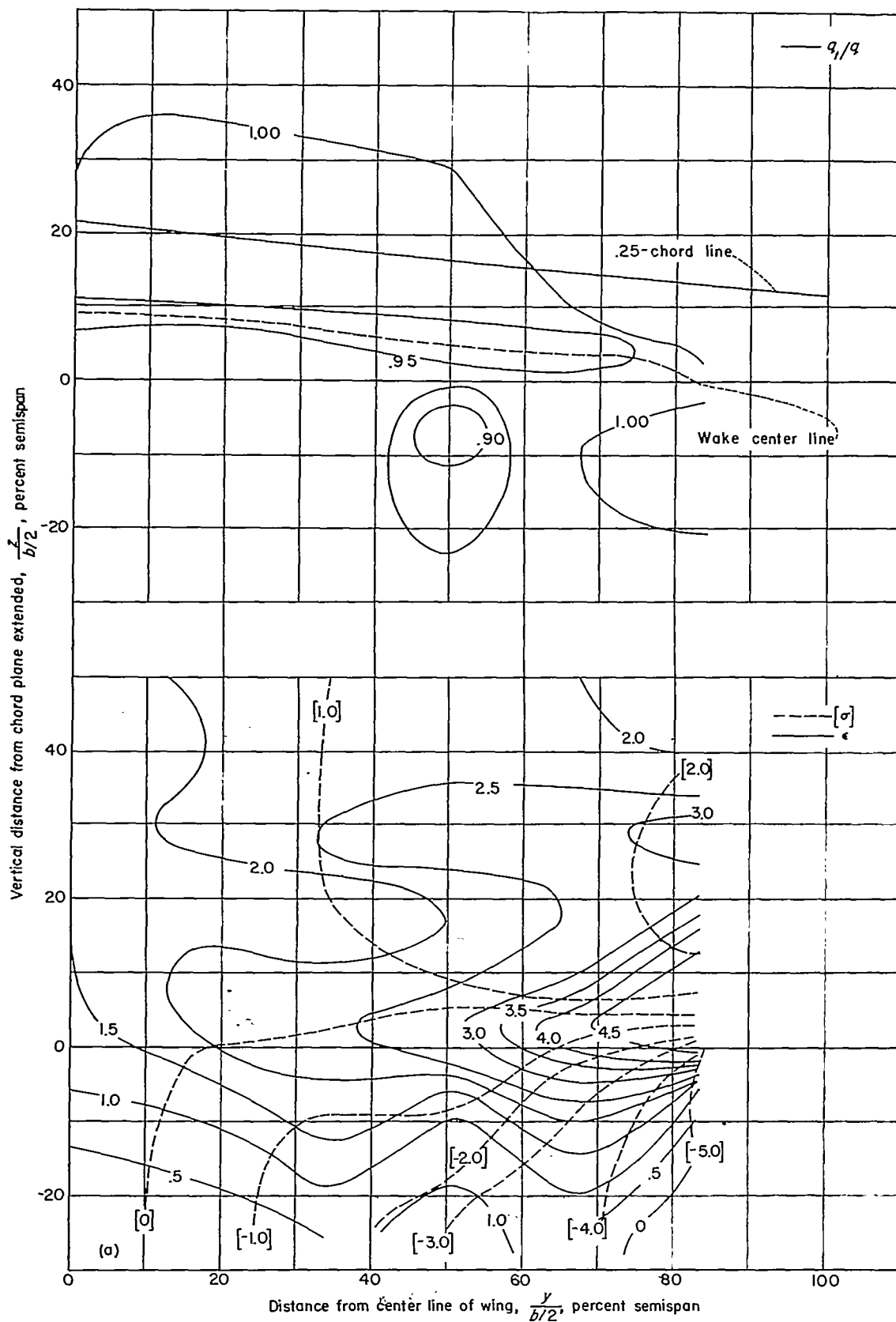
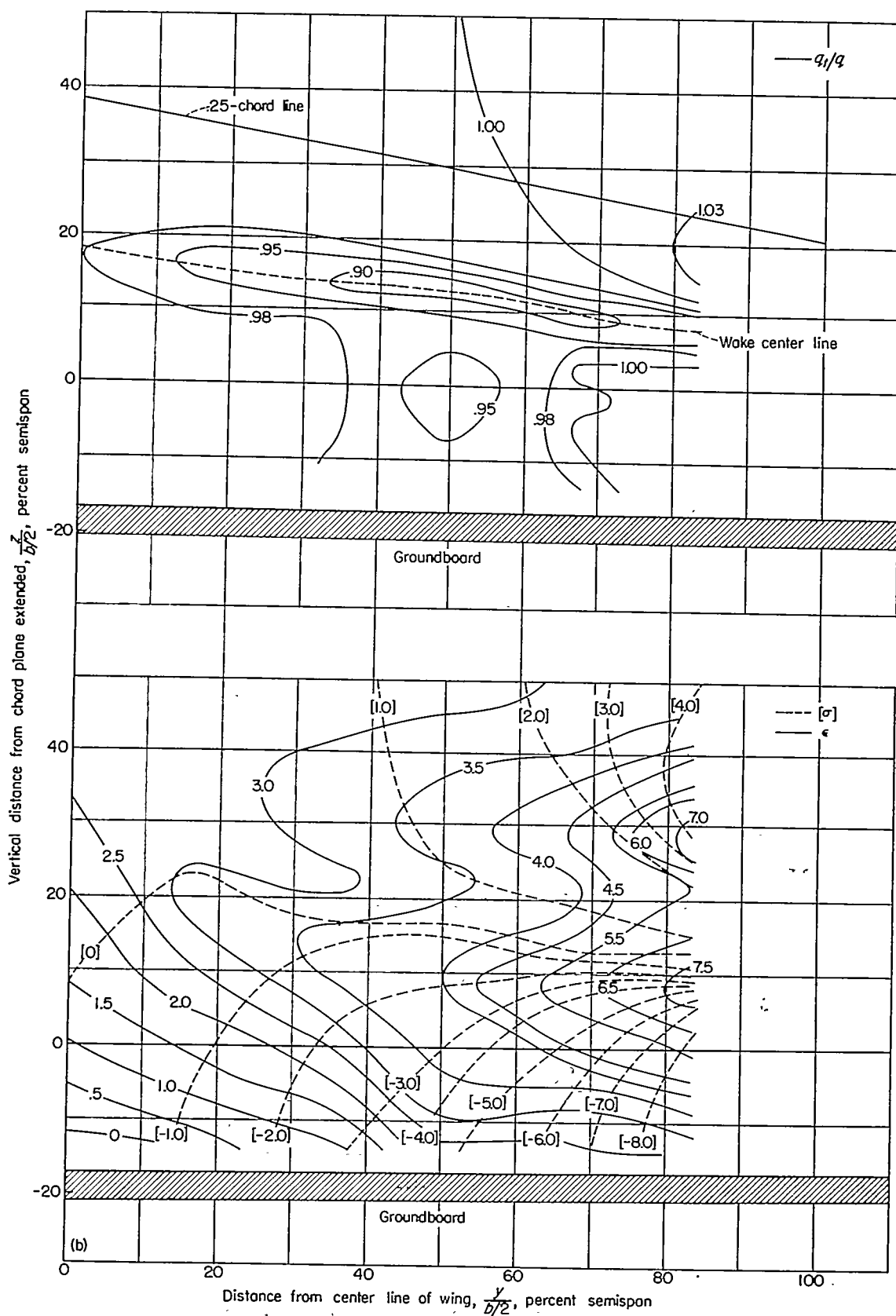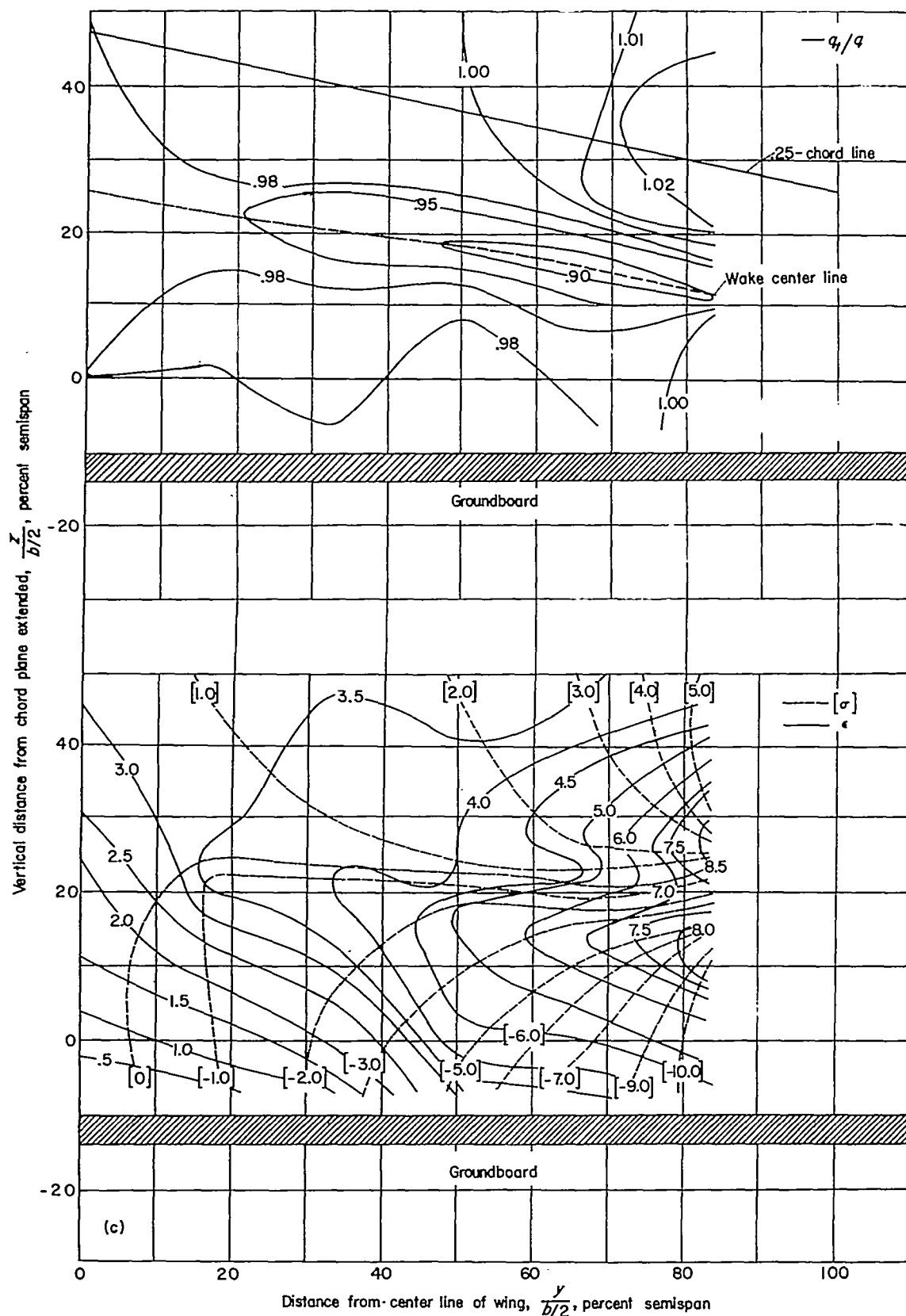(b) $\alpha=11.9°$; $C_L=0.80$.

FIGURE 14.—Continued.
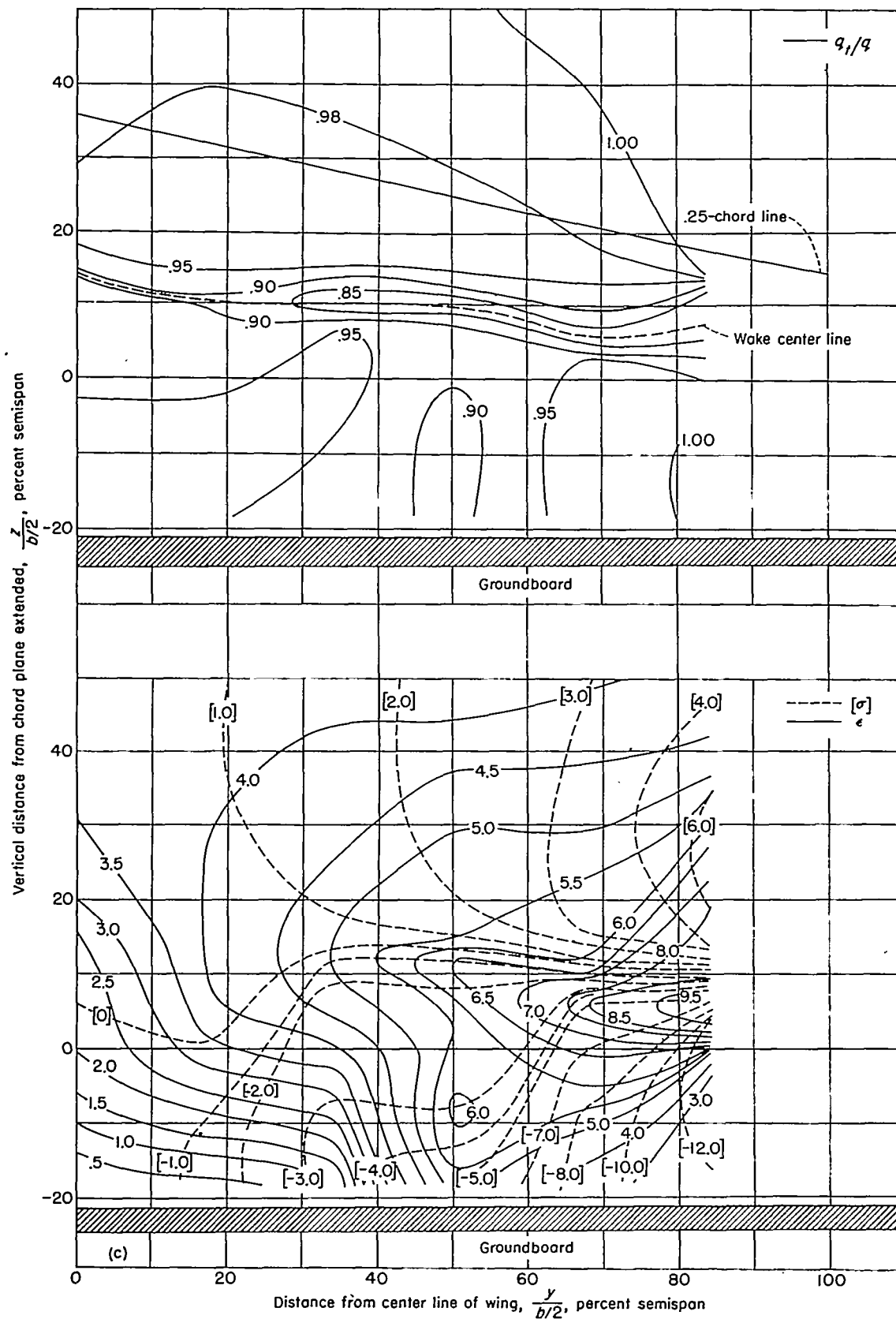
(o) $\alpha = 14.6°$; $C_L = 0.95$.
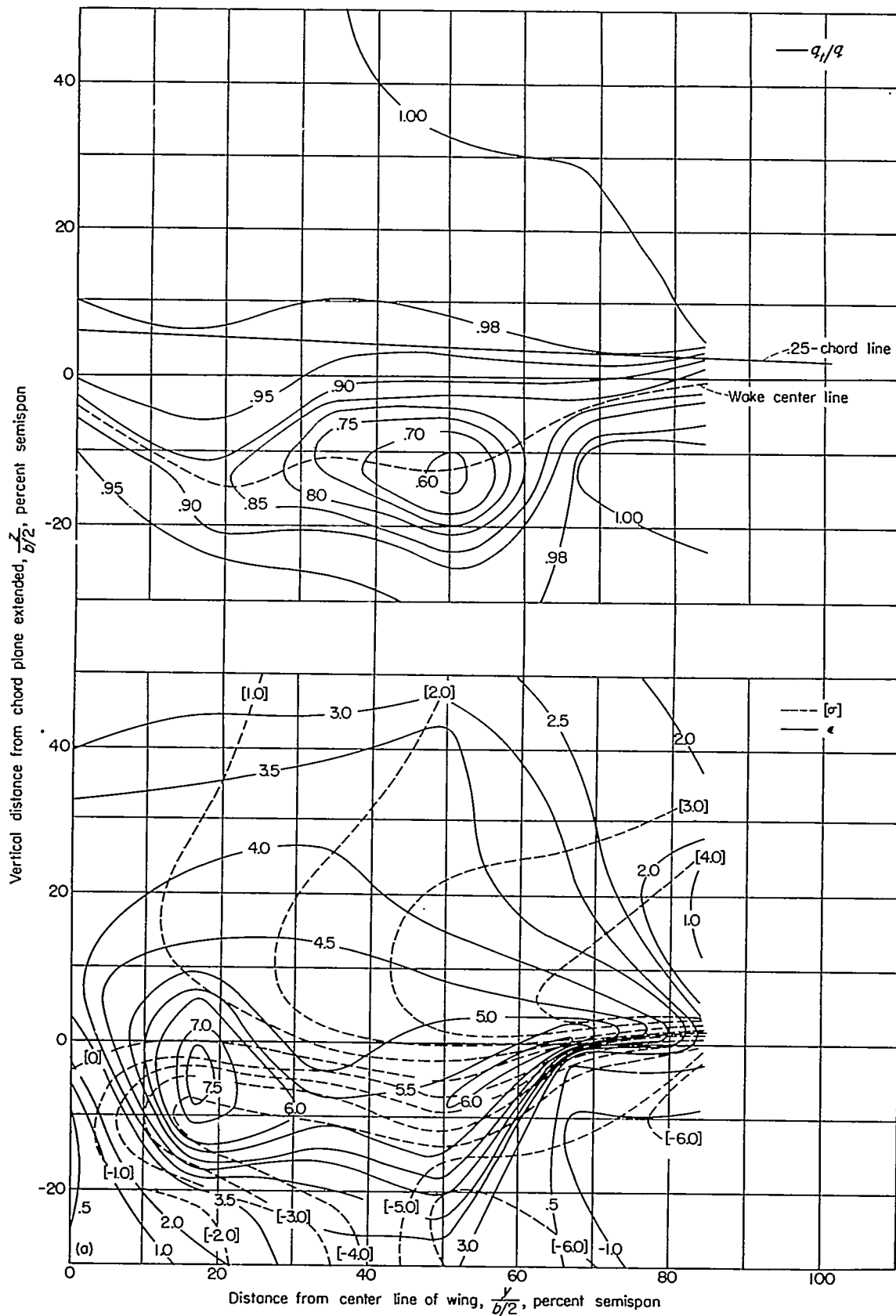
FIGURE 14.—Concluded.

(a) $\alpha = 6.7°$; $C_L = 0.48$.

FIGURE 15.—Contours of downwash and sidewash angles in degrees and of dynamic-pressure ratio behind a 42° sweptback wing. Longitudinal plane of survey at 2.8$\bar{c}$; flaps neutral; ground distance, 0.92$\bar{c}$.

(b) $\alpha = 11.9°$; $C_L = 0.80$.

FIGURE 15.—Continued.

(c) $\alpha=14.6°$; $C_L=0.95$.

FIGURE 15.—Concluded.

(a) $\alpha=2.4°$; $C_L=0.59$.

FIGURE 16.—Contours of downwash and sidewash angles in degrees and of dynamic-pressure ratio behind a 42° sweptback wing. Longitudinal plane of survey at $2.0\bar{c}$; flaps deflected 60°; ground distance, $0.92\bar{c}$.
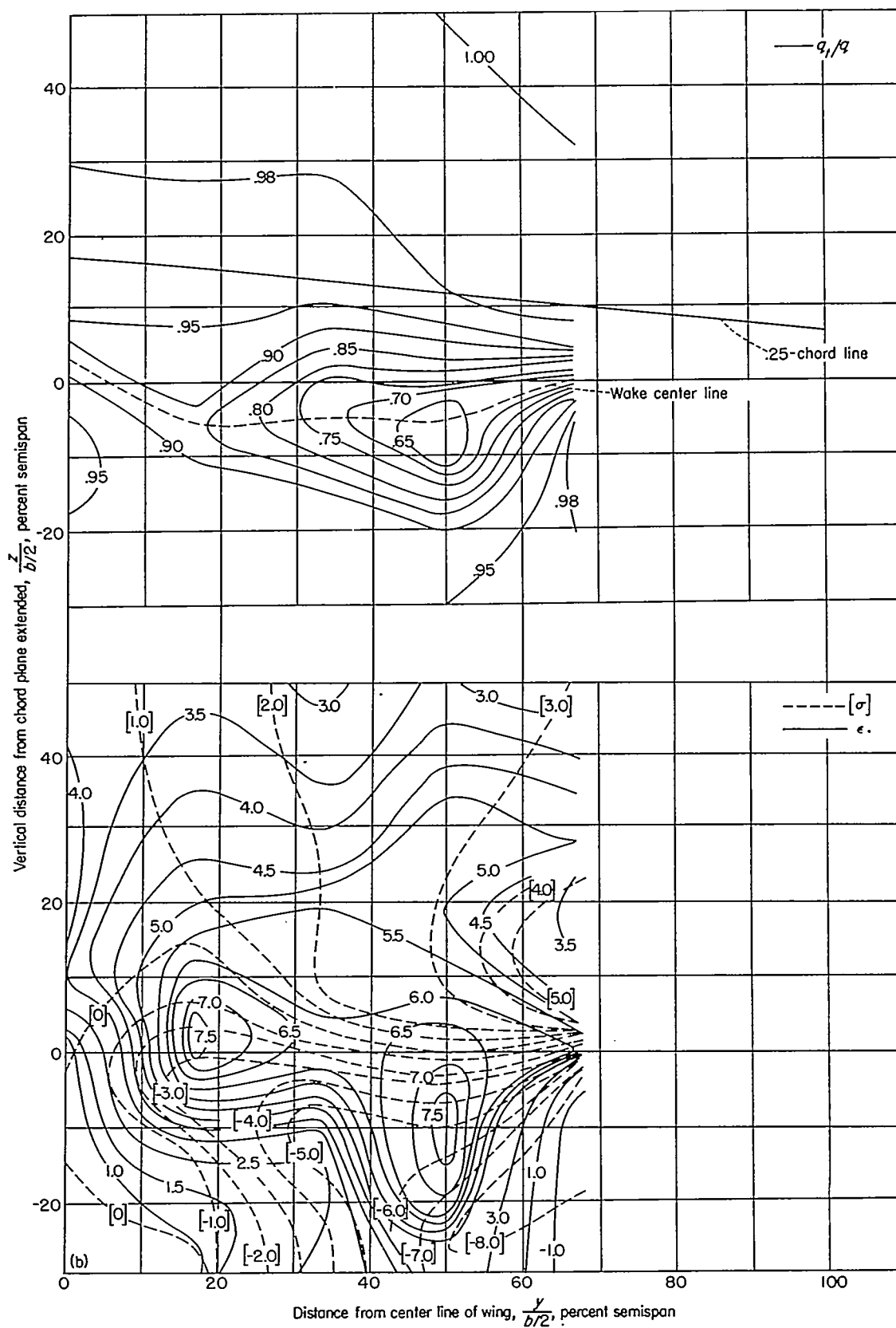
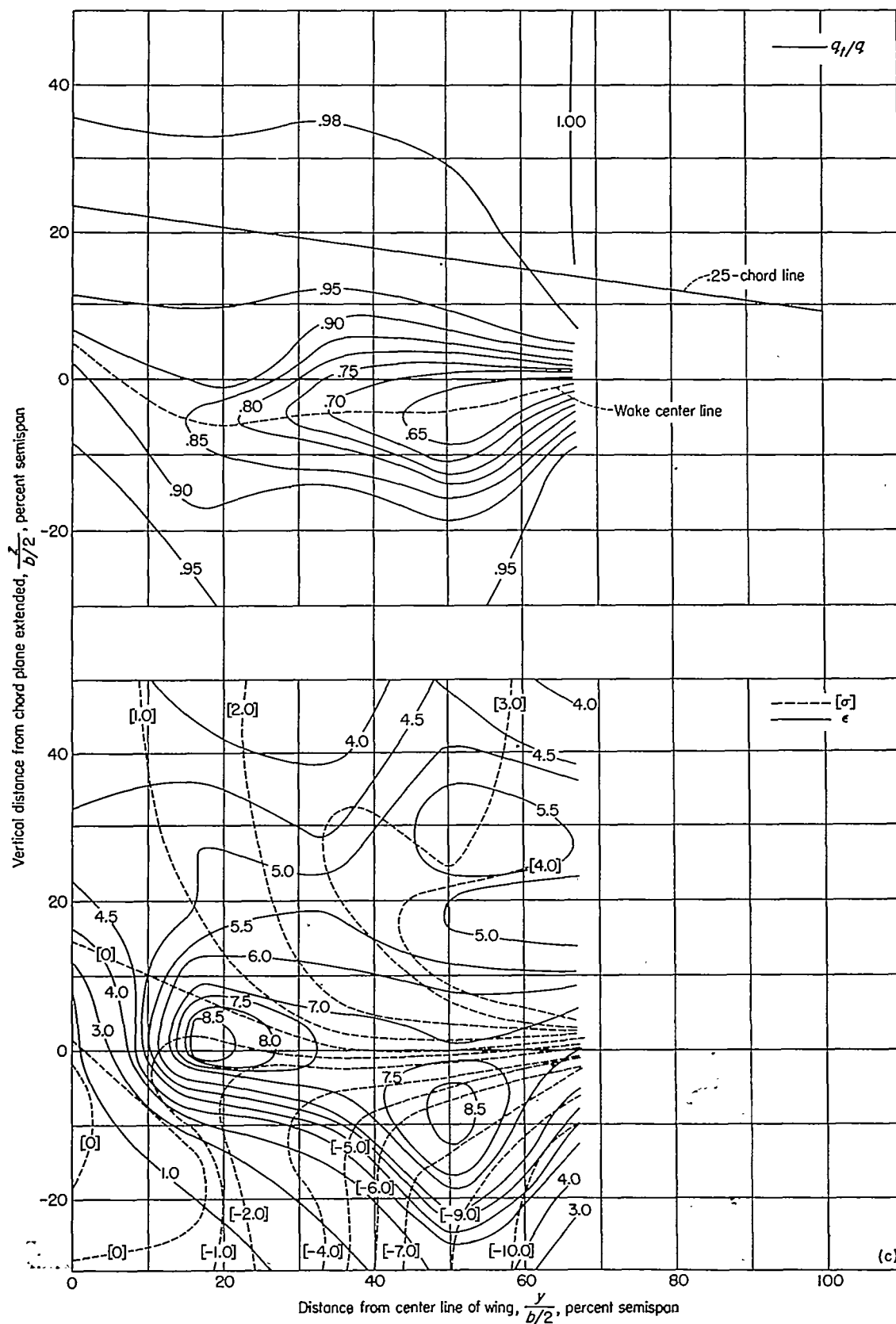(b) $\alpha = 7.1°$; $C_L = 0.89$.

FIGURE 16.—Continued.

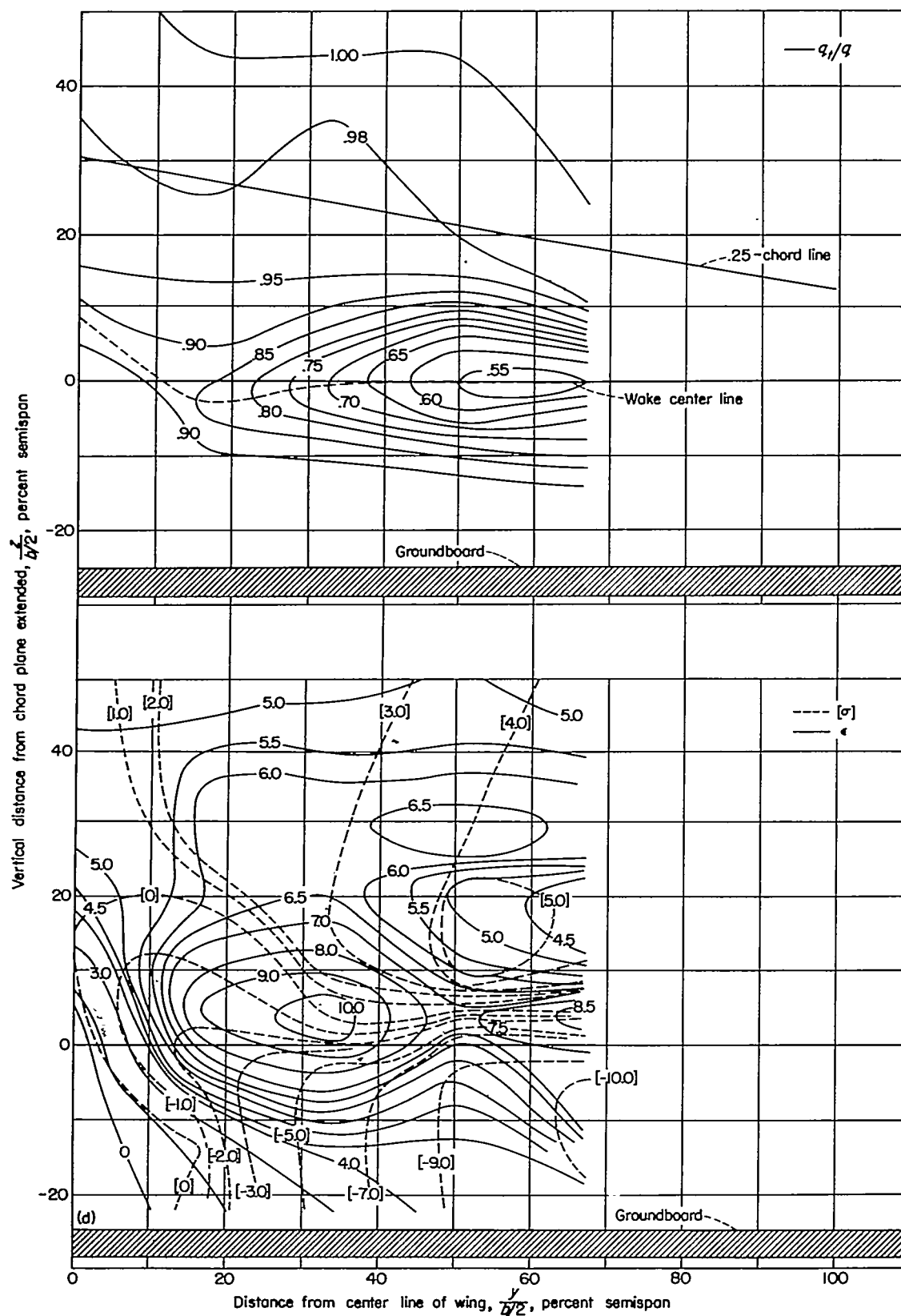(c) $\alpha = 9.7°$; $C_L = 1.04$.

FIGURE 16.—Continued.

(d) $\alpha=12.5°$; $C_L=1.18$.
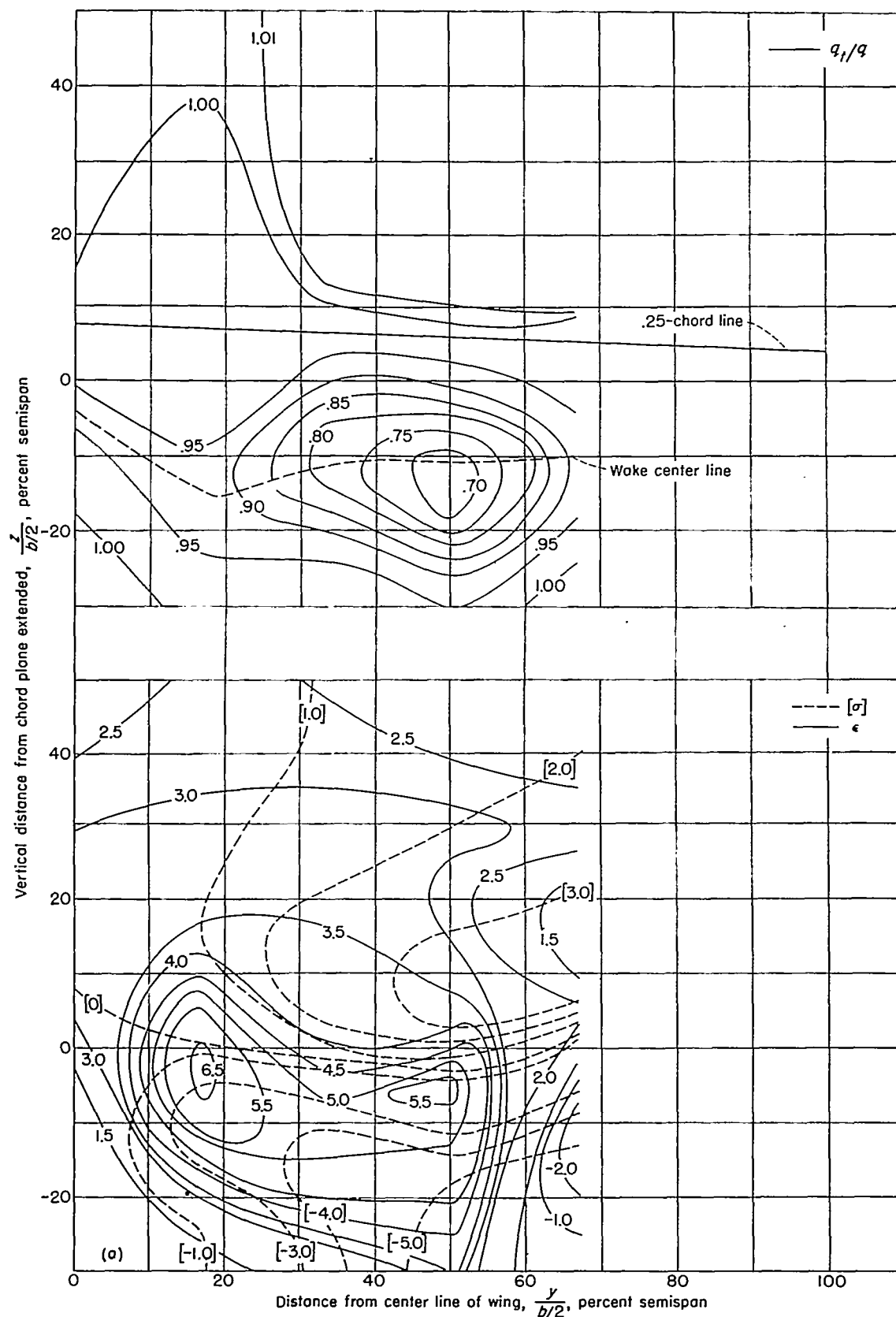
FIGURE 16.—Concluded.

(a) $\alpha = 2.4°$; $C_L = 0.59$.

FIGURE 17.—Contours of downwash and sidewash angles in degrees and of dynamic-pressure ratio behind a 42° sweptback wing. Longitudinal plane of survey at $2.8\bar{c}$; flaps deflected 60°; ground distance, $0.92\bar{c}$.

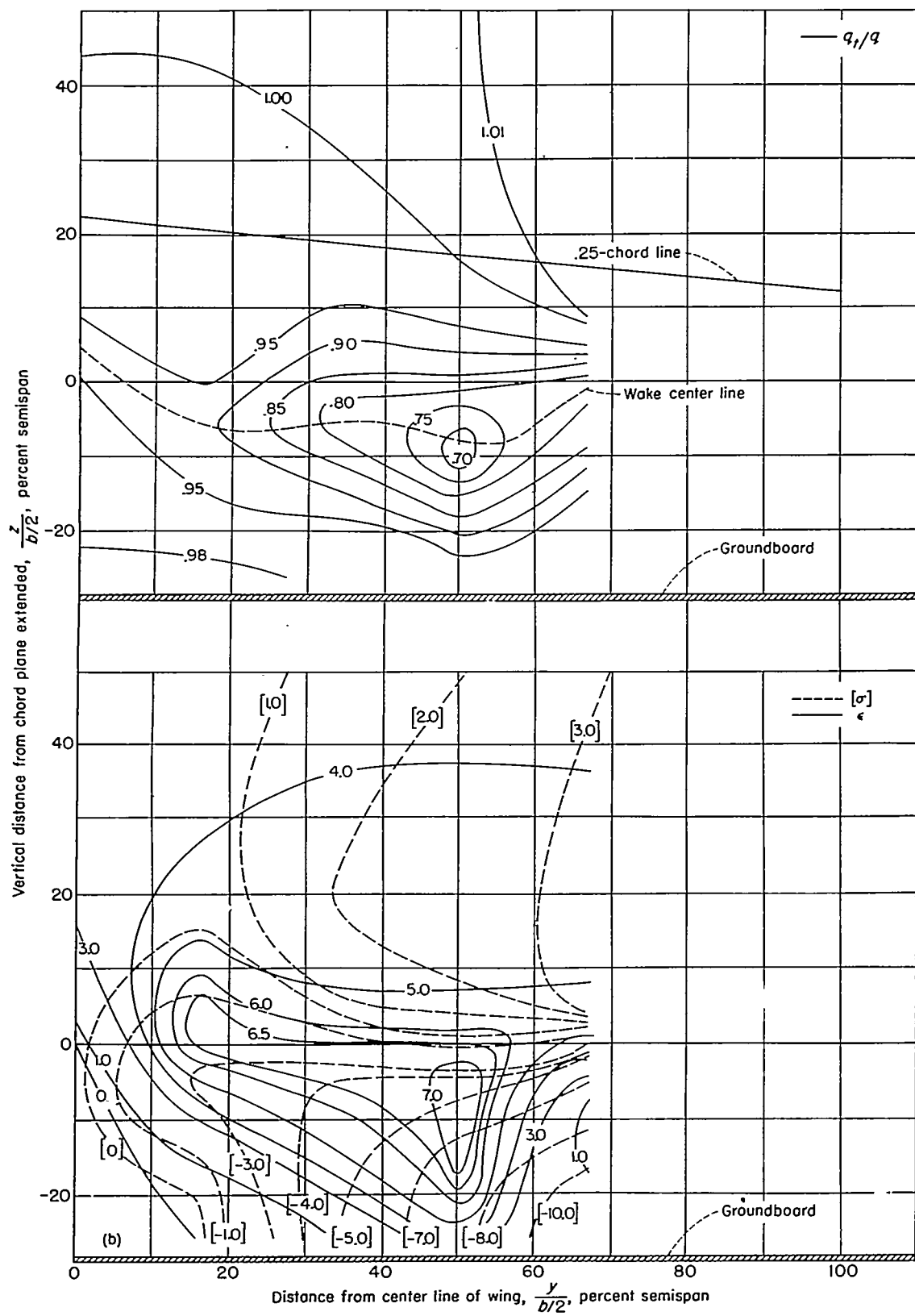(b) $\alpha = 7.1°$; $C_L = 0.89$.

FIGURE 17.—Continued.

Vertical distance from chord plane extended, $\frac{z}{b/2}$, percent semispan

Distance from center line of wing, $\frac{y}{b/2}$, percent semispan

(c) $\alpha=9.7°$; $C_L=1.04$.

FIGURE 17.—Continued.

(d) $\alpha=12.5°$; $C_L=1.18$.

FIGURE 17.—Concluded.

(a) $\alpha = 6.7°$; $C_L = 0.51$.

FIGURE 18.—Contours of downwash and sidewash angles in degrees and of dynamic-pressure ratio behind a 42° sweptback wing.   Longitudinal plane of survey at $2.0\bar{c}$; flaps neutral; ground distance, $0.68\bar{c}$.
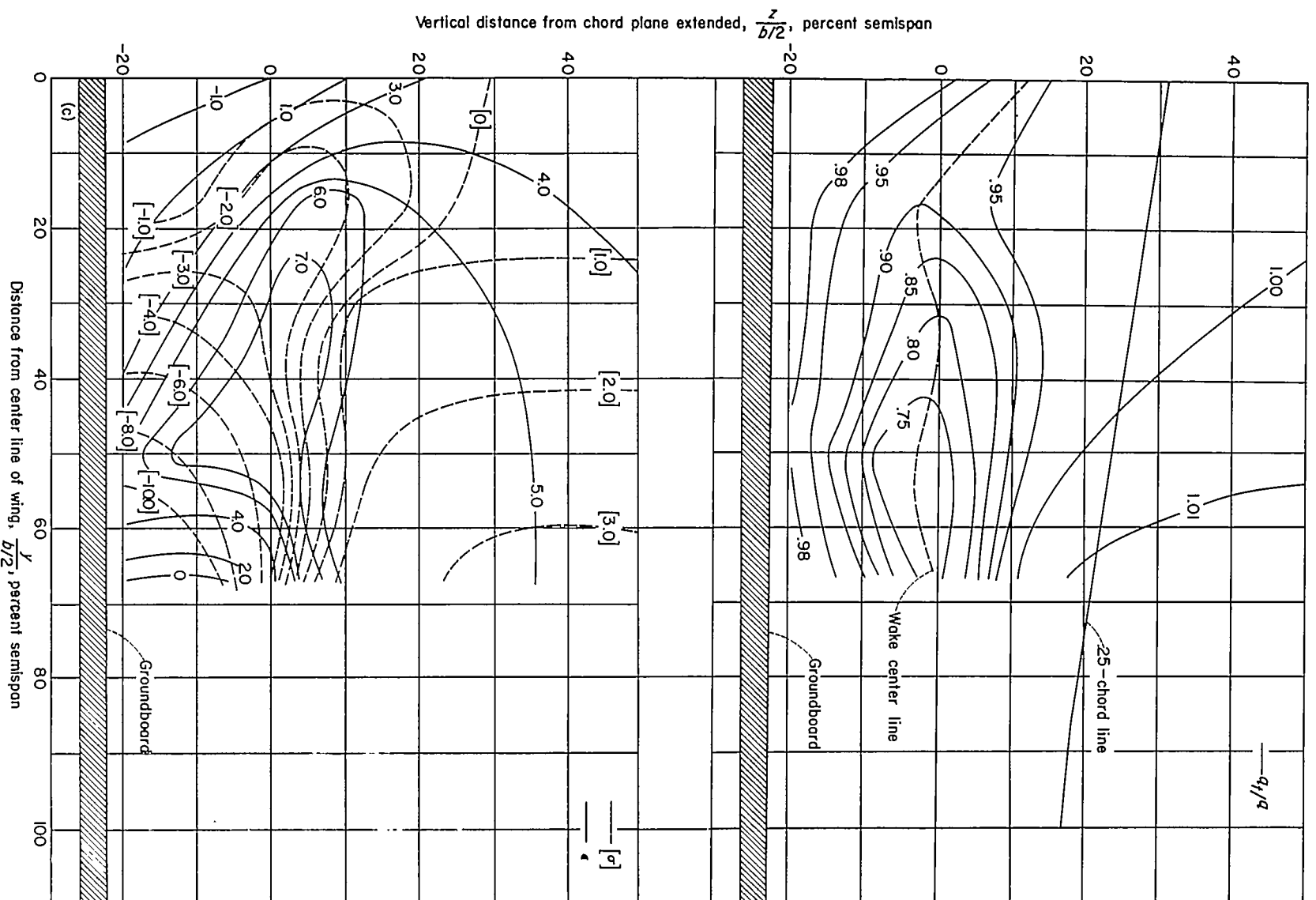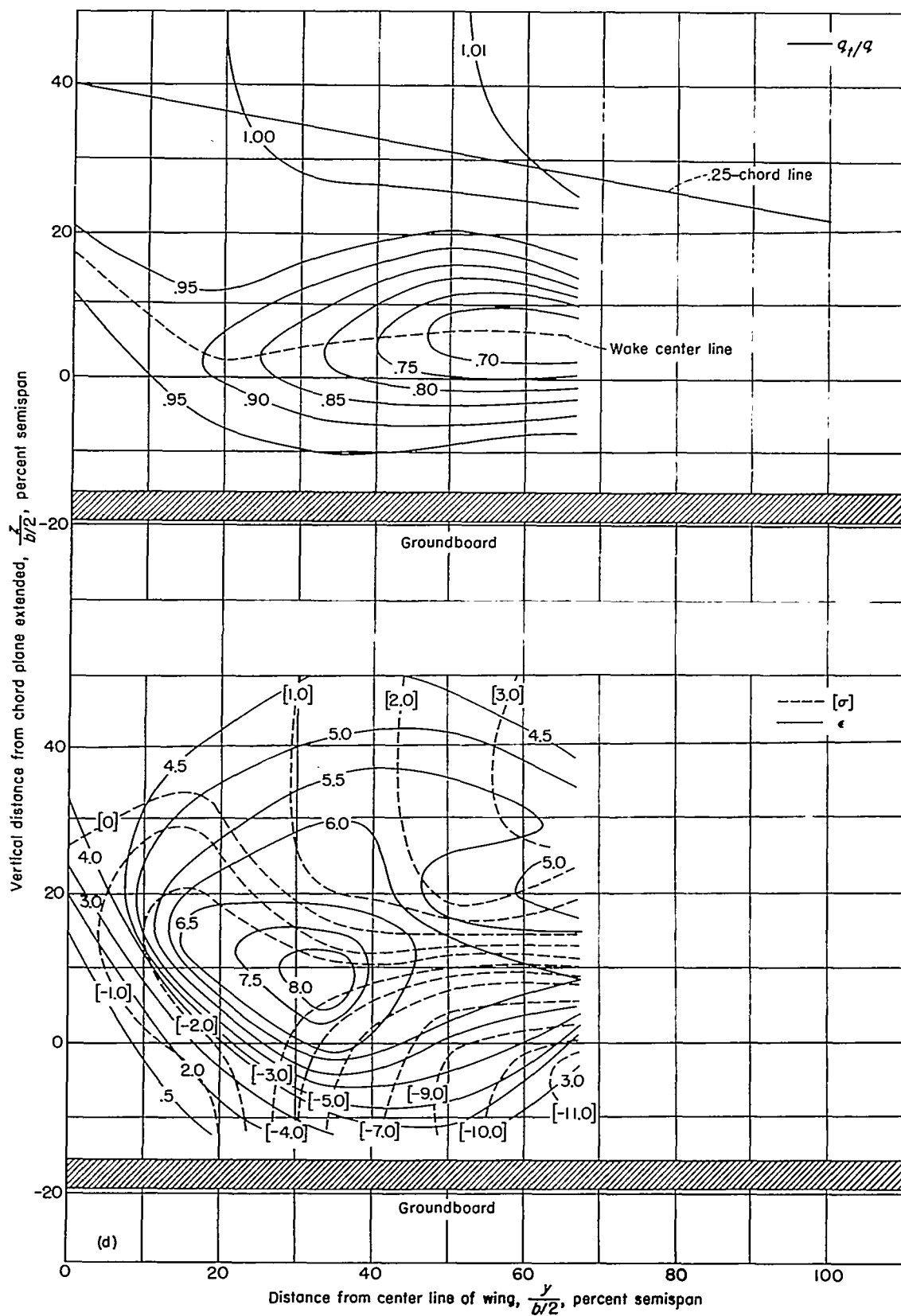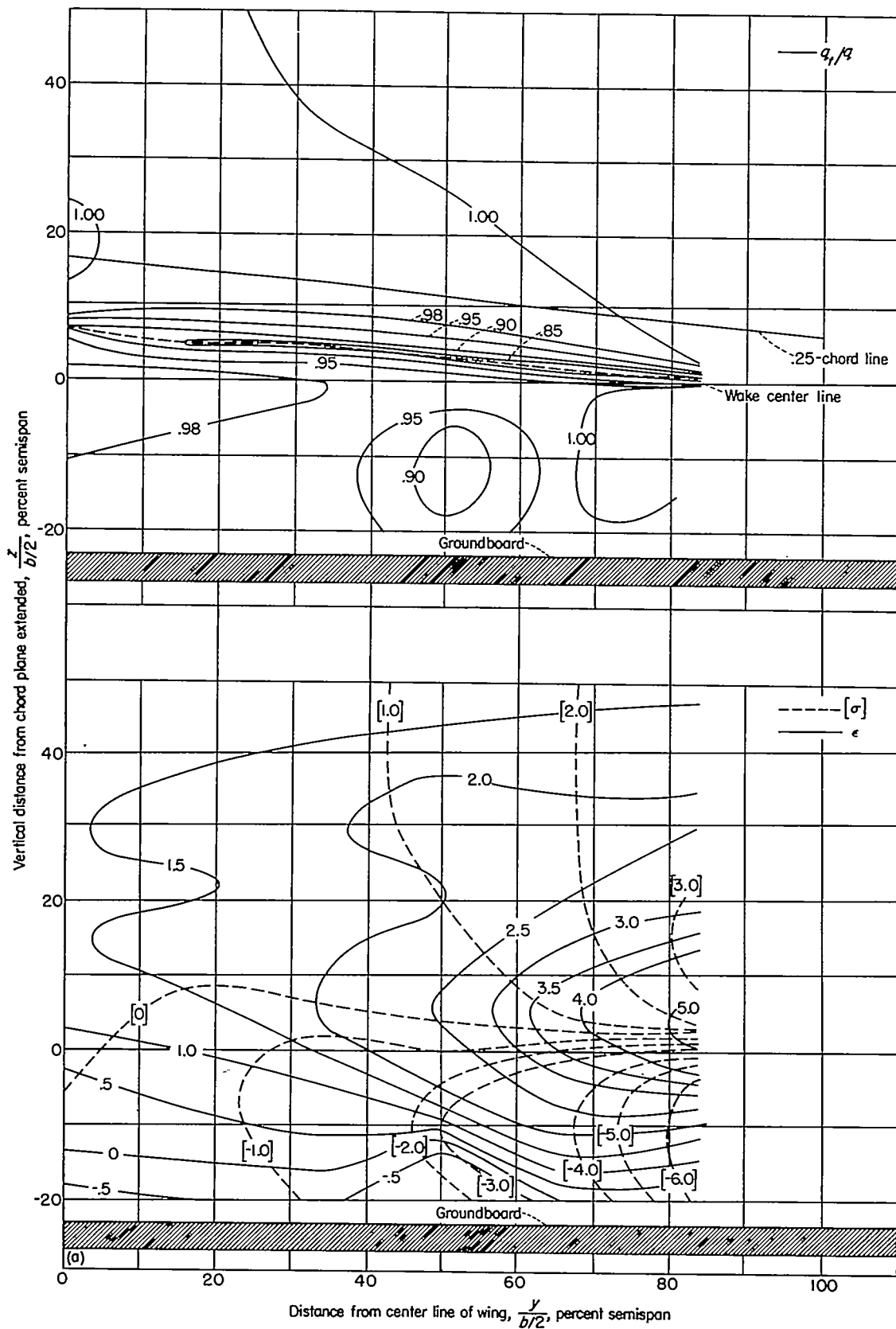
(b) $\alpha=11.9°$; $C_L=0.83$..

FIGURE 18.—Continued.

(c) $\alpha = 14.6°$; $C_L = 0.98$.

FIGURE 18.—Concluded.

(a) $\alpha=6.7°$; $C_L=0.51$.

FIGURE 19.—Contours of downwash and sidewash angles in degrees and of dynamic-pressure ratio behind a 42° sweptback wing. Longitudinal plane of survey at 2.8$\bar{c}$; flaps neutral; ground distance, 0.68$\bar{c}$.
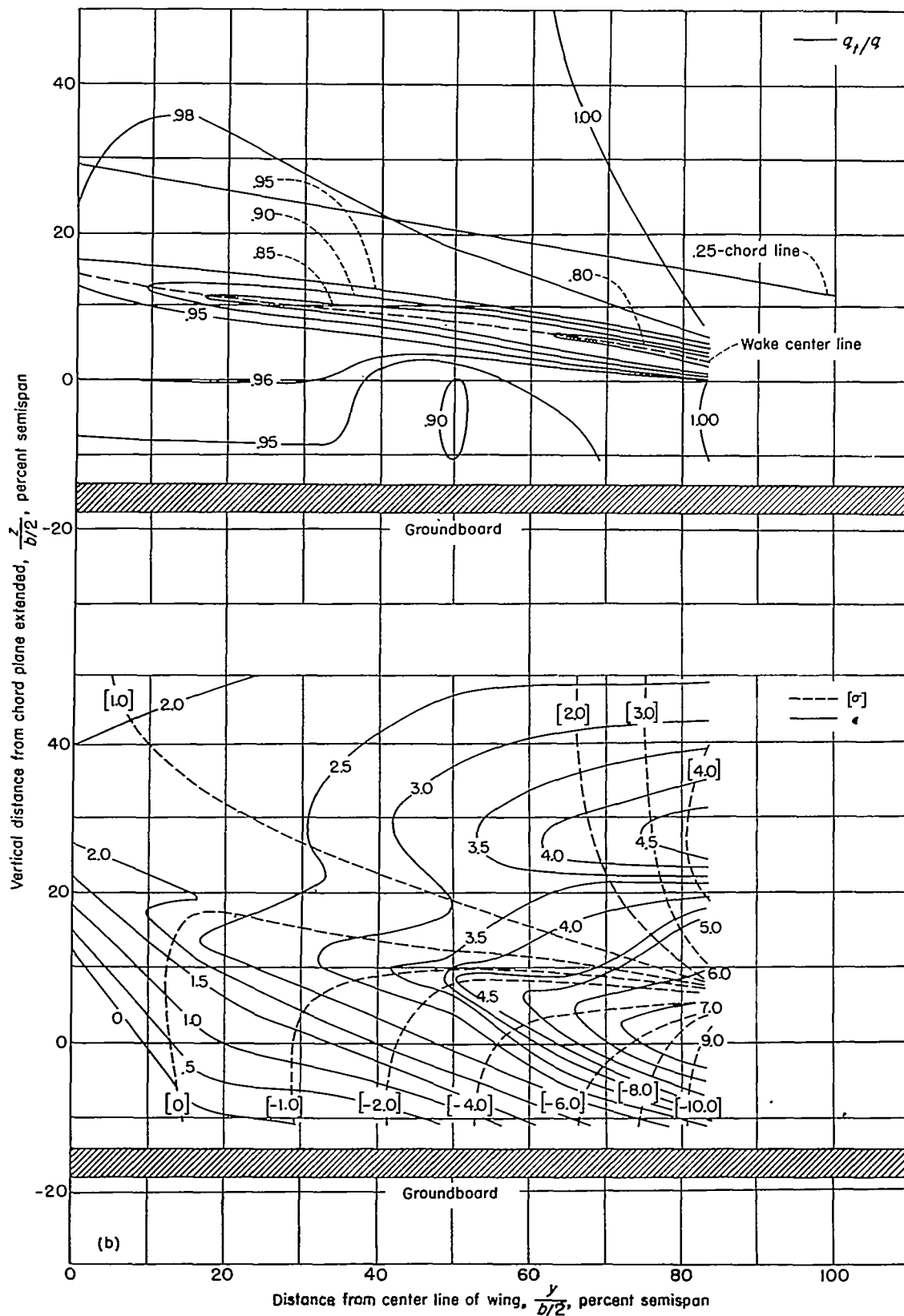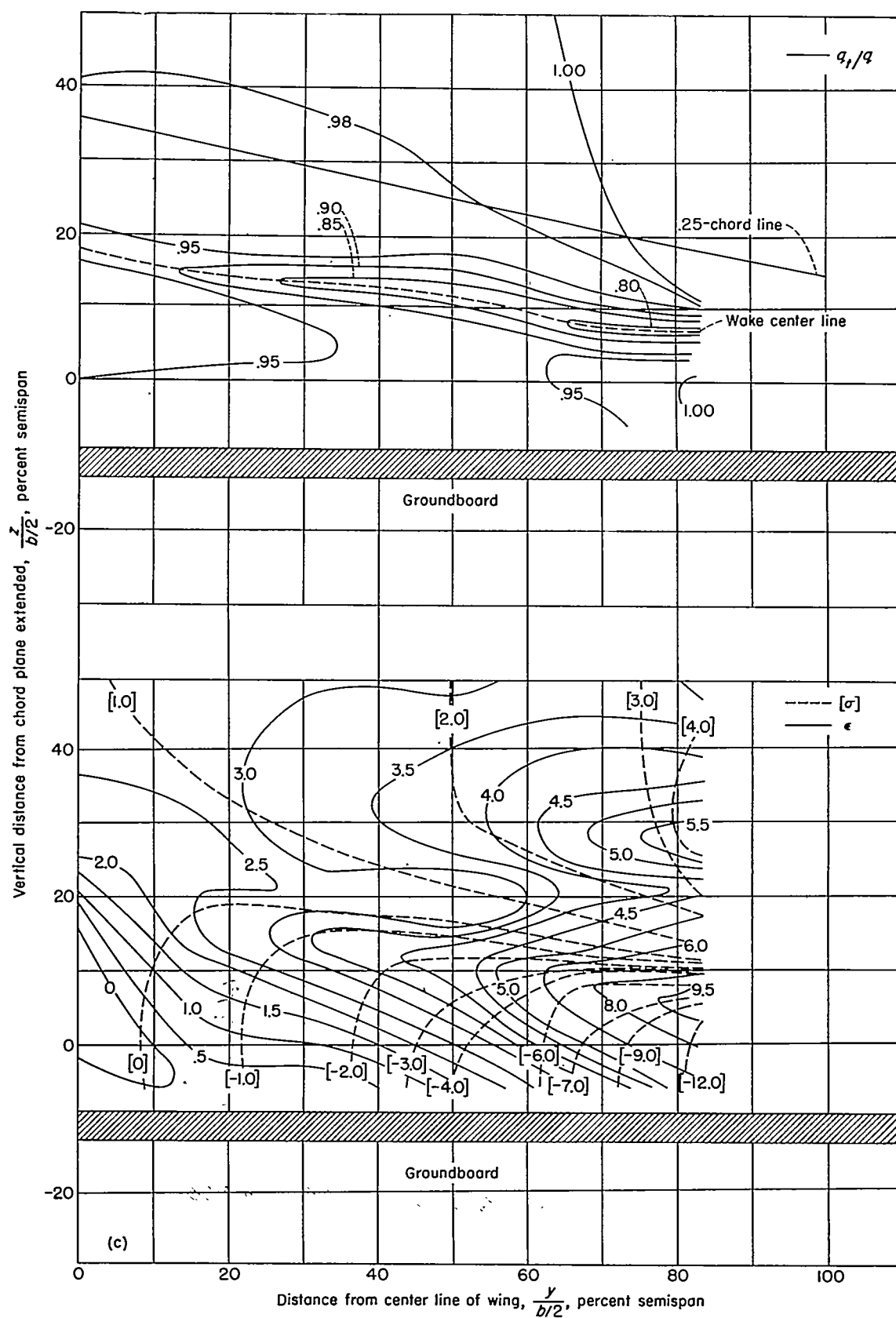
(b) $\alpha = 11.9°$; $C_L = 0.83$.
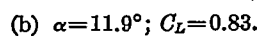
FIGURE 19.—Continued.
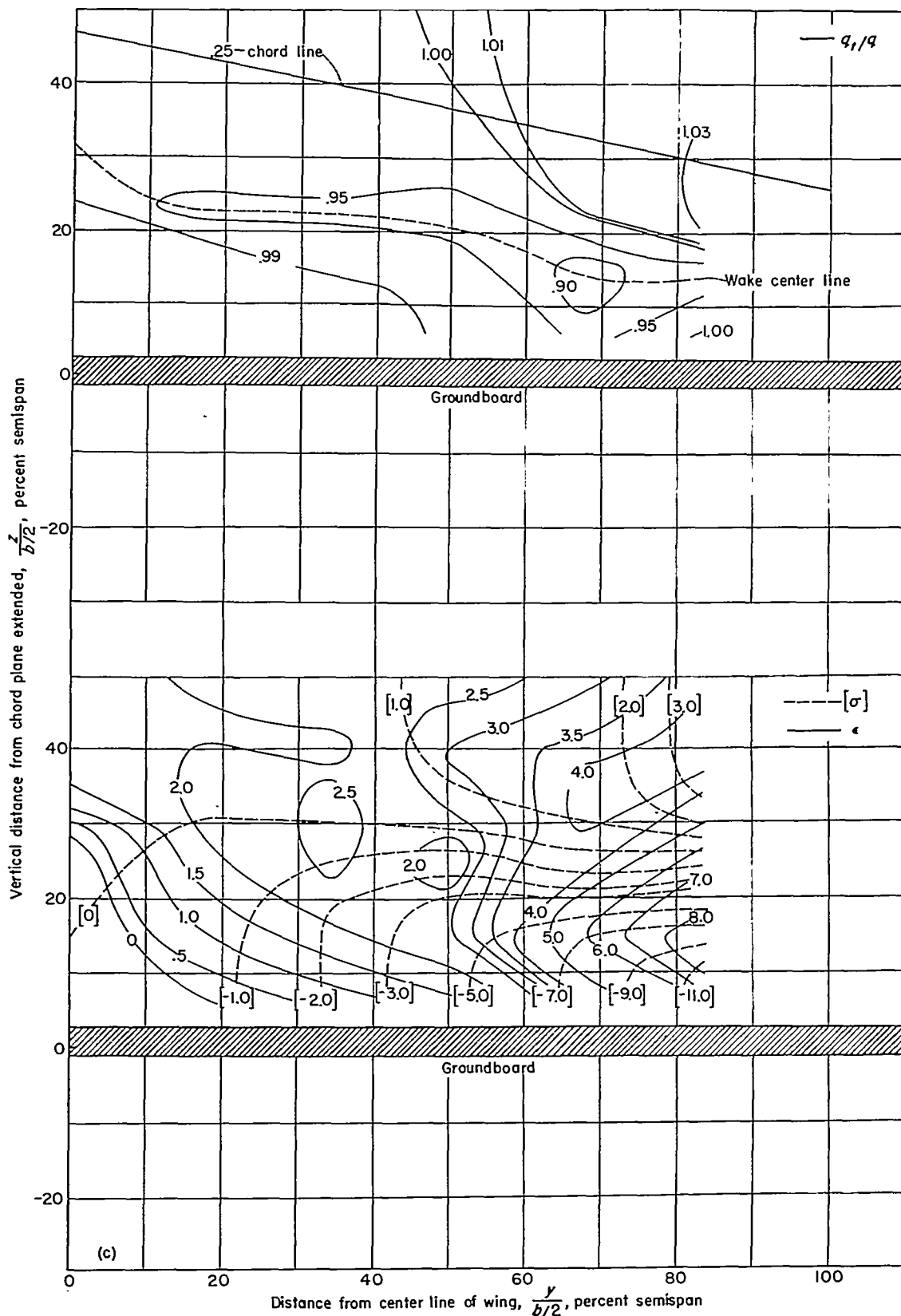
(c) $\alpha = 14.6°$; $C_L = 0.98$.

Figure 19.—Concluded.

(a) $\alpha=2.4°$; $C_L=0.62$.

FIGURE 20.—Contours of downwash and sidewash angles in degrees and of dynamic-pressure ratio behind a 42° sweptback wing. Longitudinal plane of survey at $2.0\bar{c}$; flaps deflected 60°; ground distance, $86.0\bar{c}$.

(b) $\alpha = 7.3°$; $C_L = 0.91$.

FIGURE 20.—Continued.
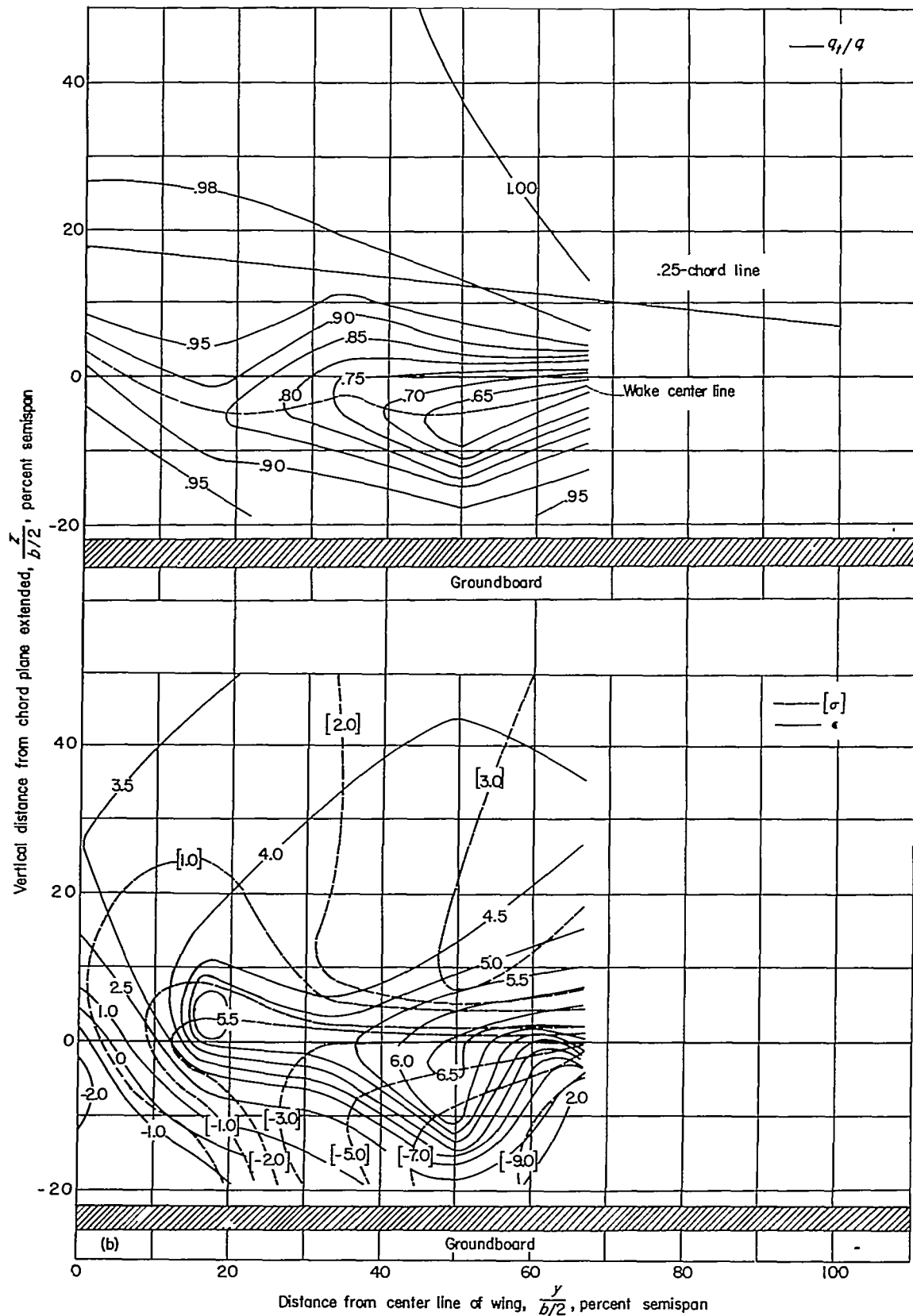
(c) $\alpha=10.0°$; $C_L=1.00$.

Figure 20.—Continued.
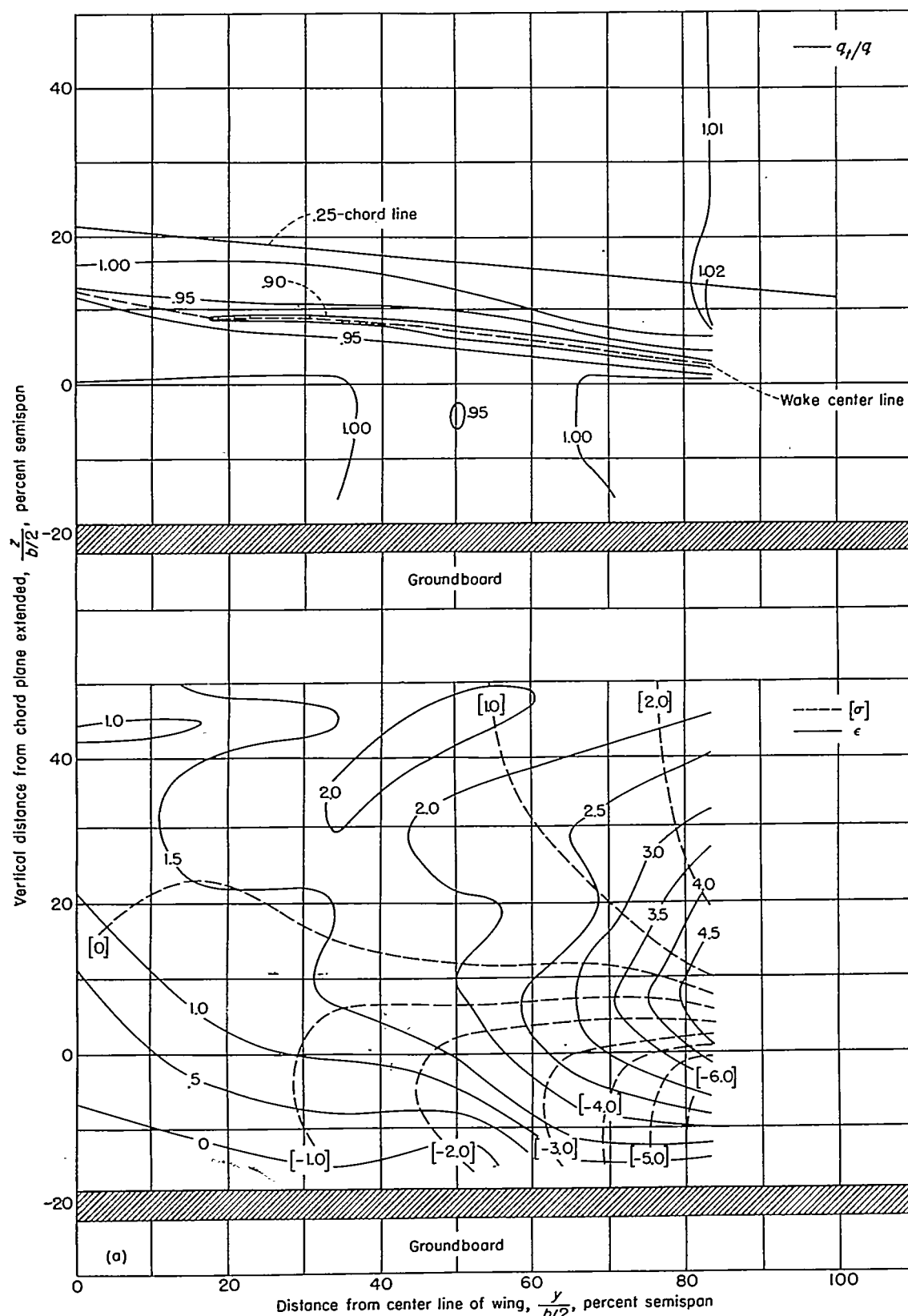
(d) $\alpha=13.6°$; $C_L=1.20$.

FIGURE 20.—Concluded.

(a) $\alpha=2.4°$; $C_L=0.62$.

FIGURE 21.—Contours of downwash and sidewash angles in degrees and of dynamic-pressure ratio behind a 42° sweptback wing. Longitudinal plane of survey at 2.8$\bar{c}$; flaps deflected 60°; ground distance, 0.68$\bar{c}$.
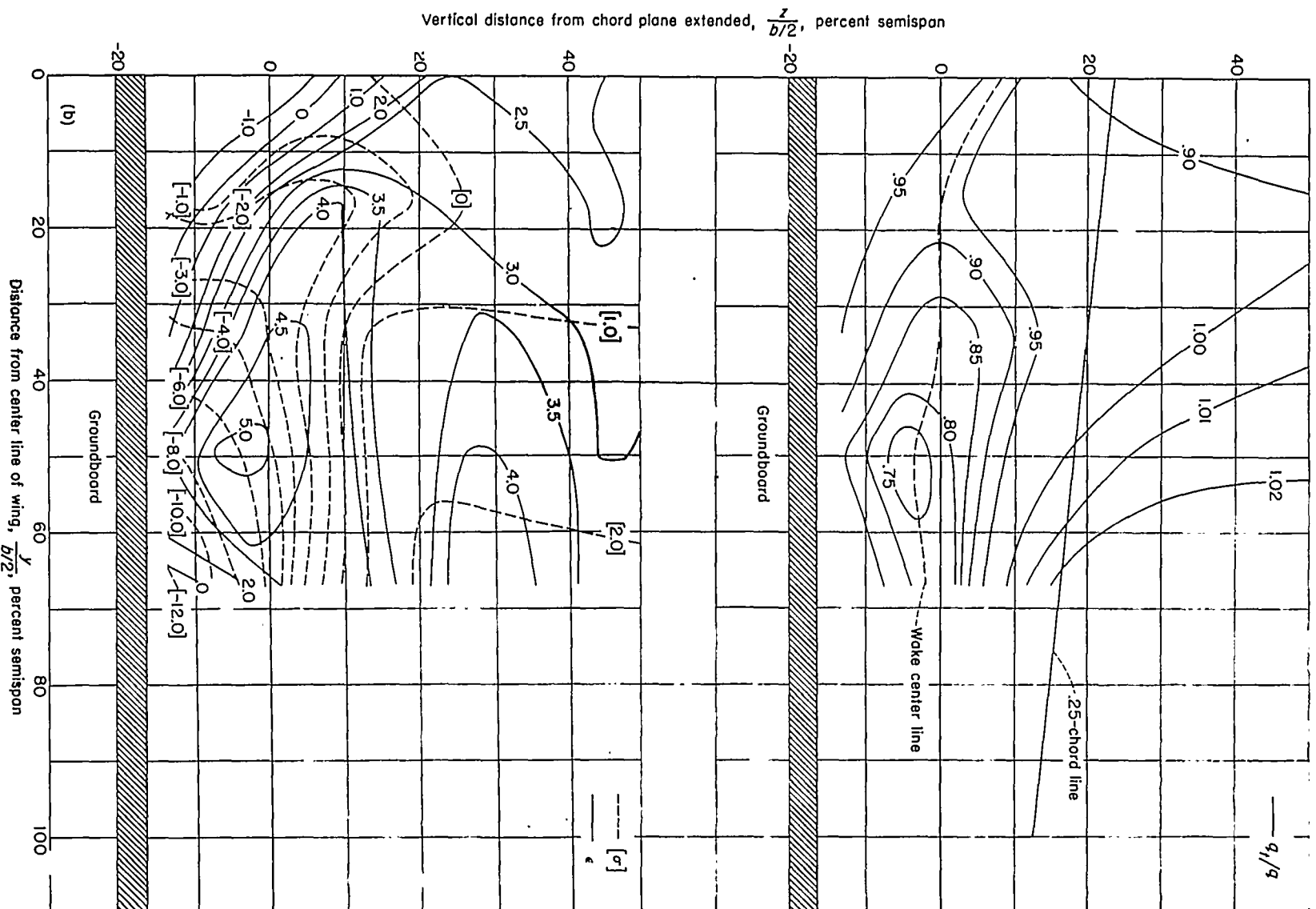
(b) $\alpha = 7.3°$; $C_L = 0.91$.
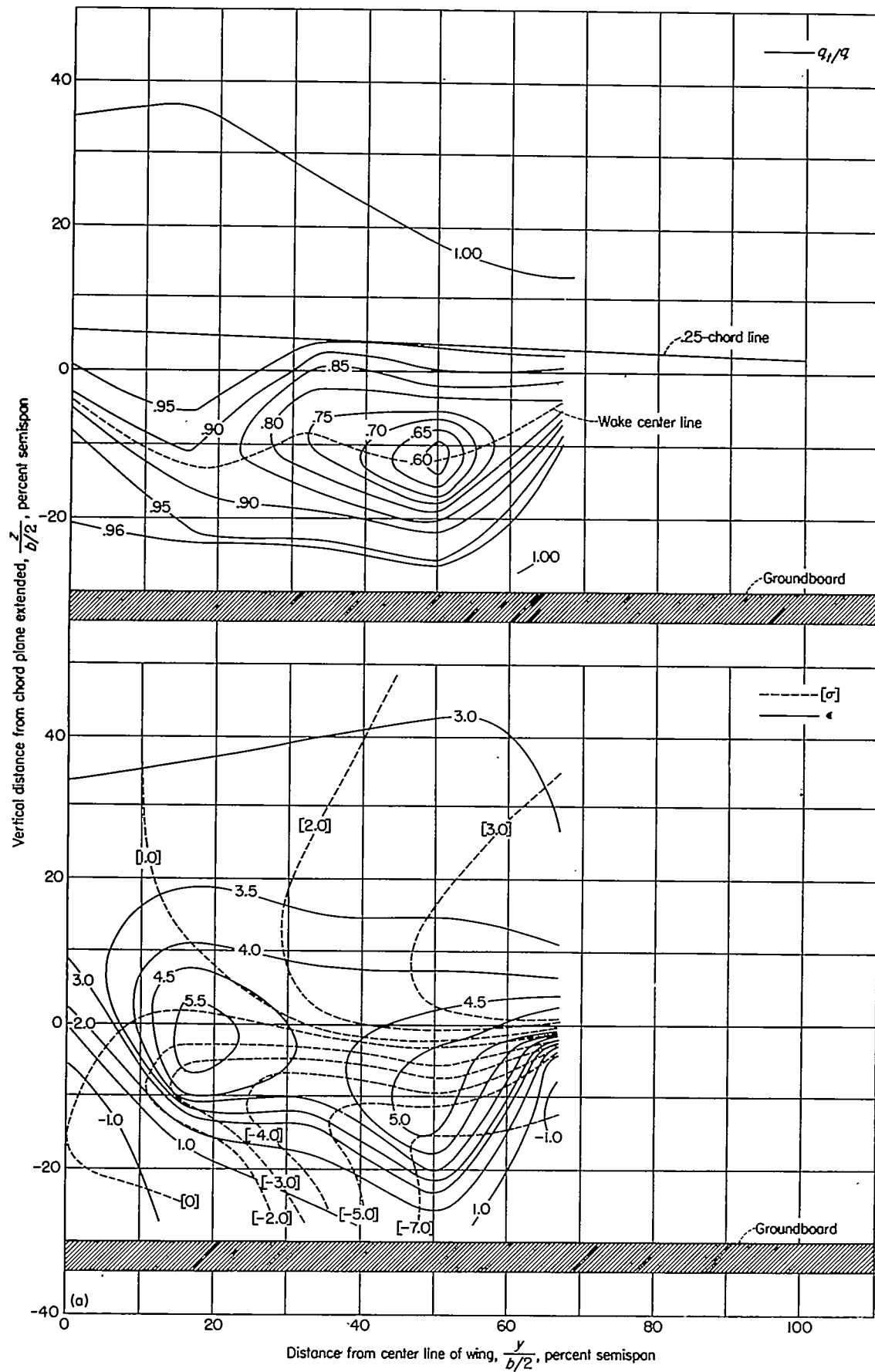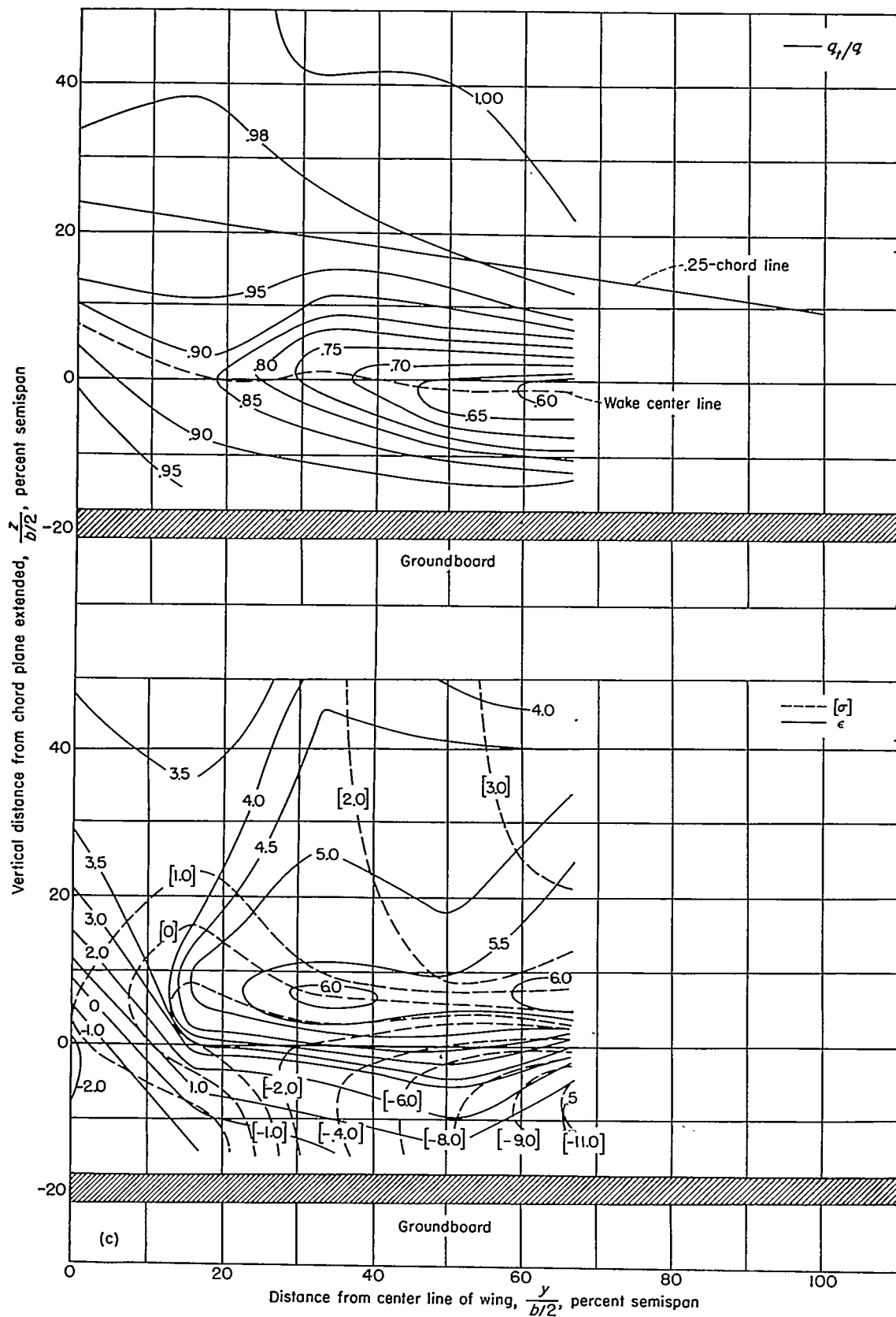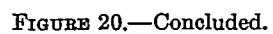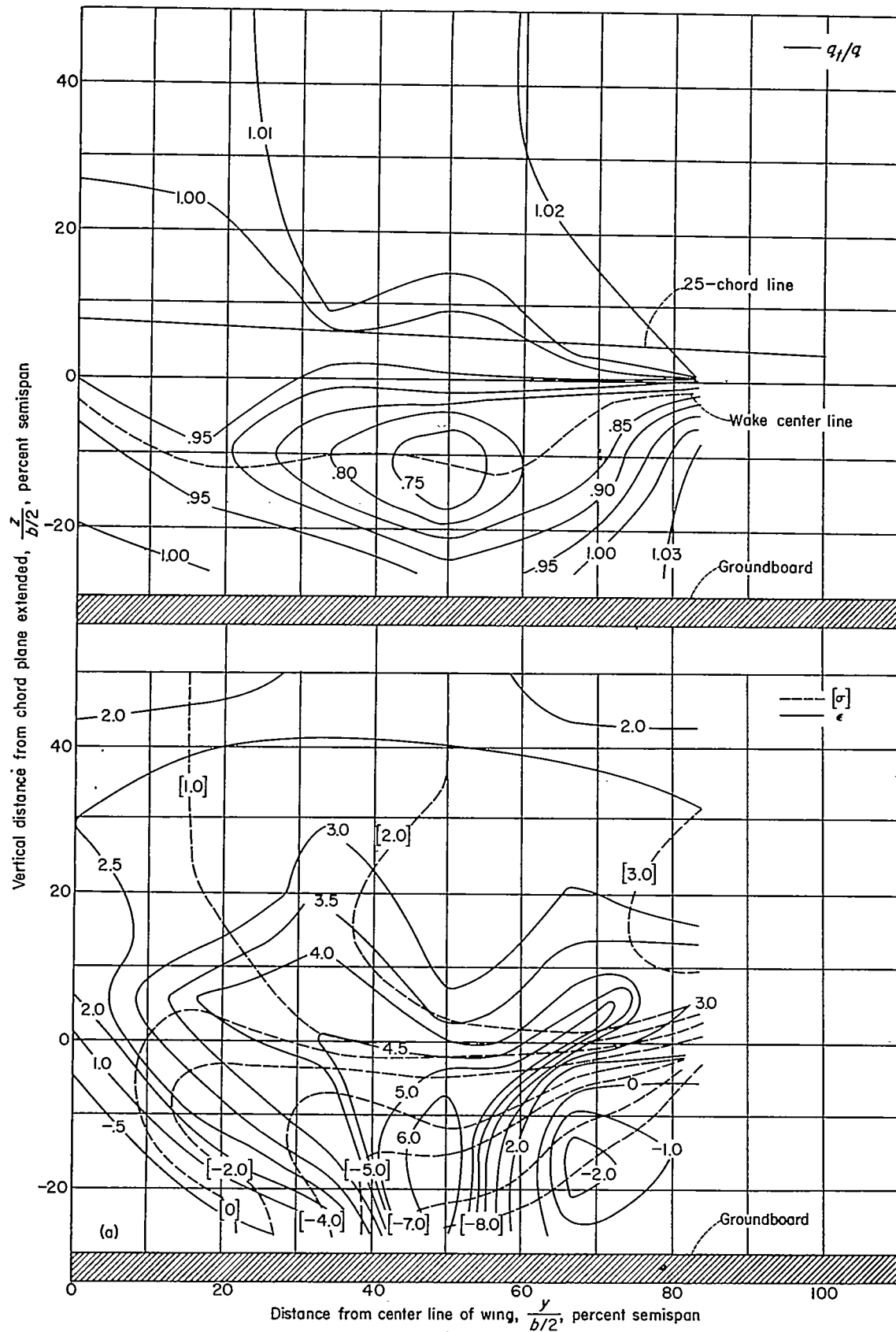
FIGURE 21.—Continued.
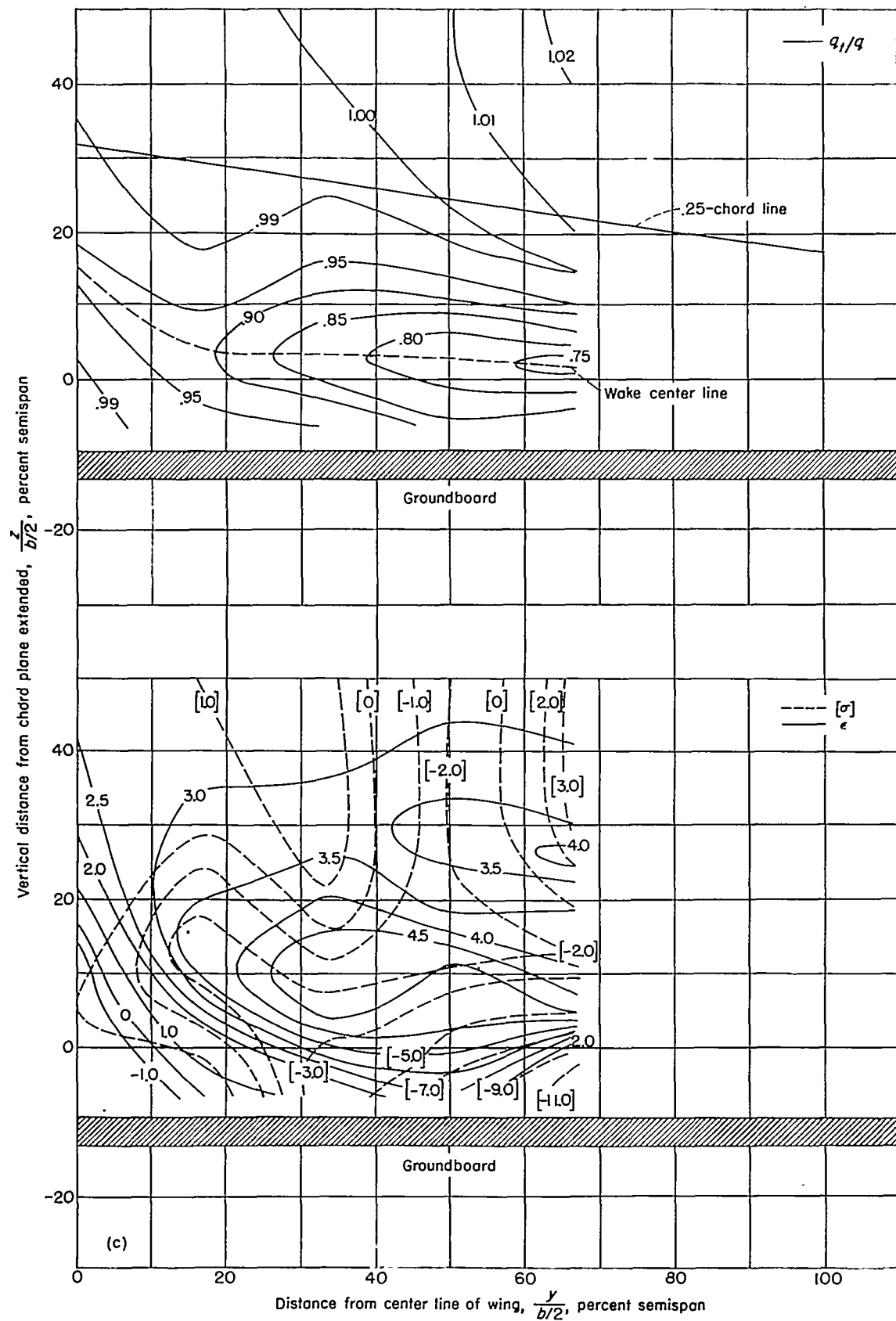
(c) $\alpha=10.0°$; $C_L=1.00$.

FIGURE 21.—Continued.

(d) $\alpha=13.6°$; $C_L=1.20$.

FIGURE 21.—Concluded.
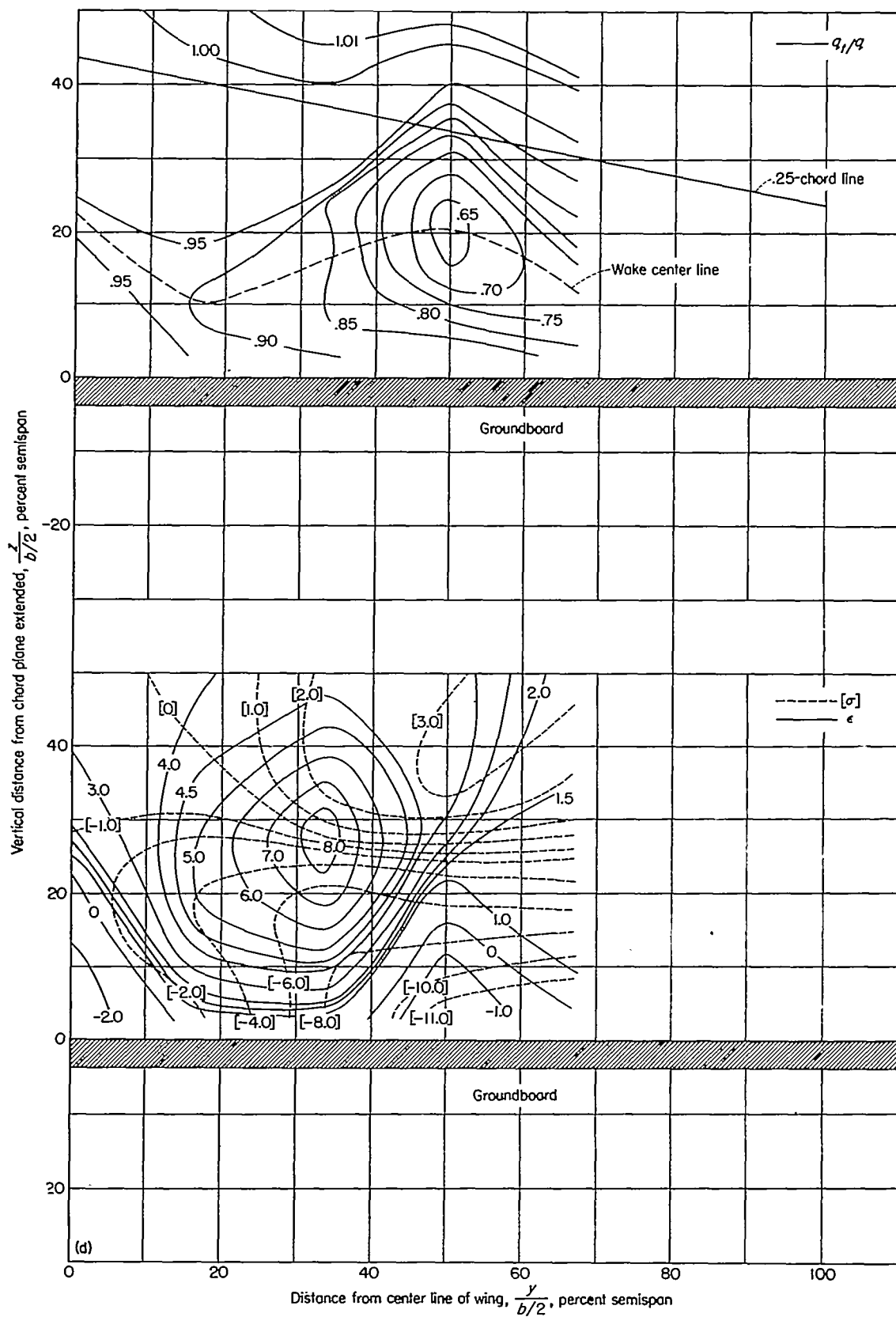
AVERAGE VALUES OF DOWNWASH AND DYNAMIC PRESSURE

Variations of average downwash and dynamic-pressure ratio with angle of attack have been presented in figures 22 to 25 to show the effects of tail span and tail location (vertical and longitudinal) on the stability of a wing-tail combination. Integrations were made across the contour charts at various vertical positions and spans of a fictitious tail of constant chord and zero sweep. At each longitudinal survey plane ($2.0\bar{c}$ and $2.8\bar{c}$), integrations were made across tail

spans of $0.25\frac{b}{2}$ and $0.50\frac{b}{2}$ and at ground distances of $0.38b/2$ above, $0.25b/2$ above, on, and $0.25b/2$ below the chord plane extended. Where physical limitations prohibited data to be obtained $0.25b/2$ below the chord plane extended, several variations have been presented for tail positions z of $0.05b/2$ and $0.125b/2$ below the chord plane extended.

Inasmuch as the data presented are for a wing alone, the results are not necessarily indicative of those that would be obtained with a fuselage present.

(a) Survey plane, $2.0\bar{c}$.   (b) Survey plane, $2.8\bar{c}$.

FIGURE 22.—The variation of average downwash angle with angle of attack for various ground distances, tail lengths (survey plane), and tail spans. Flaps neutral.

(a) Survey plane, $2.0\bar{c}$.   (b) Survey plane, $2.8\bar{c}$.

FIGURE 23.—The variation of average downwash angle with angle of attack for various ground distances, tail lengths (survey plane), and tail spans. Flaps deflected 60°.

(a) Survey plane, $2.0\bar{c}$.

(b) Survey plane, $2.8\bar{c}$.

FIGURE 24.—The variation of average dynamic-pressure ratio with angle of attack for various ground distances, tail lengths (survey plane), and tail spans. Flaps neutral.

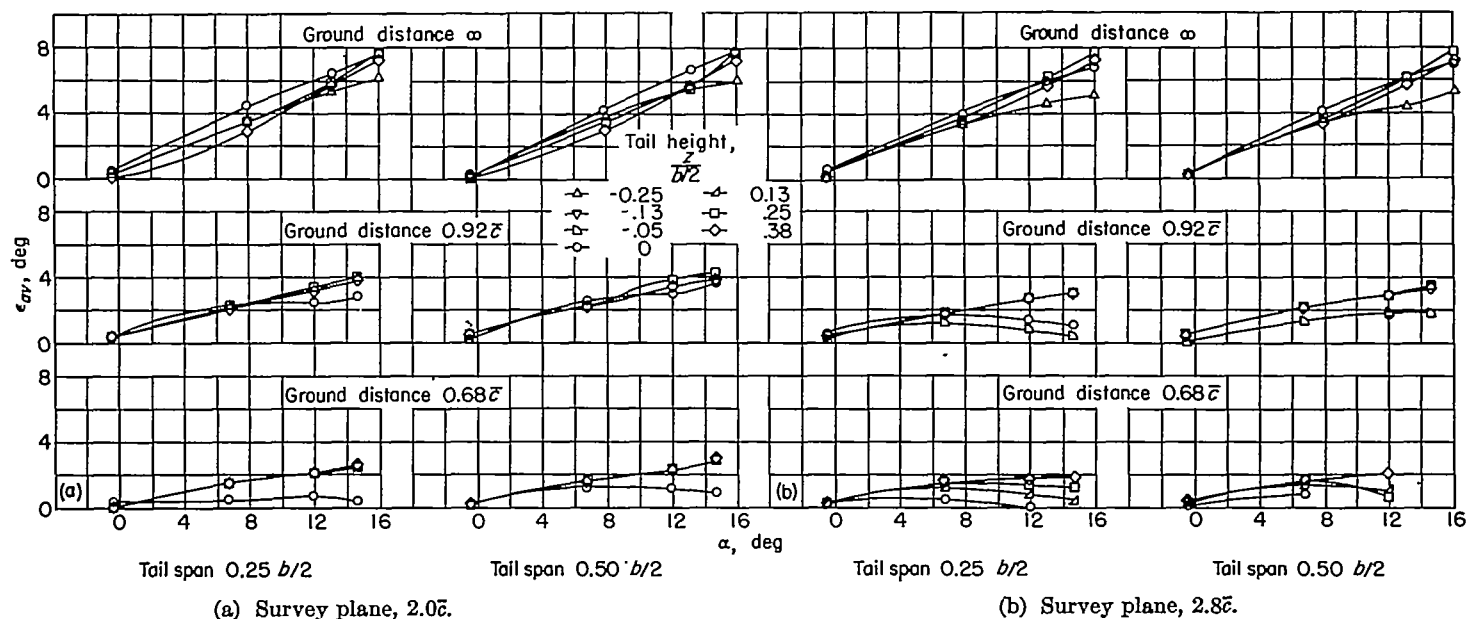(a) Survey plane, $2.0\bar{c}$

(b) Survey plane, $2.8\bar{c}$

FIGURE 25.—The variation of average dynamic-pressure ratio with angle of attack for various ground distances, tail lengths (survey plane), and tail spans. Flaps deflected 60°.
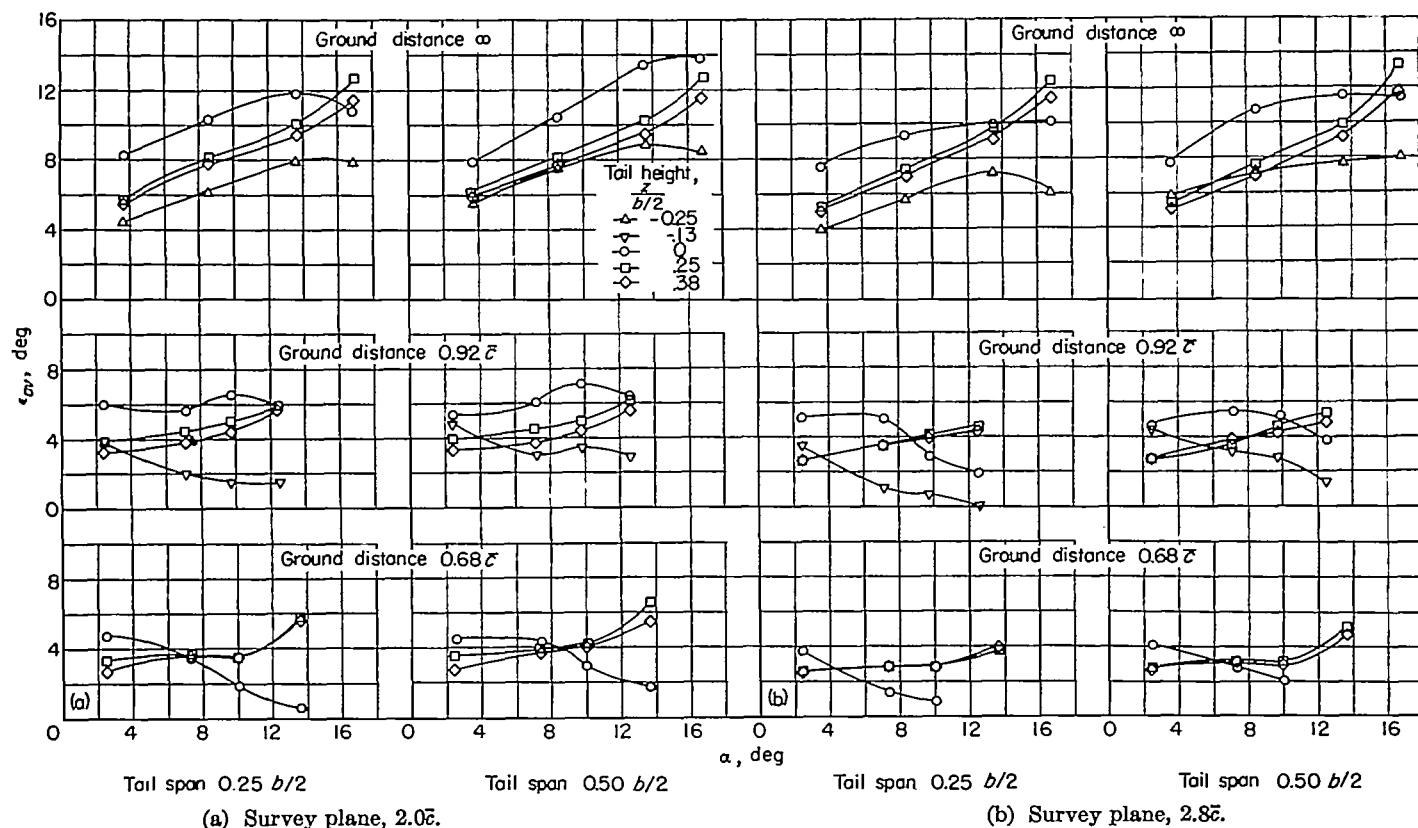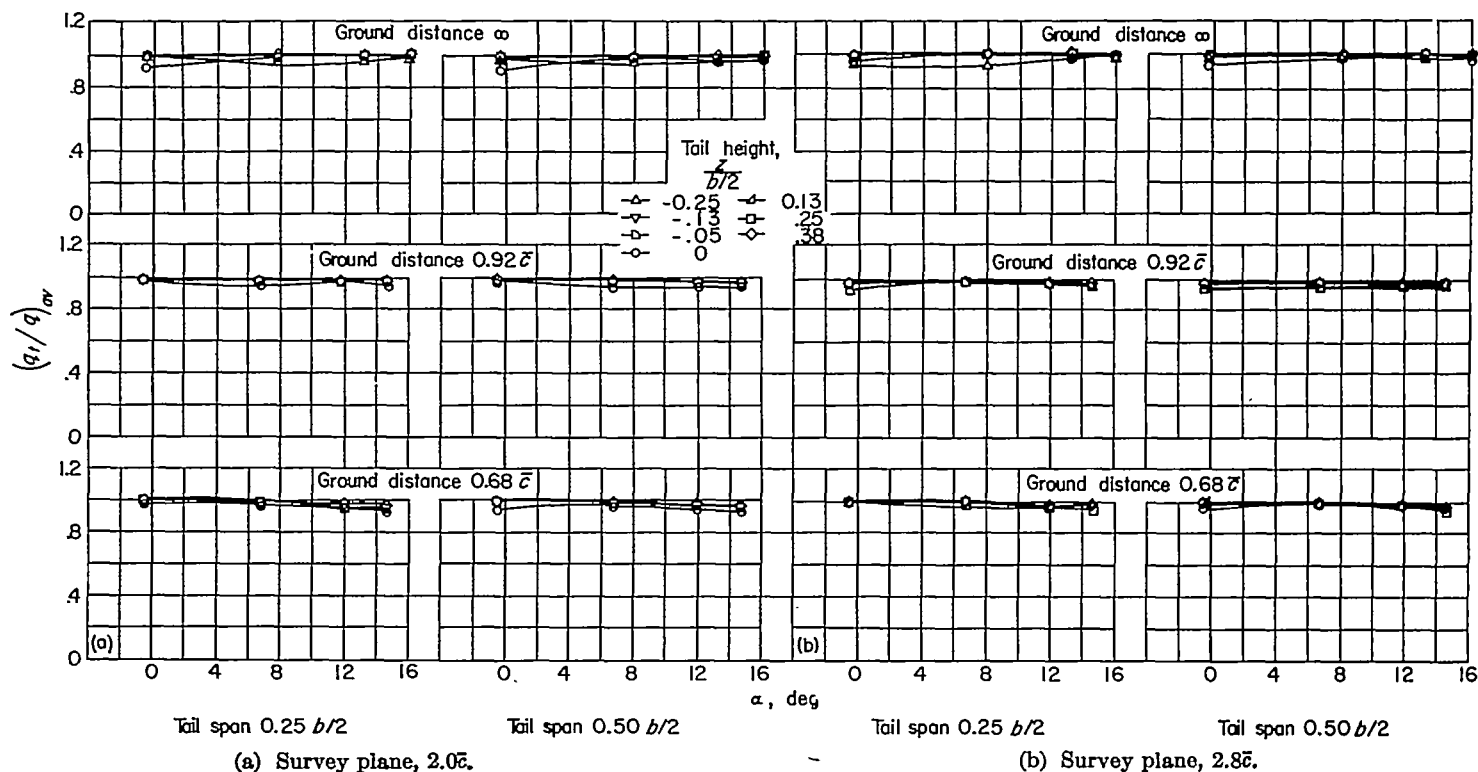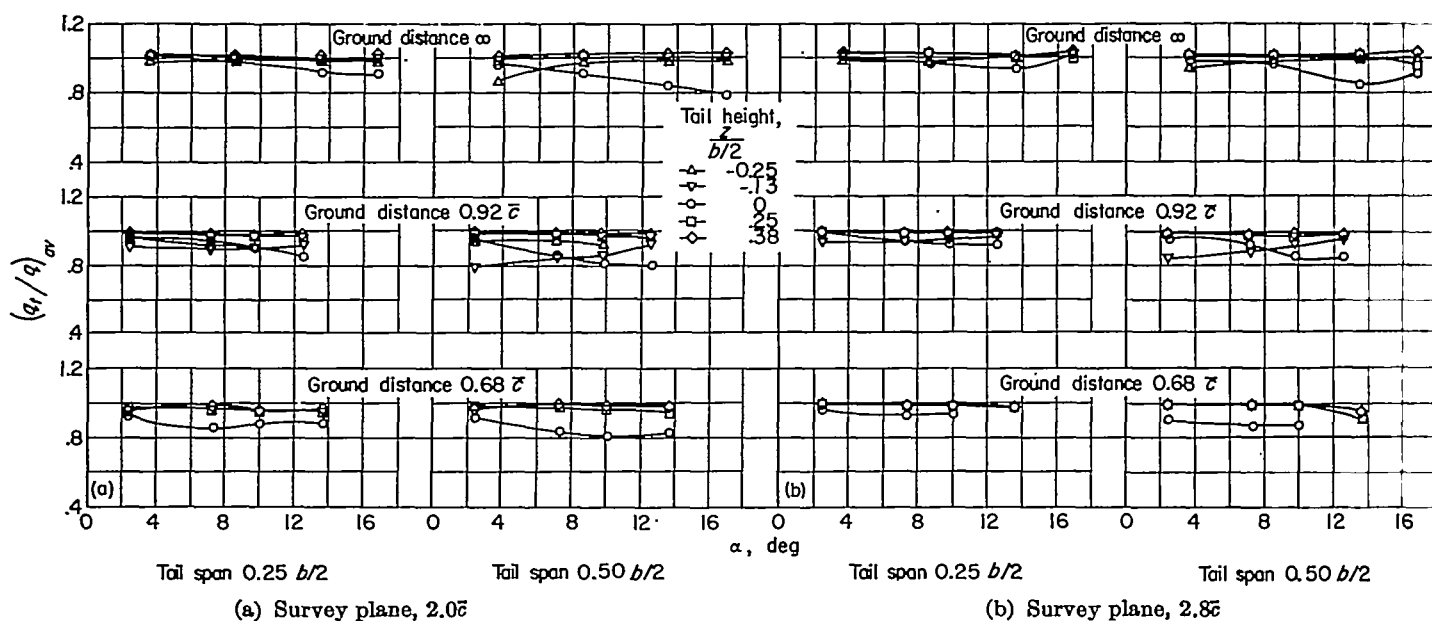
The data presented in figures 22 and 23 show that, for the wing with flaps neutral, the size of tail span (up to $0.50b/2$) has very little effect on $d\epsilon/d\alpha$ either with or without the ground; whereas, for the flapped wing, an increase in span causes an increase in $d\epsilon/d\alpha$. The increased values of $d\epsilon/d\alpha$ for the flapped wing can be attributed to the influence of the flap-tip vortex.

Near maximum lift, the greater tail length (survey plane at $2.8\bar{c}$) resulted in a slight decrease in $d\epsilon/d\alpha$ for the wing with flaps neutral and a greater decrease for the wing with flaps deflected.

The most important parameter, as regards horizontal-tail location for either the plain or flapped wing, appears to be the vertical position. Almost without exception, the values of $d\epsilon/d\alpha$ are decreasing near the maximum lift of the wing for tail locations on or below the chord plane extended, while for tail locations from the chord plane to $0.38b/2$ above, the values of $d\epsilon/d\alpha$ are increasing. The low values of $d\epsilon/d\alpha$ for low tail locations indicate that an increase in stability will probably be obtained as the tail is lowered. Although the values of $d\epsilon/d\alpha$ are decreasing near maximum lift for the tail location on the chord plane extended, the influence of the wake (figs. 24 and 25) may be detrimental at this location. The contours of dynamic-pressure ratio indicate that when the flaps are deflected, the wake is approximately $0.18b/2$ below the chord plane extended at low angles of attack. At high angles of attack or when the wing with flaps deflected is in the presence of the ground, the wake has moved up to within $0.10b/2$ of the chord plane extended.

The presence of the ground substantially reduced the values of $d\epsilon/d\alpha$ and at the lowest ground distance actually produced slight negative values of $d\epsilon/d\alpha$ near maximum lift for the wing with flaps neutral. The values of $d\epsilon/d\alpha$ for the wing with flaps deflected became even more negative at low ground distances than those for the wing with flaps neutral, and although negative values of $d\epsilon/d\alpha$ will improve the stability, such variations may be undesirable from the standpoint of trim (figs. 22 and 23).

The data obtained for the wing with flaps neutral and with flaps deflected 60° with and without the ground present indicate that, from a consideration of downwash and dynamic pressure, the most favorable tail location would be below the chord plane extended and with the greater tail length.

CALCULATED DOWNWASH

The possibility of using lifting-line theory to determine the downwash behind sweptback wings has been briefly investigated. The procedure for the calculations is given in the appendix. Experimental results have been compared with variations of downwash with vertical distance, calculated at the plane of symmetry and at a spanwise station $0.33b/2$ (figs. 26 and 27). The vertical reference point in figure 26 is the 0.25-chord point of the root chord and in figure 27 it is the 0.25-chord point of the chord at spanwise station $0.33b/2$. The spanwise variations of maximum downwash obtained experimentally are presented in figure 28. Also included in this figure are values of downwash calculated at the center of the vortex sheet and, as can be seen in

(a) Survey plane, $2.0\bar{c}$.

(b) Survey plane, $2.8\bar{c}$.
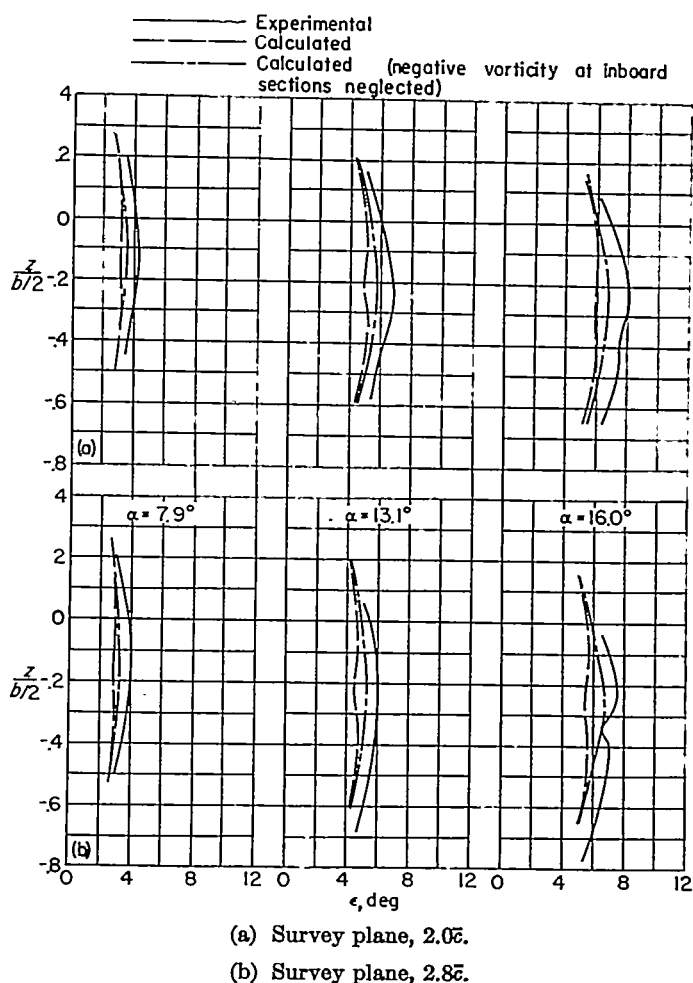
FIGURE 26.—Variation of calculated and experimental values of downwash with vertical distance at the plane of symmetry. (Vertical reference point 0.25 chord at plane of symmetry.)
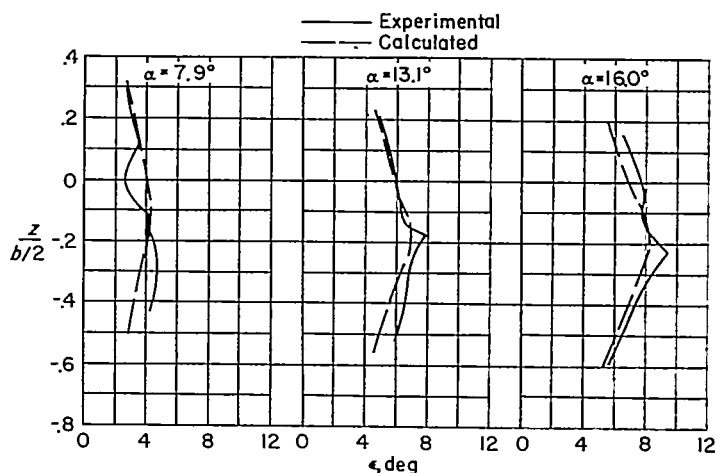
FIGURE 27.—Variation of calculated and experimental values of downwash with vertical distance at a spanwise station $0.33b/2$. (Vertical reference point 0.25 chord at spanwise station $0.33b/2$.) Survey plane, $2.0\bar{c}$.

figure 26, they do not necessarily represent the maximum values obtained.

It is apparent in figure 26 that the lifting-line theory, as applied in the present calculations, underestimates the experimental downwash in the plane of symmetry. For the angle-of-attack range shown, the value of $d\epsilon/d\alpha$ calculated is approximately 20 percent lower than that obtained
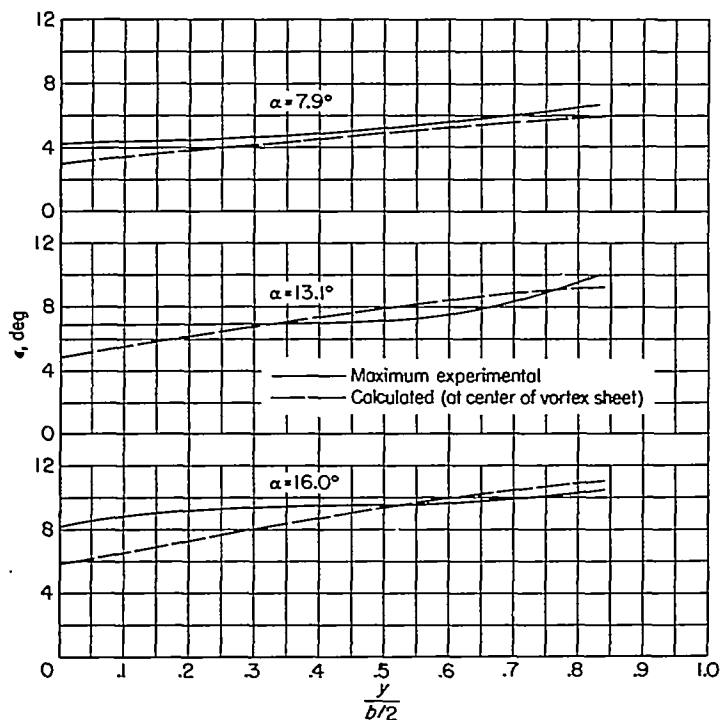
FIGURE 28.—Spanwise variation of maximum experimental downwash and calculated downwash at the center of the vortex sheet.

experimentally. The results presented in figures 27 and 28 show that the agreement improves outboard of the plane of symmetry. The assumption was made in the calculations that the vortex sheet was shed along the 0.25-chord line and that the wing was at an angle of attack of 0°. The calculations were repeated by taking into account the tilt of the vortex sheet (extending from the 0.25-chord line) as the angle of attack increased. The results of these calculations were essentially in agreement with the original calculations. In order to evaluate the upwash contributed by the negative vorticity shed over the inboard sections of the wing, calculations were made with the negative vorticity neglected. The downwash angles obtained are shown in figure 26 and the calculated value of $d\epsilon/d\alpha$ is now only 10 percent lower than the experimental value. Neglecting the negative vorticity at the inboard sections had a negligible effect on the downwash calculated at stations outboard of the plane of symmetry.

Reference 8 indicates that, for downwash calculations behind straight wings, the displacement of the vortex sheet must be accounted for and the distention of the vortex sheet may be neglected. The displacement of the vortex sheet, as calculated by the method of reference 8, appears adequate for sweptback wings (figs. 26 and 27); whereas the distention of the vortex sheet behind a sweptback wing may not be small enough to neglect.

CONCLUDING REMARKS

An investigation has been conducted to determine the ground interference effects on the aerodynamic and flow characteristics of a 42° sweptback wing. The simulated ground tests were made at ground distances 0.68 and 0.92 of the mean aerodynamic chord. The model was tested with flaps neutral and with inboard trailing-edge split flaps deflected 60° and outboard leading-edge flaps deflected. The results of the tests indicated:

1. The nature and magnitudes of the effects of ground interference on the aerodynamic characteristics of the swept-back wing are, in general, comparable to those obtained on unswept wings. The sweptback wing in the presence of the ground board sustained an increase in lift-curve slope and a decrease in drag. The value of maximum lift for the sweptback wing increased for the flaps-neutral configuration and decreased for the flaps-deflected configuration as the distance from the ground became smaller.

2. The longitudinal stability at the stall for the sweptback wing with and without flaps deflected was not materially affected by the presence of the ground. There was, however, at the lowest distance from the ground a destabilizing change in pitching-moment slope several degrees prior to the stall for the flaps-deflected configuration. Because of the complexity of the phenomena at the stall, the possibility exists that the data for the sweptback wing tested are not indicative of the type of stability to be obtained at ground distances greater than one mean aerodynamic chord.

3. The qualitative results of the airstream survey for the ground-out condition are, in general, consistent with the results which would be expected from a consideration of the span loading associated with sweptback wings. It was found also that, without the ground present, the tip vortices for the plain wing were shed at a position that would be expected for a straight tapered wing.

4. The variations of average downwash and average dynamic-pressure ratio with angle of attack indicate that for either model configuration the most preferable tail location would be below the chord plane extended and at the most rearward survey position. In the presence of the ground, negative variations of average downwash with angle of attack were obtained, and though such variations would increase the degree of stability, they may be undesirable from the standpoint of trim.

5. Calculations of downwash by the lifting-line method (as applied) underestimated the experimental downwash at the plane of symmetry but resulted in reasonable estimates of the experimental downwash outboard of the plane of symmetry.

LANGLEY AERONAUTICAL LABORATORY,
  NATIONAL ADVISORY COMMITTEE FOR AERONAUTICS,
  LANGLEY FIELD, VA., *December 17, 1954.*

APPENDIX

METHOD OF DOWNWASH CALCULATIONS

The reasonable agreement, attained for unswept wings, between values of downwash calculated by the method presented in references 7 and 8 and those obtained by experiment suggests an extension of the method to account for the sweep of the lifting line. Obvious objections to simplifications imposed by the lifting-line method have been discussed in reference 1 for the case of an unswept wing and it can be assumed that they apply in essence to sweptback wings as well. Although the aspect ratios of sweptback wings are, in general, smaller than those of the unswept wings treated in references 7 and 8, the lifting-line theory may still be expected to render approximate estimates of the downwash in the region of the tail plane. Little is known of the downward displacement and distention of the vortex sheet behind a sweptback wing; hence, for the present calculations, the assumptions made for unswept wings are applied.

The Biot-Savart equation has been expanded, as in reference 8, to determine the induced downward velocity due to the bound vortex and two trailing vortices, with the assumption, however, that the bound vortex is swept along the 0.25-chord line. The resulting induced downward velocity for any point whose coordinates are x, y, z may be expressed in terms of stream velocity as:

$$\frac{w}{V} = -\int_0^1 \left(\frac{cc_l}{b}\right) (g_1)\, ds + \int_0^{-1} \left(\frac{cc_l}{b}\right) (g_2)\, ds$$

where

$$g_1 = \frac{1}{4\pi}\left(\frac{(s-y)}{[(s-y)^2+z^2]}\left[1+\frac{x-s\tan\Lambda}{\sqrt{(s-y)^2+(x-s\tan\Lambda)^2+z^2}}\right]+\right.$$

$$\frac{(x-y\tan\Lambda)\cos\Lambda}{(x-y\tan\Lambda)^2\cos^2\Lambda+z^2]}\left\{\frac{\frac{s}{\cos\Lambda}-\sqrt{y^2+x^2-[(x-y\tan\Lambda)\cos\Lambda]^2}}{\sqrt{(s-y)^2+(x-s\tan\Lambda)^2+z^2}}+\frac{\sqrt{y^2+x^2-[(x-y\tan\Lambda)\cos\Lambda]^2}}{\sqrt{y^2+x^2+z^2}}\right\}\left.\right)$$

$$g_2 = \frac{1}{4\pi}\left(\frac{(s+y)}{[(s+y)^2+z^2]}\left[1+\frac{x-s\tan\Lambda}{\sqrt{(s+y)^2+(x-s\tan\Lambda)^2+z^2}}\right]+\right.$$

$$\frac{(x+y\tan\Lambda)\cos\Lambda}{[(x+y\tan\Lambda)^2\cos^2\Lambda+z^2]}\left\{\frac{\frac{s}{\cos\Lambda}-\sqrt{y^2+x^2-[(x+y\tan\Lambda)\cos\Lambda]^2}}{\sqrt{(s+y)^2+(x-s\tan\Lambda)^2+z^2}}+\frac{\sqrt{y^2+x^2-[(x+y\tan\Lambda\cos\Lambda]^2}}{\sqrt{y^2+x^2+z^2}}\right\}\left.\right)$$

and

$$\frac{cc_l}{b}=\frac{2\tau}{Vb}$$

The integration was performed by numerical summation with vorticity shed every $0.1\frac{b}{2}$ outboard of the plane of symmetry. Then the downwash angle can be evaluated:

$$\epsilon'=\frac{w}{V}\ (57.3)$$

The displacement of the vortex sheet according to reference 8 is

$$h=\int_{T.E.}^x \tan\epsilon\, dx$$

For the present calculations, the span-load curve was computed by an empirical method which adapts Schrenk's method to sweptback wings (ref. 11). As previously indicated, the downwash is directly affected by the shape of the span load distribution. For more precise evaluation of the downwash, it is recommended that a span load distribution calculated by one of the more rigorous lifting-surface methods described in reference 12 be used.

REFERENCES

1. Wieselsberger, C.: Wing Resistance Near the Ground. NACA TM 77, 1922.
2. Pistolesi, E.: Ground Effect—Theory and Practice. NACA TM 828, 1937.
3. Reid, Elliott G.: A Full-Scale Investigation of Ground Effect. NACA Rep. 265, 1927.
4. Recant, Isidore G.: Wind-Tunnel Investigation of Ground Effect on Wings With Flaps. NACA TN 705, 1939.

5. Katzoff, S., and Sweberg, Harold H.: Ground Effect on Downwash Angles and Wake Location. NACA Rep. 738, 1943.
6. Tani, Itiro, Taima, Masuo, and Simidu, Sodi: The Effect of Ground on the Aerodynamic Characteristics of a Monoplane Wing. Rep. No. 156 (vol. XIII, 2), Aero. Res. Inst., Tokyo Imperial Univ., Sept. 1937.
7. Silverstein, Abe, and Katzoff, S.: Design Charts for Predicting Downwash Angles and Wake Characteristics Behind Plain and Flapped Wings. NACA Rep. 648, 1939.
8. Silverstein, Abe, Katzoff, S., and Bullivant, W. Kenneth: Downwash and Wake Behind Plain and Flapped Airfoils. NACA Rep. 651, 1939.
9. Purser, Paul E., Spearman, M. Leroy, and Bates, William R.: Preliminary Investigation at Low Speed of Downwash Charac-

teristics of Small-Scale Sweptback Wings. NACA TN 1378, 1947.
10. Tolhurst, William H., Jr.: An Investigation of the Downwash and Wake Behind Large-Scale Swept and Unswept Wings. NACA RM A7L05, 1948.
11. Diederich, Franklin W.: A Simple Approximate Method for Calculating Spanwise Lift Distributions and Aerodynamic Influence Coefficients at Subsonic Speeds. NACA TN 2751, 1952.
12. Schneider, William C.: A Comparison of the Spanwise Loading Calculated by Various Methods With Experimental Loadings Obtained on a 45° Sweptback Wing of Aspect Ratio 8 at a Reynolds Number of 4.0×10^6. NACA Rep. 1208, 1954. (Supersedes NACA RM L51G30.)